Clumped同位素的理论和应用

刘琪（副研究员）

中国科学院地球化学研究所 矿床地球化学国家重点实验室

课程大纲

- Clumped同位素的分馏理论
- ^{13}C-^{18}O clumped同位素体系
- 新兴clumped同位素体系
- 国内相关领域的发展

Clumped同位素的分馏理论

定义和随机分布

Clumped Isotopes

John Eiler
Caltech

Clumped同位素：研究分子内含有两个或两个以上稀有同位素的同位素体丰度。

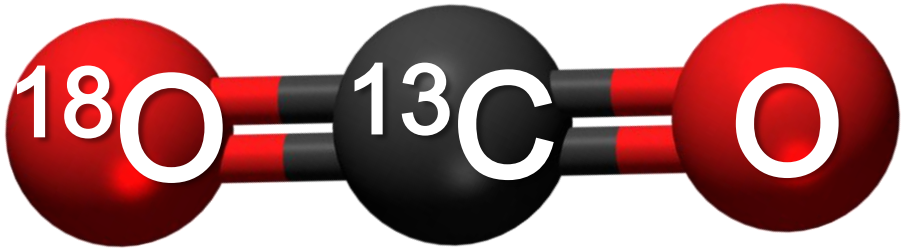

“稀-稀”同位素体

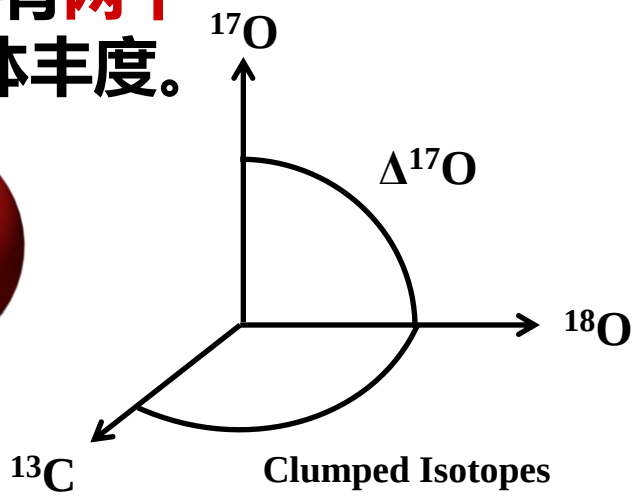

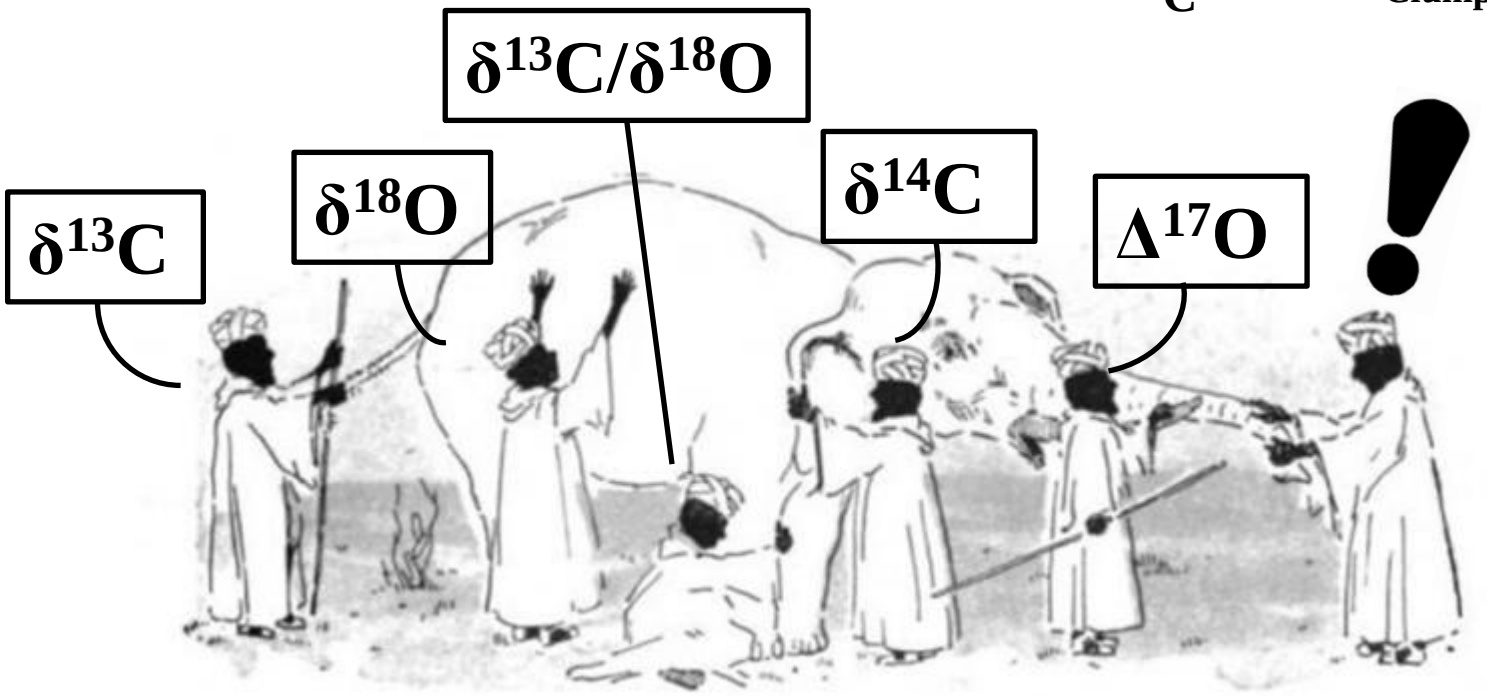

定义

R：同位素体的丰度比值

∞：随机分布

$\Delta^{18}O^{18}O = \Delta 36$

$$A^*B^*X$$

$$=\left(\frac{R_{A^*B^*X}}{R^{\infty}_{A^*B^*X}}-1\right)\times 1000$$

$$=\left(\frac{R_{A^*B^*X}}{R^{\infty}_{A^*B^*X}}-1\right)\times 1000-\left(\frac{R_{A^*BX}}{R^{\infty}_{A^*BX}}-1\right)\times 1000-\left(\frac{R_{AB^*X}}{R^{\infty}_{AB^*X}}-1\right)\times 1000$$

减小实验误差，与平衡常数对应

$$=1000\ln\left(\frac{R_{A^*B^*X}}{R^{\infty}_{A^*B^*X}}\right)-1000\ln\left(\frac{R_{A^*BX}}{R^{\infty}_{A^*BX}}\right)-1000\ln\left(\frac{R_{AB^*X}}{R^{\infty}_{AB^*X}}\right)$$

无需担心定义差别

According to our definition of Δ_i and the Eq. (24) in Wang et al. (2004), we have

$$A^*BX + AB^*X = A^*B^*X + ABX \quad (A.1)$$

$$K_{A^*B^*X} = \frac{[A^*B^*X][ABX]}{[A^*BX][AB^*X]} \quad (A.2)$$

$$K^{\infty}_{A^*B^*X} = \frac{[A^*B^*X]^{\infty}[ABX]^{\infty}}{[A^*BX]^{\infty}[AB^*X]^{\infty}} \quad (A.3)$$

$$\frac{K_{A^*B^*X}}{K^{\infty}_{A^*B^*X}} = \frac{\frac{\delta_{A^*B^*X}}{1000}+1}{\left(\frac{\delta_{A^*BX}}{1000}+1\right)\left(\frac{\delta_{AB^*X}}{1000}+1\right)} \quad (A.4)$$

$$\ln\left(\frac{K_{A^*B^*X}}{K^{\infty}_{A^*B^*X}}\right) = \ln\left(\frac{\delta_{A^*B^*X}}{1000}+1\right) - \ln\left(\frac{\delta_{A^*BX}}{1000}+1\right) - \ln\left(\frac{\delta_{AB^*X}}{1000}+1\right) \quad (A.5)$$

Using Taylor series expansion to the second order (i.e., $\ln(x+1) = x - x^2/2$, when $-1 < x \leqslant 1$), we get

$$\ln\left(\frac{K_{A^*B^*X}}{K^{\infty}_{A^*B^*X}}\right) \approx \left[\frac{\delta_{A^*B^*X}}{1000} - \frac{1}{2}\left(\frac{\delta_{A^*B^*X}}{1000}\right)^2\right] - \left[\frac{\delta_{A^*BX}}{1000} - \frac{1}{2}\left(\frac{\delta_{A^*BX}}{1000}\right)^2\right] - \left[\frac{\delta_{AB^*X}}{1000} - \frac{1}{2}\left(\frac{\delta_{AB^*X}}{1000}\right)^2\right] \quad (A.6)$$

$$1000\ln\left(\frac{K_{A^*B^*X}}{K^{\infty}_{A^*B^*X}}\right) + \frac{(\delta_{A^*B^*X})^2 - (\delta_{A^*BX})^2 - (\delta_{AB^*X})^2}{2000} \approx \delta_{A^*B^*X} - \delta_{A^*BX} - \delta_{AB^*X} = \Delta_{A^*B^*X} \quad (A.7)$$

Because in the approximation of Eq. (27) of Wang et al. (2004), δ_{A^*BX} and δ_{AB^*X} is very close to 0.

$$\delta_{A^*B^*X} \approx \Delta_{A^*B^*X} \quad (A.8)$$

$$\Delta_{A^*B^*X} \approx 1000\ln\left(\frac{K_{A^*B^*X}}{K^{\infty}_{A^*B^*X}}\right) + \frac{(\Delta_{A^*B^*X})^2}{2000} \approx \left(\frac{K_{A^*B^*X}}{K^{\infty}_{A^*B^*X}}-1\right)\times 1000 \quad (A.9)$$

When δ_{A^*BX} and δ_{AB^*X} is very small, a better approximation is

$$\frac{K_{A^*B^*X}}{K^{\infty}_{A^*B^*X}} = \frac{\frac{\delta_{A^*B^*X}}{1000}+1}{\left(\frac{\delta_{A^*BX}}{1000}+1\right)\left(\frac{\delta_{AB^*X}}{1000}+1\right)} \approx 1 + \frac{\delta_{A^*B^*X}}{1000} - \frac{\delta_{A^*BX}}{1000} - \frac{\delta_{AB^*X}}{1000} \quad (A.10)$$

Therefore, $\Delta_{A^*B^*X} = \delta_{A^*B^*X} - \delta_{A^*BX} - \delta_{AB^*X} \approx \left(\frac{K_{A^*B^*X}}{K^{\infty}_{A^*B^*X}}-1\right)\times 1000.$ (A.11)

Moreover, if we define

$$\delta'_{A^*B^*X} = 1000\ln\left(\frac{R_i}{R_i^{\infty}}\right) \quad (A.12)$$

$$\frac{K_{A^*B^*X}}{K^{\infty}_{A^*B^*X}} = \frac{\exp\left(\frac{\delta'_{A^*B^*X}}{1000}\right)}{\exp\left(\frac{\delta'_{A^*BX}}{1000}\right)\exp\left(\frac{\delta'_{AB^*X}}{1000}\right)} \quad (A.13)$$

$$\Delta_{A^*B^*X} = \delta'_{A^*B^*X} - \delta'_{A^*BX} - \delta'_{AB^*X} = 1000\ln\left(\frac{K_{A^*B^*X}}{K^{\infty}_{A^*B^*X}}\right) \quad (A.14)$$

The above definition of Δ_i is preferred by Ono et al. (2014).

Liu & Liu, GCA, 2016

$$\delta_i = \left(\frac{R_i}{R_i^{\infty}}-1\right)\times 1000$$

$$\Delta_{A^*B^*X} = \delta_{A^*B^*X} - \delta_{A^*BX} - \delta_{AB^*X} \approx \left(\frac{K_{A^*B^*X}}{K^{\infty}_{A^*B^*X}}-1\right)\times 1000$$

$$\delta'_{A^*B^*X} = 1000\ln\left(\frac{R_i}{R_i^{\infty}}\right)$$

$$\Delta_{A^*B^*X} = \delta'_{A^*B^*X} - \delta'_{A^*BX} - \delta'_{AB^*X} = 1000\ln\left(\frac{K_{A^*B^*X}}{K^{\infty}_{A^*B^*X}}\right)$$

定义

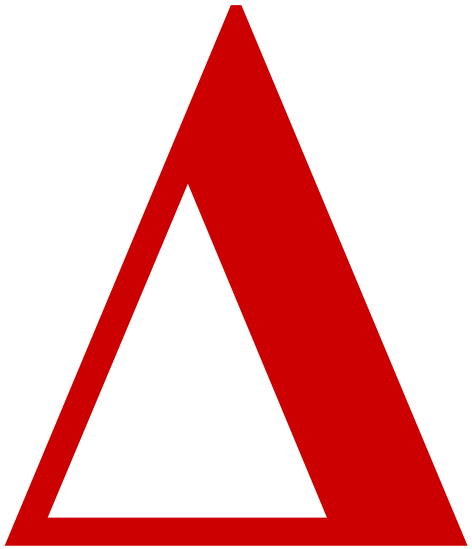

$A*B*X$

>0

$=0$

<0

Isotope clumping and anticlumping in oxygen and methane

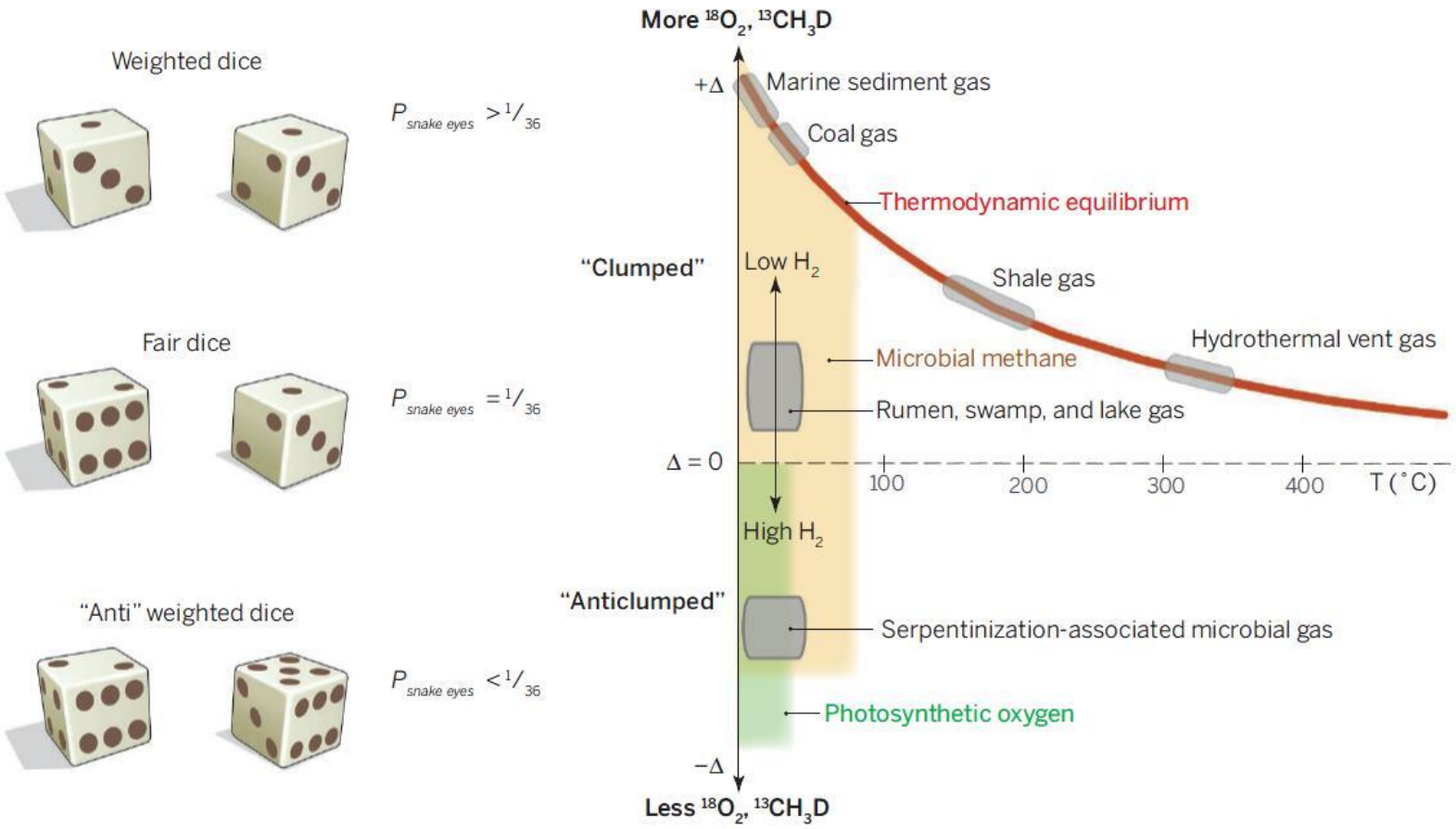

More than a roll of the dice. The appearance of more than one rare, heavy isotope in a molecule (a heavy isotope "clump") is not random. Instead, the isotopic dice are weighted. Clumps are strongly favored under conditions of chemical equilibrium, whereas kinetic processes related to biosynthesis may have lower preference for clumps and in some cases may select against clumps, leading to "anticlumped" products. Natural methane gas shows both behaviors (*6*), whereas the isotope content of photosynthetic oxygen is random or anticlumped (i.e., below chance levels) (*5*).

(Passey, Science, 2015)

随机分布

Abundances of isotopologues of CO_2 and CO_3, assuming bulk $^{13}C/^{12}C$ ratios equal to PDB, bulk $^{18}O/^{17}O/^{16}O$ ratios equal to SMOW, and a stochastic (random) distribution of isotopes

C	Mass	Abundance
Isotopes		
^{12}C	12	98.89%
^{13}C	13	1.11%
O		
^{16}O	16	99.759%
^{17}O	17	370 ppm
^{18}O	18	0.204%

CO_2	Mass	Abundance
Isotopologue		
$^{16}O^{12}C^{16}O$	44	98.40%
$^{16}O^{13}C^{16}O$	45	1.10%
$^{17}O^{12}C^{16}O$	45	730 ppm
$^{18}O^{12}C^{16}O$	46	0.40%
$^{17}O^{13}C^{16}O$	46	8.19 ppm
$^{17}O^{12}C^{17}O$	46	135 ppb
$^{18}O^{13}C^{16}O$	47	45 ppm
$^{17}O^{12}C^{18}O$	47	1.5 ppm
$^{17}O^{13}C^{17}O$	47	1.5 ppb
$^{18}O^{12}C^{18}O$	48	4.1 ppm
$^{17}O^{13}C^{18}O$	48	16.7 ppb
$^{18}O^{13}C^{18}O$	49	46 ppb

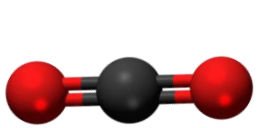

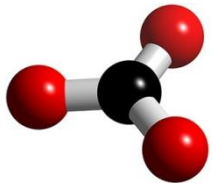

CO_3	Mass	Abundance
Isotopologue		
$^{12}C^{16}O^{16}O^{16}O$	60	98.20%
$^{13}C^{16}O^{16}O^{16}O$	61	1.10%
$^{12}C^{17}O^{16}O^{16}O$	61	0.11%
$^{12}C^{18}O^{16}O^{16}O$	62	0.60%
$^{13}C^{17}O^{16}O^{16}O$	62	12 ppm
$^{12}C^{17}O^{17}O^{16}O$	62	405 ppb
$^{13}C^{18}O^{16}O^{16}O$	63	67 ppm
$^{12}C^{17}O^{18}O^{16}O$	63	4.4 ppm
$^{13}C^{17}O^{17}O^{16}O$	63	4.54 ppb
$^{12}C^{17}O^{17}O^{17}O$	63	50 ppt
$^{12}C^{18}O^{18}O^{16}O$	64	12 ppm
$^{13}C^{17}O^{18}O^{16}O$	64	50 ppb
$^{12}C^{17}O^{17}O^{18}O$	64	828 ppt
$^{13}C^{17}O^{17}O^{17}O$	64	0.5 ppt
$^{13}C^{18}O^{18}O^{16}O$	65	138 ppb
$^{12}C^{17}O^{18}O^{18}O$	65	4.5 ppb
$^{13}C^{17}O^{17}O^{18}O$	65	9 ppt
$^{12}C^{18}O^{18}O^{18}O$	66	8 ppb
$^{13}C^{17}O^{18}O^{18}O$	66	51 ppt
$^{13}C^{18}O^{18}O^{18}O$	67	94 ppt

以PDB和SMOW为碳、氧同位素初始值的随机分布结果。

(Ghosh et al., GCA, 2006)

随机分布

Abundances of isotopologues of CO_2 and CO_3, assuming bulk $^{13}C/^{12}C$ ratios equal to PDB, bulk $^{18}O/^{17}O/^{16}O$ ratios equal to SMOW, and a stochastic (random) distribution of isotopes

C	Mass	Abundance
Isotopes		
^{12}C	12	98.89%
^{13}C	13	1.11%
O		
^{16}O	16	99.759%
^{17}O	17	370 ppm
^{18}O	18	0.204%

CO_2	Mass	Abundance
Isotopologue		
$^{16}O^{12}C^{16}O$	44	98.40%
$^{16}O^{13}C^{16}O$	45	1.10%
$^{17}O^{12}C^{16}O$	45	730 ppm
$^{18}O^{12}C^{16}O$	46	0.40%
$^{17}O^{13}C^{16}O$	46	8.19 ppm
$^{17}O^{12}C^{17}O$	46	135 ppb
$^{18}O^{13}C^{16}O$	47	45 ppm
$^{17}O^{12}C^{18}O$	47	1.5 ppm
$^{17}O^{13}C^{17}O$	47	1.5 ppb
$^{18}O^{12}C^{18}O$	48	4.1 ppm
$^{17}O^{13}C^{18}O$	48	16.7 ppb
$^{18}O^{13}C^{18}O$	49	46 ppb

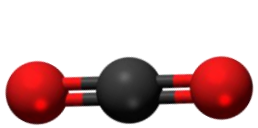

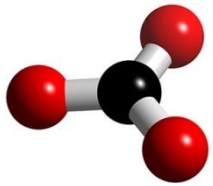

CO_3	Mass	Abundance
Isotopologue		
$^{12}C^{16}O^{16}O^{16}O$	60	98.20%
$^{13}C^{16}O^{16}O^{16}O$	61	1.10%
$^{12}C^{17}O^{16}O^{16}O$	61	0.11%
$^{12}C^{18}O^{16}O^{16}O$	62	0.60%
$^{13}C^{17}O^{16}O^{16}O$	62	12 ppm
$^{12}C^{17}O^{17}O^{16}O$	62	405 ppb
$^{13}C^{18}O^{16}O^{16}O$	63	67 ppm
$^{12}C^{17}O^{18}O^{16}O$	63	4.4 ppm
$^{13}C^{17}O^{17}O^{16}O$	63	4.54 ppb
$^{12}C^{17}O^{17}O^{17}O$	63	50 ppt
$^{12}C^{18}O^{18}O^{16}O$	64	12 ppm
$^{13}C^{17}O^{18}O^{16}O$	64	50 ppb
$^{12}C^{17}O^{17}O^{18}O$	64	828 ppt
$^{13}C^{17}O^{17}O^{17}O$	64	0.5 ppt
$^{13}C^{18}O^{18}O^{16}O$	65	138 ppb
$^{12}C^{17}O^{18}O^{18}O$	65	4.5 ppb
$^{13}C^{17}O^{17}O^{18}O$	65	9 ppt
$^{12}C^{18}O^{18}O^{18}O$	66	8 ppb
$^{13}C^{17}O^{18}O^{18}O$	66	51 ppt
$^{13}C^{18}O^{18}O^{18}O$	67	94 ppt

$^{16}O^{12}C^{16}O$=99.759%×98.89%×99.759%=98.41%

$^{17}O^{12}C^{16}O$=370ppm×98.89%×99.759%×2=730ppm

$^{18}O^{13}C^{16}O$=0.204%×1.11%×99.759%×2=45ppm

$^{17}O^{13}C^{18}O$=370ppm×1.11%×0.204%×2=16.8ppb

ppm=1×10^{-6}（百万分之一）

ppb =1×10^{-9}（十亿分之一）

$^{13}C^{18}O^{16}O^{16}O$=？？？

（Ghosh et al., GCA, 2006）

随机分布

Abundances of isotopologues of CO_2 and CO_3, assuming bulk $^{13}C/^{12}C$ ratios equal to PDB, bulk $^{18}O/^{17}O/^{16}O$ ratios equal to SMOW, and a stochastic (random) distribution of isotopes

C	Mass	Abundance
Isotopes		
^{12}C	12	98.89%
^{13}C	13	1.11%
O		
^{16}O	16	99.759%
^{17}O	17	370 ppm
^{18}O	18	0.204%

CO_2	Mass	Abundance
Isotopologue		
$^{16}O^{12}C^{16}O$	44	98.40%
$^{16}O^{13}C^{16}O$	45	1.10%
$^{17}O^{12}C^{16}O$	45	730 ppm
$^{18}O^{12}C^{16}O$	46	0.40%
$^{17}O^{13}C^{16}O$	46	8.19 ppm
$^{17}O^{12}C^{17}O$	46	135 ppb
$^{18}O^{13}C^{16}O$	47	45 ppm
$^{17}O^{12}C^{18}O$	47	1.5 ppm
$^{17}O^{13}C^{17}O$	47	1.5 ppb
$^{18}O^{12}C^{18}O$	48	4.1 ppm
$^{17}O^{13}C^{18}O$	48	16.7 ppb
$^{18}O^{13}C^{18}O$	49	46 ppb

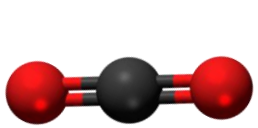

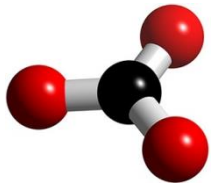

CO_3	Mass	Abundance
Isotopologue		
$^{12}C^{16}O^{16}O^{16}O$	60	98.20%
$^{13}C^{16}O^{16}O^{16}O$	61	1.10%
$^{12}C^{17}O^{16}O^{16}O$	61	0.11%
$^{12}C^{18}O^{16}O^{16}O$	62	0.60%
$^{13}C^{17}O^{16}O^{16}O$	62	12 ppm
$^{12}C^{17}O^{17}O^{16}O$	62	405 ppb
$^{13}C^{18}O^{16}O^{16}O$	63	67 ppm
$^{12}C^{17}O^{18}O^{16}O$	63	4.4 ppm
$^{13}C^{17}O^{17}O^{16}O$	63	4.54 ppb
$^{12}C^{17}O^{17}O^{17}O$	63	50 ppt
$^{12}C^{18}O^{18}O^{16}O$	64	12 ppm
$^{13}C^{17}O^{18}O^{16}O$	64	50 ppb
$^{12}C^{17}O^{17}O^{18}O$	64	828 ppt
$^{13}C^{17}O^{17}O^{17}O$	64	0.5 ppt
$^{13}C^{18}O^{18}O^{16}O$	65	138 ppb
$^{12}C^{17}O^{18}O^{18}O$	65	4.5 ppb
$^{13}C^{17}O^{17}O^{18}O$	65	9 ppt
$^{12}C^{18}O^{18}O^{18}O$	66	8 ppb
$^{13}C^{17}O^{18}O^{18}O$	66	51 ppt
$^{13}C^{18}O^{18}O^{18}O$	67	94 ppt

$^{16}O^{12}C^{16}O$=99.759%×98.89%×99.759%=98.41%

$^{17}O^{12}C^{16}O$=370ppm×98.89%×99.759%×2=730ppm

$^{18}O^{13}C^{16}O$=0.204%×1.11%×99.759%×2=45ppm

$^{17}O^{13}C^{18}O$=370ppm×1.11%×0.204%×2=16.8ppb

ppm=1×10^{-6}（百万分之一）

ppb =1×10^{-9}（十亿分之一）

$^{13}C^{18}O^{16}O^{16}O$=1.11%×0.204%×99.759%×99.759%×3=67.6ppm

（Ghosh et al., GCA, 2006）

知识点：

1）随机分布是高温极限下的分布状态，只受概率控制；

同位素分馏

Clumped同位素有别于随机分布的情况，是同位素分馏的结果：

平衡分馏（热力学控制，$\Delta_{A*B*X} > 0$）

动力学分馏（化学反应、生物效应等，$\Delta_{A*B*X} > 0, \Delta_{A*B*X} < 0$ ）

组合效应（反应底物对同位素的选择差异，主要$\Delta_{A*B*X} < 0$）

扩散

混合

……

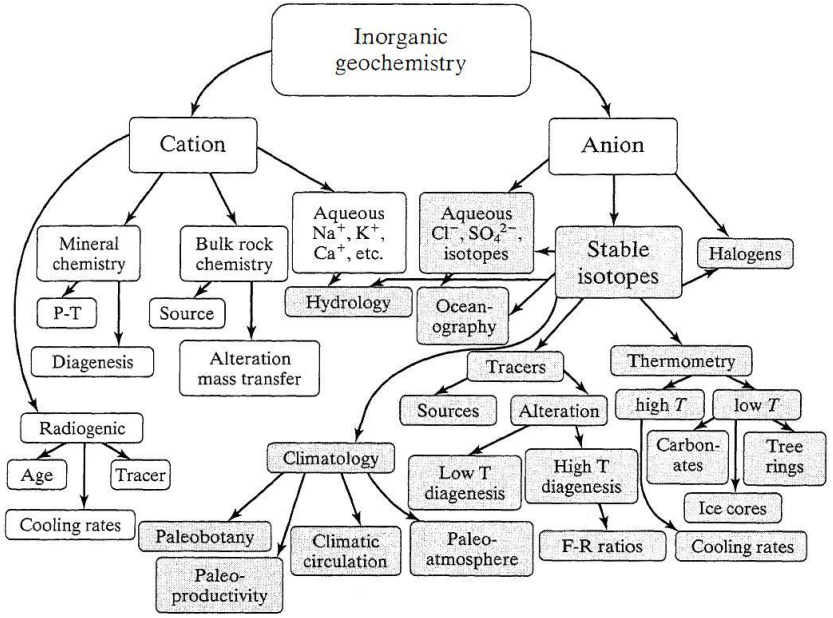

(Sharp, Principles of Stable Isotope Geochemistry, 2006)

Clumped同位素的分馏理论

平衡分馏

平衡分馏

化学平衡：

一种热力学状态，即可逆反应的正、反方向的反应速率相等；
处于平衡条件下，各组分浓度不发生改变；
条件改变（例如温度），各组分浓度随之改变；
通过何种途径达到平衡不重要。

同位素平衡：

只与能量（振动、转动、平动和电子能）和温度有关，（有时与压力有关）。

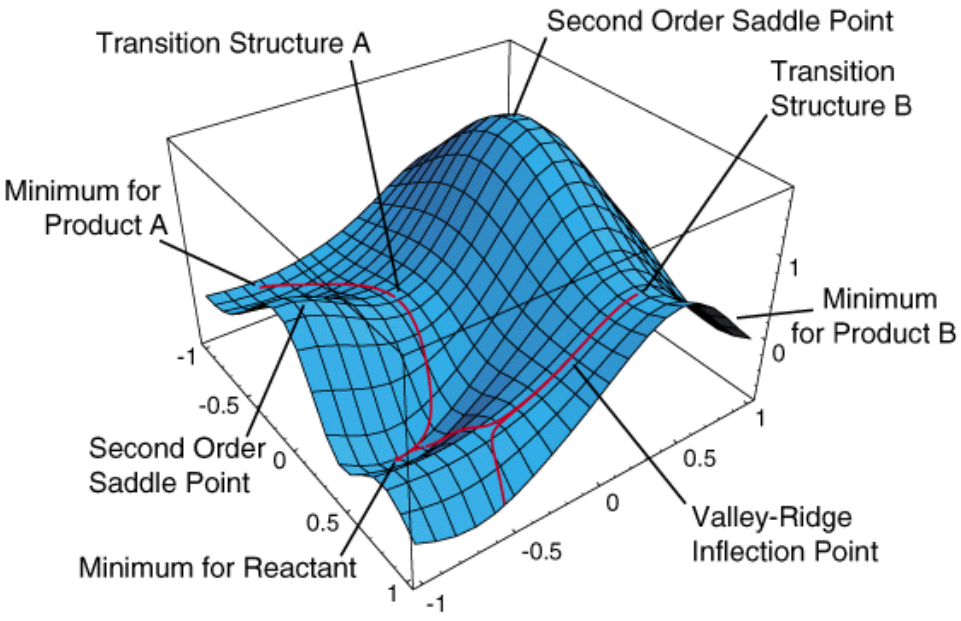

为什么 Δ > 0？

答："稀-稀"同位素体具有更低的零点能，更低的能量更有利于成键。

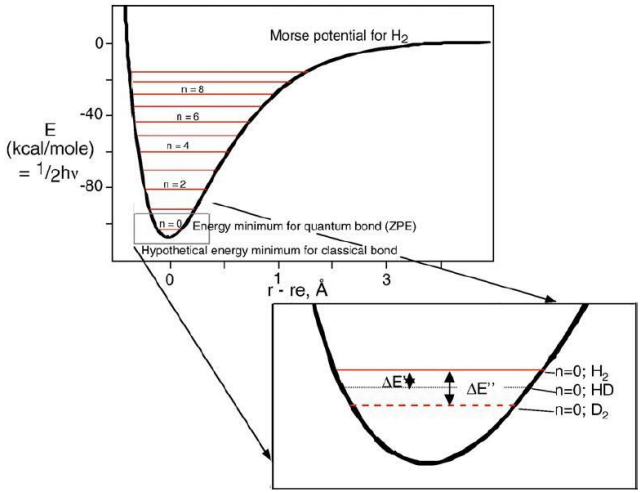

平衡分馏

Geochimica et Cosmochimica Acta, Vol. 68, No. 23, pp. 4779–4797, 2004

0016-7037/04 $30.00 + .00

ELSEVIER

doi:10.1016/j.gca.2004.05.039

Equilibrium thermodynamics of multiply substituted isotopologues of molecular gases

ZHENGRONG WANG,* EDWIN A. SCHAUBLE,† and JOHN M. EILER
Division of Geological and Planetary Sciences, M/C 100-23, California Institute of Technology, Pasadena, California 91125, USA

CO_2, 内平衡反应:

row 5 :

$$^{16}O^{12}C^{16}O + {}^{16}O^{13}C^{17}O \overset{K_1}{=} {}^{16}O^{13}C^{16}O + {}^{16}O^{12}C^{17}O \quad K_1 = \frac{x_2x_3}{x_1x_5}$$

row 6 :

$$^{16}O^{12}C^{16}O + {}^{17}O^{12}C^{17}O \overset{K_2}{=} 2\,{}^{16}O^{12}C^{17}O \quad K_2 = \frac{x_3^2}{x_1x_6}$$

row 7 :

$$^{16}O^{12}C^{16}O + {}^{16}O^{13}C^{18}O \overset{K_3}{=} {}^{16}O^{13}C^{16}O + {}^{16}O^{12}C^{18}O \quad K_3 = \frac{x_2x_4}{x_1x_7}$$

row 8 :

$$^{16}O^{12}C^{16}O + {}^{17}O^{12}C^{18}O \overset{K_4}{=} {}^{16}O^{12}C^{17}O + {}^{16}O^{12}C^{18}O \quad K_4 = \frac{x_3x_4}{x_1x_8}$$

row 9 :

$$2\,{}^{16}O^{12}C^{16}O + {}^{17}O^{13}C^{17}O \overset{K_5}{=} {}^{16}O^{13}C^{16}O + 2\,{}^{16}O^{12}C^{17}O \quad K_5 = \frac{x_4^2}{x_1x_{10}}$$

row 10 :

$$^{16}O^{12}C^{16}O + {}^{18}O^{12}C^{18}O \overset{K_6}{=} 2\,{}^{16}O^{12}C^{18}O \quad K_6 = \frac{x_4^2}{x_1x_{10}}$$

row 11 :

$$2\,{}^{16}O^{12}C^{16}O + {}^{17}O^{13}C^{18}O \overset{K_7}{=} {}^{16}O^{13}C^{16}O + {}^{16}O^{12}C^{17}O + {}^{16}O^{12}C^{18}O \quad K_7 = \frac{x_2x_3x_4}{x_1^2x_{11}}$$

row 12 :

$$2\,{}^{16}O^{12}C^{16}O + {}^{18}O^{13}C^{18}O \overset{K_8}{=} {}^{16}O^{13}C^{16}O + 2\,{}^{16}O^{12}C^{18}O \quad K_8 = \frac{x_2^2x_2}{x_1^2x_{12}}$$

$$\ln\left(\frac{\Delta_4}{1000}+1\right) = \ln\left(\frac{\Delta_2}{1000}+1\right) + \ln\left(\frac{\Delta_3}{1000}+1\right) - \ln\left(\frac{\Delta_1}{1000}+1\right) - \ln\frac{K}{K_r}$$

$$\Delta_4 \approx \Delta_2 + \Delta_3 - 1000\ln\frac{K}{K_r}$$

$$\Delta_4 \approx -1000\ln\frac{K}{K_r}$$

1）建立clumped同位素理论基础；

2）通过内平衡反应求解平衡常数；

3）计算气态分子的clumped同位素信号的温度依赖性。

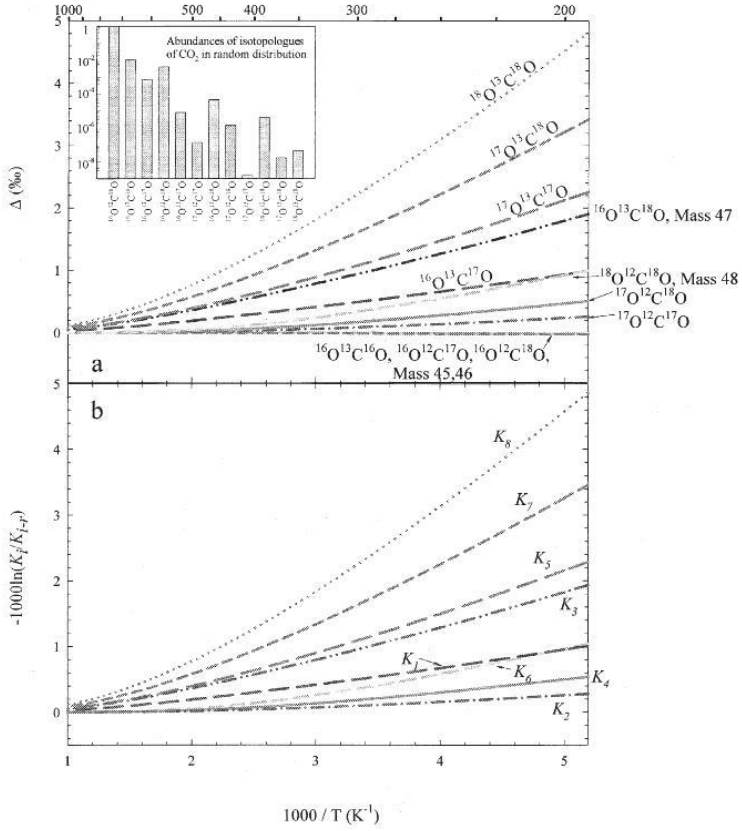

平衡分馏

Available online at www.sciencedirect.com
SciVerse ScienceDirect
Geochimica et Cosmochimica Acta 77 (2012) 292–303
Geochimica et Cosmochimica Acta
www.elsevier.com/locate/gca

1）建立兴趣分子与单原子间的同位素平衡；

$$CO_2+{}^{13}C+{}^{18}O={}^{13}C{}^{18}OO+C+O$$

Theoretical estimation of the equilibrium distribution of clumped isotopes in nature

Xiaobin Cao, Yun Liu *

State Key Laboratory of Ore Deposit Geochemistry, Institute of Geochemistry, Chinese Academy of Sciences, Guiyang 550002, China

Received 18 October 2010; accepted in revised form 7 November 2011; available online 15 November 2011

2）为求解复杂分子体系平衡常数提供理论方法，尤其针对同一质量数；

Table 2
The Δ_i results of CO_2 at 300 K using different methods.

	Wang et al. results	This study – using Wang et al.'s data				This study – DFT*		This study – MP2+	
		ZPE-E[a]	ZPE-A[b]	B.M.-E[c]	B.M.-A[d]	B.M.-E[c]	B.M.-A[d]	B.M.-E[c]	B.M.-A[d]
$^{16}O^{13}C^{16}O$	−0.004	−0.004	0.000	−0.004	0.000	−0.004	0.000	−0.004	0.000
$^{16}O^{12}C^{17}O$	−0.006	−0.006	0.000	−0.006	0.000	−0.006	0.000	−0.006	0.000
$^{16}O^{12}C^{18}O$	−0.011	−0.011	0.000	−0.011	0.000	−0.011	0.000	−0.011	0.000
$^{16}O^{13}C^{17}O$	0.489	0.489	0.499	0.477	0.487	0.488	0.498	0.480	0.490
$^{17}O^{12}C^{17}O$	0.085	0.087	0.099	0.087	0.099	0.093	0.105	0.081	0.092
$^{16}O^{13}C^{18}O$	0.938	0.936	0.951	0.917	0.932	0.935	0.951	0.921	0.936
$^{17}O^{12}C^{18}O$	0.168	0.167	0.184	0.172	0.189	0.183	0.201	0.160	0.177
$^{17}O^{13}C^{17}O$	1.074	1.075	1.091	1.052	1.067	1.079	1.095	1.051	1.067
$^{18}O^{12}C^{18}O$	0.333	0.330	0.353	0.340	0.363	0.362	0.384	0.316	0.339
$^{17}O^{13}C^{18}O$	1.608	1.605	1.627	1.579	1.600	1.618	1.639	1.572	1.593
$^{18}O^{13}C^{18}O$	2.219	2.216	2.243	2.180	2.207	2.240	2.267	2.166	2.192

47

平衡分馏

Available online at www.sciencedirect.com
ScienceDirect
Geochimica et Cosmochimica Acta 175 (2016) 252–270
Geochimica et Cosmochimica Acta
www.elsevier.com/locate/gca

Clumped-isotope signatures at equilibrium of CH_4, NH_3, H_2O, H_2S and SO_2

Qi Liu, Yun Liu*

$\Delta_{A^*B^*X}$

$$= \left(\frac{\mathrm{RPFR}_{A^*B^*X}}{\mathrm{RPFR}_{A^*BX} \cdot \mathrm{RPFR}_{AB^*X}} - 1 \right) \times 1000$$

平衡分馏

$$\alpha = \frac{RPFR(A)}{RPFR(B)}$$

Harold C. Urey

Jacob Bigeleisen

Maria G. Mayer

562 *Urey :*

The Thermodynamic Properties of Isotopic Substances.

Liversidge Lecture, Delivered before the Chemical Society in the Royal Institution on December 18th, 1946.

By Harold C. Urey.

(Institute of Nuclear Studies, University of Chicago.)

THE JOURNAL OF CHEMICAL PHYSICS VOLUME 15, NUMBER 5 MAY, 1947

Calculation of Equilibrium Constants for Isotopic Exchange Reactions

Jacob Bigeleisen and Maria Goeppert Mayer

Argonne National Laboratory, Chicago, Illinois and Institute for Nuclear Studies, University of Chicago*

(Received February 5, 1947)

It is pointed out that the possibility of chemical separation of isotopes is a quantum effect. This permits a direct calculation of the difference in the free energies of two isotopic molecules. Tables and approximation methods are given which permit a rapid calculation of equilibrium constants if the frequency shifts on isotopic substitution are known. Several applications are discussed.

RPFR

Reduced Partition Function Ratio

$$= \prod_i \left\{ \frac{u_i^*}{u_i} \frac{\exp(-u_i^*/2)}{\exp(-u_i/2)} \frac{[1-\exp(-u_i)]}{[1-\exp(-u_i^*)]} \right\}$$

平衡分馏

Available online at www.sciencedirect.com
ScienceDirect
Geochimica et Cosmochimica Acta 175 (2016) 252–270
Geochimica et Cosmochimica Acta
www.elsevier.com/locate/gca

Clumped-isotope signatures at equilibrium of CH_4, NH_3, H_2O, H_2S and SO_2

Qi Liu, Yun Liu*

$\Delta_{A^*B^*X}$

$$= \left(\frac{\mathrm{RPFR}_{A^*B^*X}}{\mathrm{RPFR}_{A^*BX} \cdot \mathrm{RPFR}_{AB^*X}} - 1 \right) \times 1000$$

知识点：

1）随机分布是高温极限下的分布状态，只受概率控制；

2）同位素平衡分馏参数，是温度（T）的函数；

^{13}C-^{18}O clumped同位素体系

平衡分馏的应用

Thermo SCIENTIFIC

Finigan

MAT 253

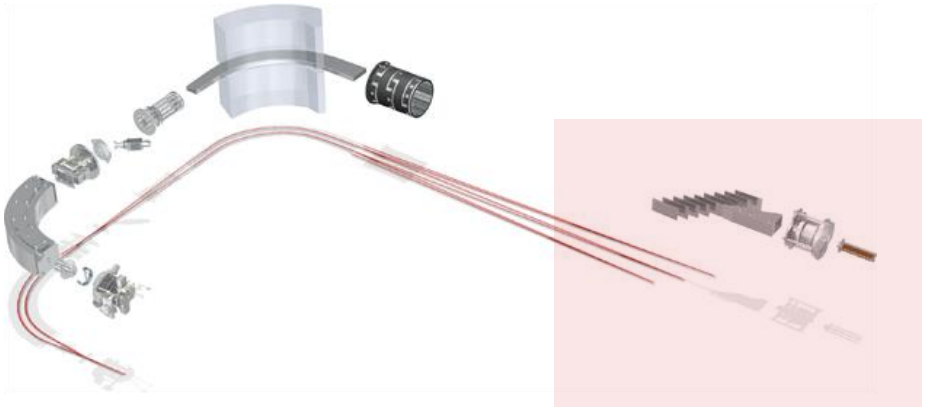

增加法拉第杯，以接收m/e为44-49的信号。

CO_2质量数47的R^{47}值。

^{13}C-^{18}O clumping

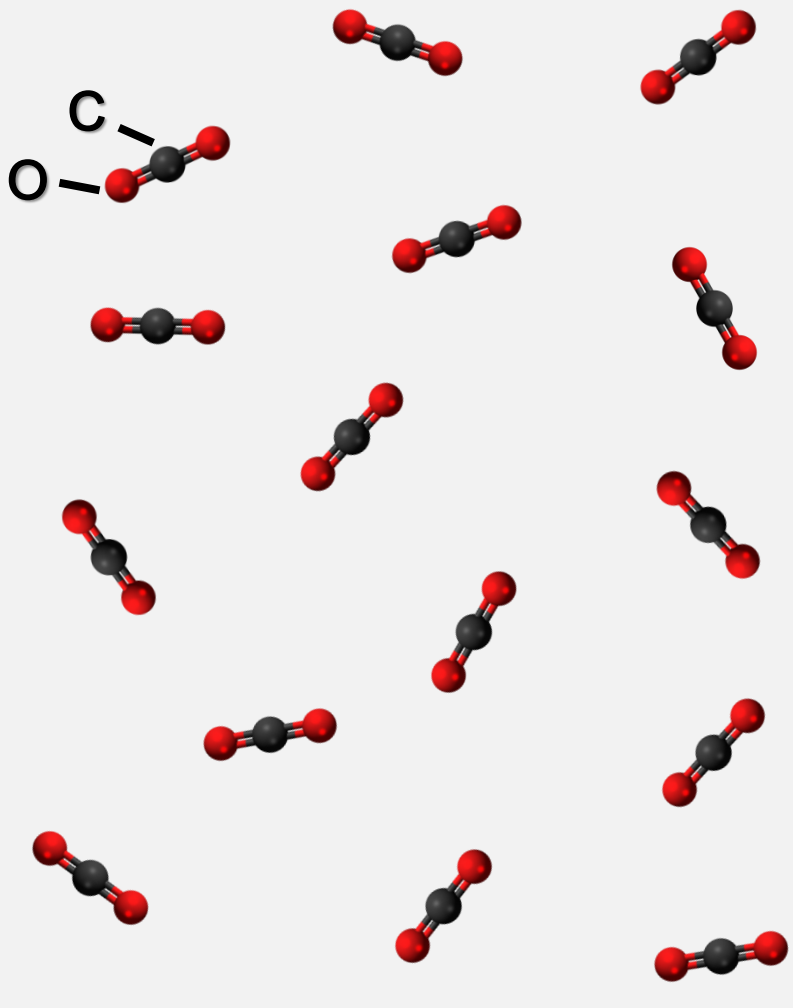

CO_2

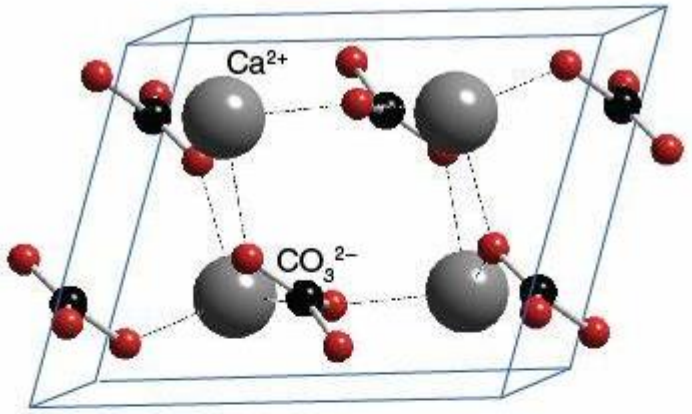

Calcite

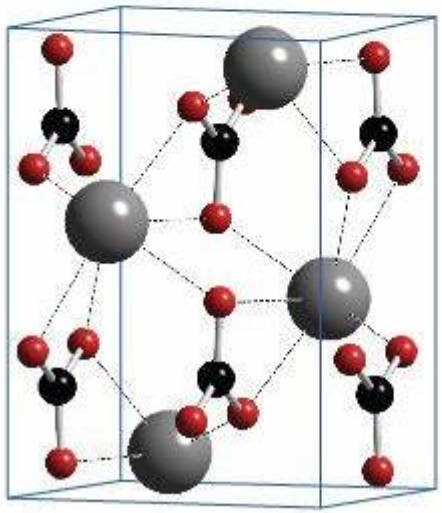

Aragonite

^{13}C-^{18}O clumping

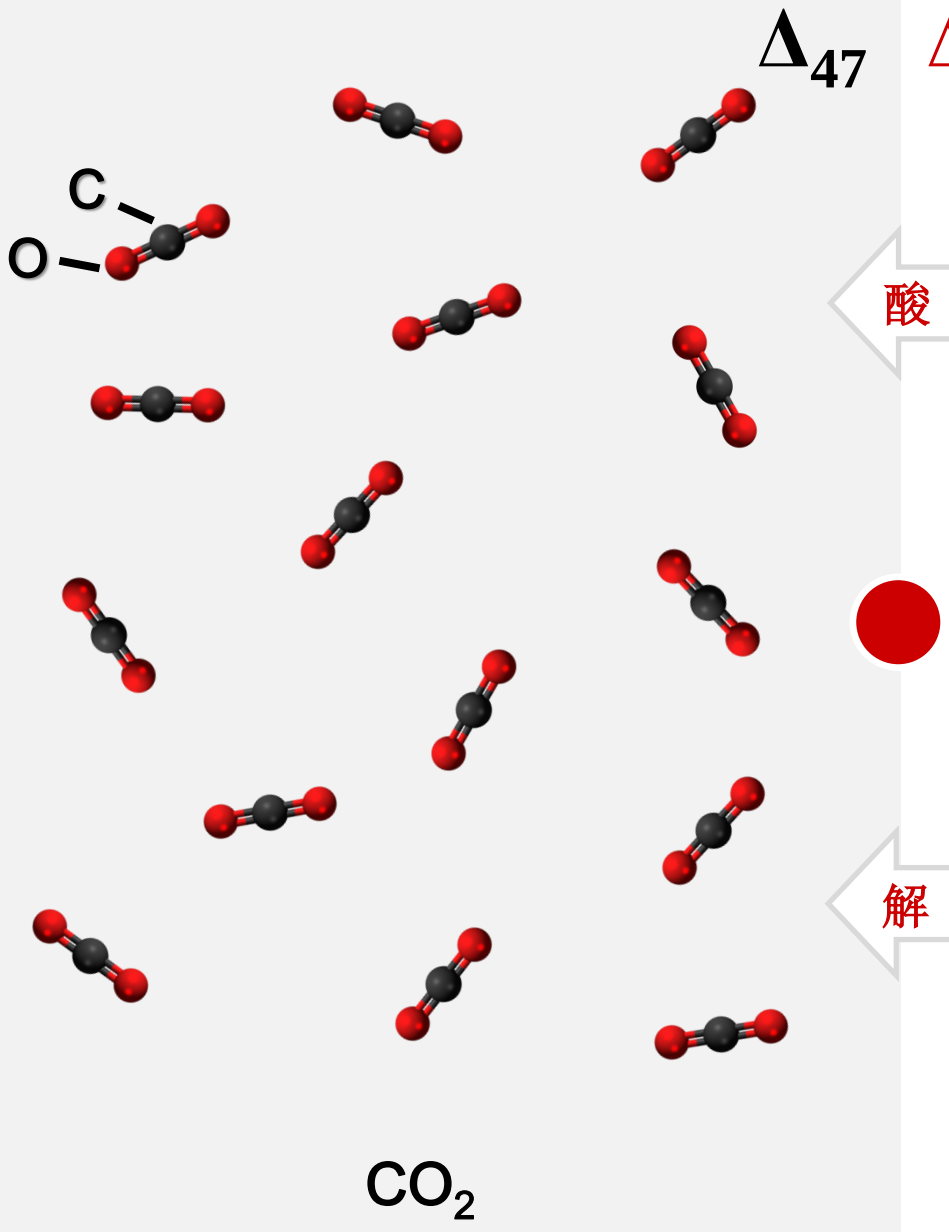

Δ_{63}

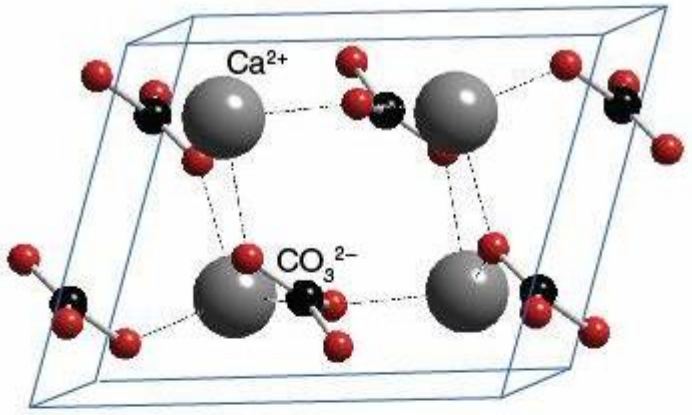

Calcite

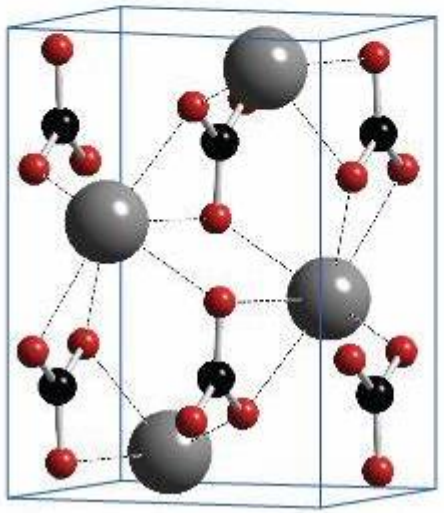

Aragonite

温度曲线

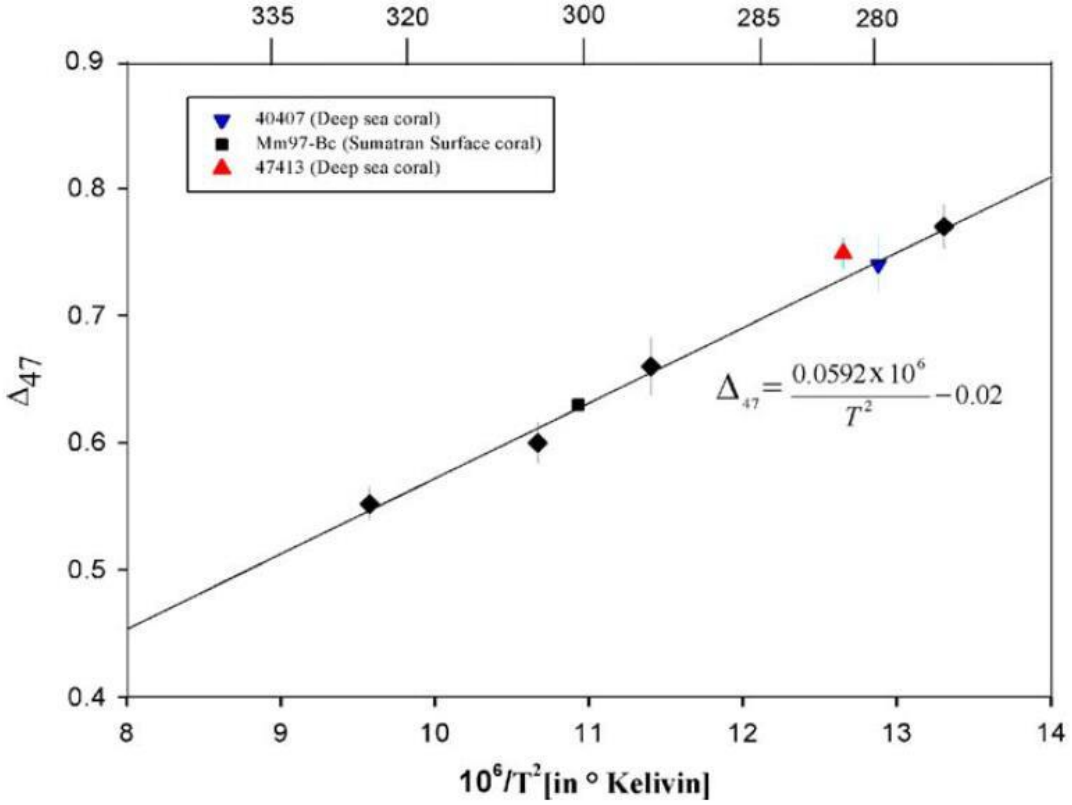

Fig. 5. Values of Δ_{47} of CO_2 extracted from calcites grown from aqueous solution (reproduced from Fig. 4) and of deep-sea and surface corals, plotted vs. $10^6/T^2$, where T is the known growth temperature in Kelvin. Note that both surface and deep-sea aragonitic corals generally conform to the trend defined by inorganic calcites. Deep-sea coral 47413 lies slightly (0.02‰) above this trend, perhaps suggesting a subtle 'vital effect' (this aliquot of this sample exhibits extreme vital effects on its $\delta^{13}C$ and $\delta^{18}O$ values; Table 5).

单相测温：

收集生长温度不同，处于同位素平衡的深海珊瑚和浅海珊瑚；

获取珊瑚碳酸盐经磷酸酸解后的CO_2，并分析其Δ_{47}值；

建立Δ_{47}与形成温度的关系，不需要与碳酸盐平衡的水的同位素信息。

(Ghosh et al., GCA, 2006)

古海洋温度

nature Vol 449|13 September 2007|doi:10.1038/nature06085

LETTERS

Coupling of surface temperatures and atmospheric CO_2 concentrations during the Palaeozoic era

Rosemarie E. Came[1], John M. Eiler[1], Ján Veizer[2], Karem Azmy[3], Uwe Brand[4] & Christopher R. Weidman[5]

大气CO_2浓度记录显示：
543-248百万年前的古生代大部分时间，大气CO_2浓度是现今水平的数倍；
但在石炭纪，二氧化碳浓度下降到类似现今的水平；
由于CO_2的温室效应，古生代早期的地表温度被认为比现今高很多；

碳酸盐岩化石的$\delta^{18}O$记录重建的热带海洋表面温度显示：
当时的温度变化幅度很小，即全球气候可能独立于大气CO_2浓度的变化。

(Came et al., Nature, 2007)

古海洋温度

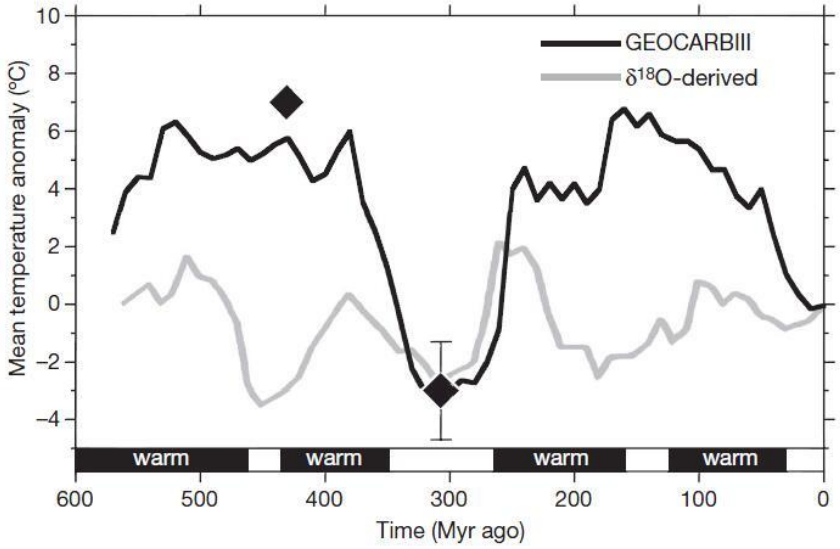

Figure 2 | Estimates of tropical temperature anomalies relative to today. The grey[4] curve represents temperature estimates based on $\delta^{18}O$ of well-preserved carbonate fossils from palaeotropical seas; the black[2] curve represents GEOCARBIII model estimates of mean global temperatures based on reconstructions of atmospheric CO_2 levels; black bars (www.scotese.com/climate.htm) at the bottom represent time intervals during which global temperatures were as much as 10 °C warmer than today based on the climate reconstruction of Scotese; filled diamonds represent our estimates of carbonate fossil growth temperatures. Error bars represent ±1 s.e. on the Δ_{47} temperatures of well-preserved samples.

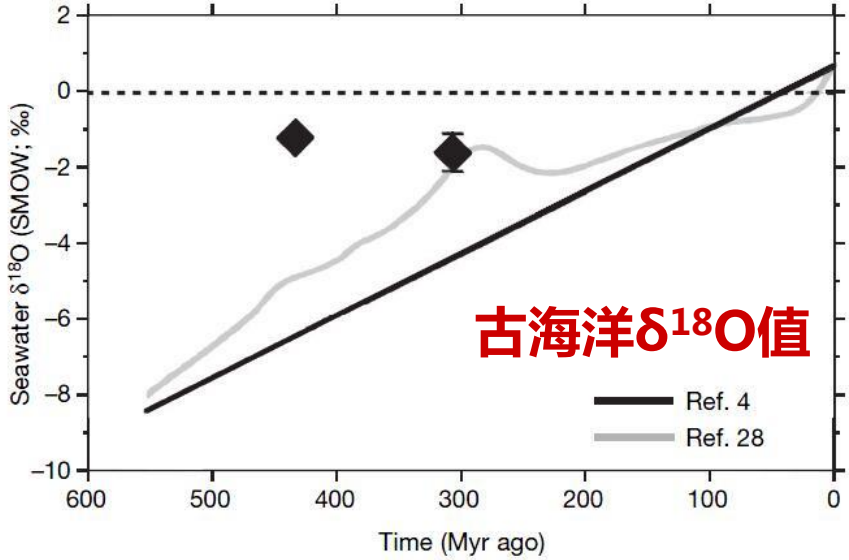

Figure 3 | Estimates of the oxygen isotopic composition of Phanerozoic sea water. The black[4] and grey[28] curves represent previous model estimates; the dashed line represents modern seawater $\delta^{18}O$ (SMOW); filled diamonds represent new estimates of Pennsylvanian and Silurian seawater $\delta^{18}O$ calculated from carbonate $\delta^{18}O$ and Δ_{47} temperatures. Error bars represent ±1 s.e. on the seawater $\delta^{18}O$ of well-preserved samples.

$$\Delta_{47} = 0.0592(10^6 T^{-2}) - 0.02$$

利用腕足类化石和软体动物贝壳的碳酸盐Δ_{47}值，重建了地质历史的海面温度。结果显示：志留纪早期(443-423百万年前）的热带海面温度明显高于现今水平（~10°C）；二氧化碳浓度与现今相近的石炭纪末期(314-300百万年前)，海面温度与现今类似；说明大气CO_2浓度的增加会推动全球气温的升高。

（Came et al., Nature, 2007）

知识点：

1）随机分布是高温极限下的分布状态，只受概率控制；

2）同位素平衡分馏参数，是温度（T）的函数；

3）碳酸盐Δ_{47}平衡信号可单相测温，结合碳酸盐$\delta^{18}O$值，可获得与之平衡的水体$\delta^{18}O$值。

高原隆升

Rapid Uplift of the Altiplano Revealed Through ^{13}C-^{18}O Bonds in Paleosol Carbonates

Prosenjit Ghosh,[1] Carmala N. Garzione,[2] John M. Eiler[1]

地表海拔信息是最难从地质记录中重建的环境变量之一：
1）确定大气压或大气厚度理论上最为可靠，但在样品可用性和解释方面存在困难，因此几乎没有什么用处；
2）利用同位素数据虽然最为实用，但难以估算气候变化或降水季节性变化的影响；
3）约束大气焓或温度的古植物学方法，依赖对植物外貌的经验判断，当应用于古代植物群落时，存在不确定性。

土壤碳酸盐：采用Altiplano中心地区的一套古土壤、砂岩、泥岩序列中，先进海拔~3800-3900米。

Table 1. Stable isotope compositions, growth temperatures, and parental water $\delta^{18}O$ values for Altiplano soil carbonates.

Sample	Age (Ma) (*15*)*	$\delta^{13}C_{PDB}$ of carbonate (*14*)	$\delta^{18}O_{PDB}$ of carbonate (*14*)	Δ_{47} of extracted CO_2 (*14*)	Temperature (°C) (*13*)	$\delta^{18}O_{SMOW}$ of water (*20*)
03BL13	11.42	−9.4	−11.4	0.612 (19)	32.8 (4.6)	−7.5 (0.9)
03BL19	11.32	−6.8	−11.1	0.651 (21)	23.8 (4.6)	−9.0 (0.9)
04BL75	10.88	−9.3	−9.8	0.634 (14)	27.7 (3.2)	−6.9 (0.6)
04BL76	10.74	−8.3	−11.7	0.632 (13)	28.2 (3.0)	−8.7 (0.6)
04BL78	10.58	−9.4	−13.0	0.644 (21)	25.6 (4.7)	−10.5 (0.9)
04BL79	10.53	−8.6	−12.3	0.630 (12)	28.6 (2.8)	−9.0 (0.5)
04BL80	10.46	−10.1	−11.6	0.620 (5)	31.0 (1.2)	−8.2 (0.2)
03BL1	10.33	−8.2	−12.5	0.628 (6)	29.2 (1.4)	−9.3 (0.3)
				11.4 to 10.3 Ma average	**28.4 (0.9)**	**−8.6 (0.4)**
04BL2	7.61	−4.6	−13.9	0.695 (9)	14.6 (1.8)	−13.7 (0.4)
04BL10	7.32	−5.9	−11.5	0.665 (10)	20.8 (2.1)	−10.0 (0.4)
				7.6 to 7.3 Ma average	**17.7 (2.2)**	**−11.8 (1.3)**
04BL21	6.74	−7.7	−14.7	0.681 (4)	17.5 (0.8)	−13.9 (0.2)
04BL24	6.64	−6.7	−13.5	0.713 (12)	11.0 (2.3)	−14.1 (0.5)
04BL25	6.53	−7.0	−14.6	0.750 (8)	4.1 (1.4)	−16.7 (0.3)
04BL30	5.83	−6.5	−14.6	0.679 (13)	18.0 (2.7)	−13.7 (0.6)
				6.7 to 5.8 Ma average	**12.6 (2.8)**	**−14.6 (0.6)**
			Suspected of diagenetic alteration			
04BL69	10.95	−9.9	−8.2	0.546 (17)	50.3 (4.9)	−1.1 (0.8)

*Italic numbers in parentheses at the head of each column refer to references explaining the sources, methods, or algorithms on which the data are based. Analytical uncertainties in $\delta^{13}C$ and $\delta^{18}O$ of carbonate average ±0.02 and ±0.1‰, respectively, and are not shown. Analytical uncertainties in Δ_{47} (numbers in parentheses) are shown for each measurement as the standard error of the mean of all mass spectrometric analyses for a given sample. These are propagated to estimate uncertainties in temperature and $\delta^{18}O$ of water.

抬升速率

利用Δ_{47}温度：
0.94±0.17 mm/year

利用水$\delta^{18}O$组成：
0.83±0.08 mm/year

然而，受环境因素影响（中新世与现今的维度、气候差别，以及蒸发作用等），该抬升速率存在误差。

经过校正：玻利维亚安第斯山脉的Altiplano高原在10.3-6.7百万年前以平均每年1.03±0.12毫米的速度抬升。

（Ghosh et al., Science, 2006）

动物体温

Body temperatures of modern and extinct vertebrates from ^{13}C-^{18}O bond abundances in bioapatite

Robert A. Eagle[a,1], Edwin A. Schauble[b], Aradhna K. Tripati[a,b,c], Thomas Tütken[d], Richard C. Hulbert[e], and John M. Eiler[a]

Table 1. Δ_{47} measurements from tooth bioapatite of modern species

Species	n *	Δ_{47}	Estimated Body Temperature (°C) †	Δ_{47} Temperature (°C) ‡
White Rhinoceros (*Ceratotherium simum*)	6	0.597 ± 0.006	37	36.6 ± 1.4
Indian Elephant (*Elephas maximus indicus*)	4	0.596 ± 0.008	37	36.9 ± 2.0
Nile Crocodile (*Crocodylus niloticus*)	7	0.638 ± 0.006	28 ± 3	26.9 ± 1.4
American Alligator (*Alligator mississippiensis*)	3	0.639 ± 0.011	28 ± 3	26.7 ± 2.5
Sand Tiger Shark (*Carcharias taurus*)	5	0.641 ± 0.013	25.3	26.2 ± 3.0
Sand Tiger Shark (*Carcharias taurus*)	3	0.654 ± 0.010	23.6	23.1 ± 2.3

± Uncertainty in Δ_{47} values represent the external precision of the measurement (one standard error). Uncertainty in Δ_{47} body temperature values represent the error in body temperatures in °C propagated from the external precision of the Δ_{47} measurement (one standard error).
*Number of distinct extractions of CO_2 from bioapatite analyzed for each species. Between 1–5 teeth for each species were analyzed. Data for individual extractions is shown in Table S1.
†Estimated from published body temperature measurements (see main text for details). In the case of sand tiger sharks the two samples were from two different aquariums with different ambient water temperatures.
‡Calculated assuming Δ_{47} values in bioapatite exhibit the same temperature dependency as inorganic calcite, given in Eq. **1**.

Table 2. Δ_{47} measurements from fossil mammoth tooth bioapatite

Sample	Locality	n *	Δ_{47}	Δ_{47} Temperature (°C)
Enamel	Rhine River	4	0.587 ± 0.011	39.1 ± 2.8
Dentin	Rhine River	3	0.643 ± 0.027	25.6 ± 6.3
Enamel	North Sea	2	0.596 ± 0.006	36.8 ± 1.3
Dentin	North Sea	2	0.620 ± 0.001	30.9 ± 0.3
Enamel	Average from both sites	6	0.590 ± 0.007	38.4 ± 1.8

± Uncertainty in Δ_{47} values represent the external precision of the measurement (one standard error if more than two analyses were made; if fewer were made, then the standard deviation is shown). Uncertainty in Δ_{47} body temperature values represent the error in body temperatures in °C propagated from the external precision of the Δ_{47} measurement (one standard error).
*Number of distinct extractions of CO_2 made from bioapatite of each species. Data for individual extractions is shown in Table S2.

(Eagle et al., PNAS, 2006)

恐龙体温

Dinosaur Body Temperatures Determined from Isotopic (^{13}C-^{18}O) Ordering in Fossil Biominerals

Robert A. Eagle,[1,2]* Thomas Tütken,[3] Taylor S. Martin,[1] Aradhna K. Tripati,[2,4] Henry C. Fricke,[5] Melissa Connely,[6] Richard L. Cifelli,[7] John M. Eiler[1]

Table 1. Δ_{47} derived body temperature determinations on well-preserved dinosaur tooth enamel. Number of analyses represent the total number of Δ_{47} measurements made on distinct extractions of CO_2 gas from tooth enamel material from each locality. Values for individual measurements and averages for each individual tooth specimen are given in tables S4 to S9. When average Δ_{47} values are calculated for each species, they are from the average of each tooth specimen and not of each individual analysis on distinct CO_2 extractions. Errors are ±1 SE of the average Δ_{47} and the propagated error in temperature calculations.

Species	Site	Number of analyses*	Δ_{47} [per mil (‰)]	Δ_{47} temperature (°C)
Brachiosaurus brancai, acquisitions from 3 teeth	Tendaguru, Tanzania	5	0.591 ± 0.004	38.2 ± 1.0
Diplodocinae, acquisitions from 2 teeth	Tendaguru, Tanzania	3	0.609 ± 0.017	33.6 ± 4.0
Camarasaurus sp., acquisitions from 3 teeth*	Oklahoma	7	0.596 ± 0.004	36.9 ± 1.0
Camarasaurus sp., acquisitions from 1 tooth†	Howe Quarry, Wyoming	3	0.614 ± 0.010	32.4 ± 2.4
Camarasaurus sp., average acquisitions from 4 teeth‡	Wyoming and Oklahoma	10	0.601 ± 0.005	35.7 ± 1.3

*One of the four specimens from Oklahoma was suspected of alteration and so was excluded from the final body temperature determinations presented here and in Fig. 1. †One of the two tooth specimens from Howe Quarry was suspected of alteration and so was excluded from the final body temperature determinations presented here and in Fig. 1. ‡All of the specimens from the Utah Quarries and Como Bluffs, Wyoming, were suspected of alteration and so were excluded from the final body temperature determinations presented here and in Fig. 1.

恐龙体温：

侏罗纪大型蜥脚类恐龙与大多数现代哺乳动物的体温相似；
该温度范围比模型预测低4-7°C摄氏度，显示恐龙体温随体重的变化而变化；
可能表明蜥脚类动物有防止体温过高的机制。

(Eagle et al., Science, 2011)

测温前提

精确测温需要满足3个条件：

1）碳酸盐岩达到同位素平衡；

动力学过程、生物效应？

2）后期不发生^{13}C-^{18}O成键改变；

成岩过程、变质作用？

3）Clumped同位素与温度的关系精准。

酸解过程？

Clumped同位素的分馏理论

动力学分馏

化学反应动力学

$$A + B \xrightarrow{k} C + D$$

基元反应，k：速率常数

$$\frac{d[C]}{dt} = \frac{d[D]}{dt} = -\frac{d[A]}{dt} = -\frac{d[B]}{dt} = k[A][B]$$

同位素：

具有相同的电子排布，因此具有相同的化学性质；
具有不同的原子核质量，因此反应常数不同；
通常，质量越轻，反应越快。
反应初期，产物富集轻同位素，反应物富集重同位素；
随着反应进行，产物同位素比值逐步变重。

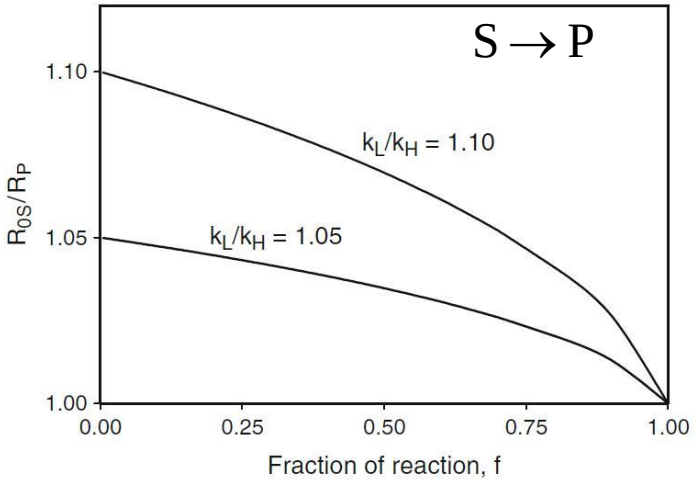

Fig. 7.4 Time dependence of isotopic ratios in product during single label competitive KIE studies

R_{0S}：反应物初始同位素比值

R_P：产生同位素比值

k_L：轻同位素速率常数

k_H：重同位素速率常数

同位素不平衡

动力学分馏会导致同位素不平衡：

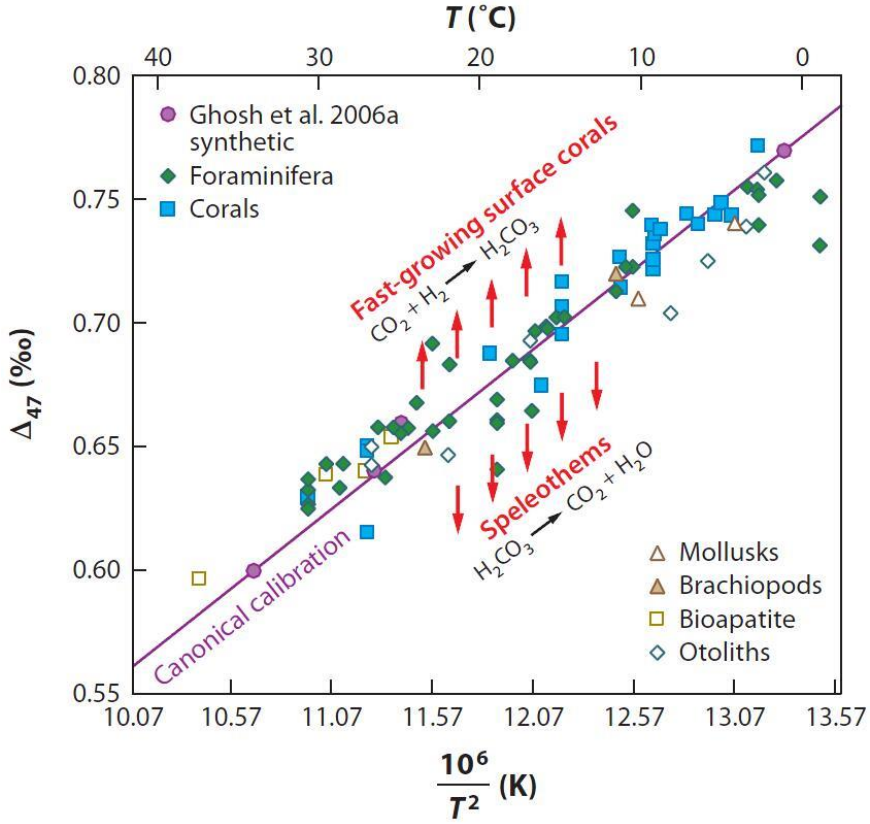

(Eiler, Annu. Rev., 2013)

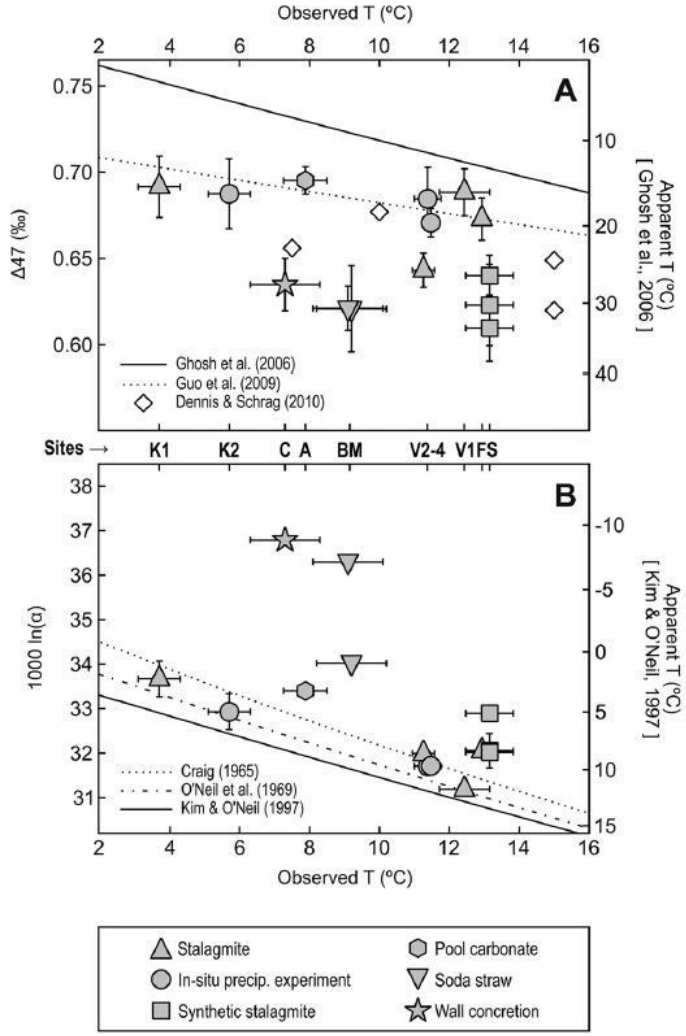

(Daëron et al., GCA, 2011)

石笋的同位素不平衡：

溶液快速去气过程，具有比平衡值更高的$\delta^{18}O$，更低的Δ_{47}值。

浅海珊瑚的同位素不平衡：

快速生长（CO_2水合过程），具有比平衡值低的$\delta^{18}O$，高的Δ_{47}值。

同位素不平衡

动力学分馏会导致同位素不平衡：

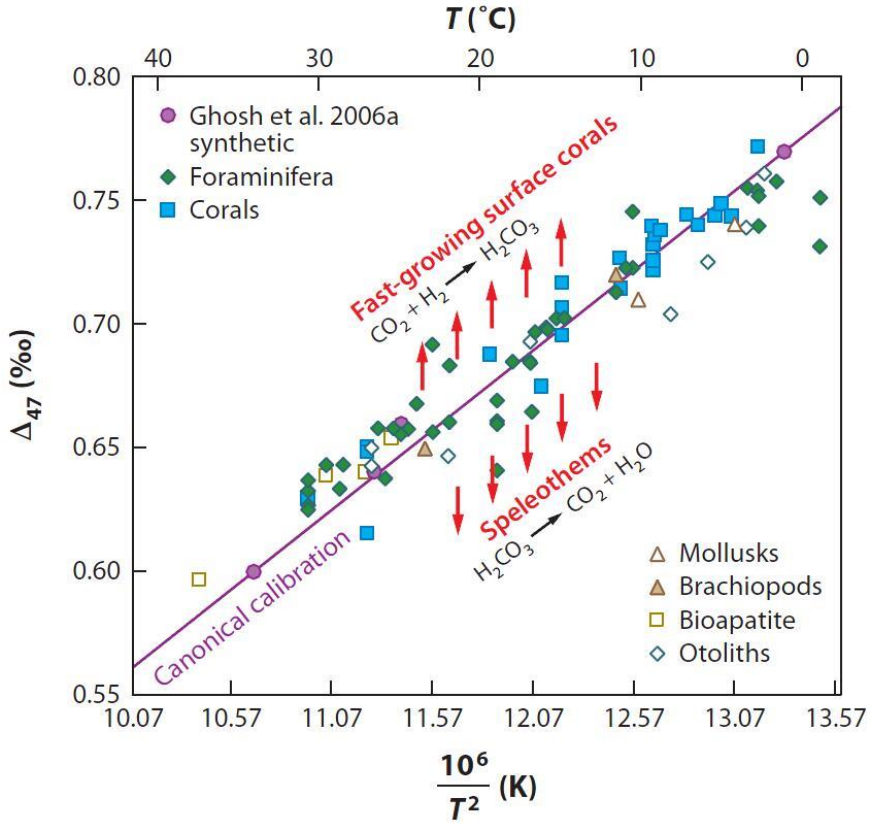

(Eiler, Annu. Rev., 2013)

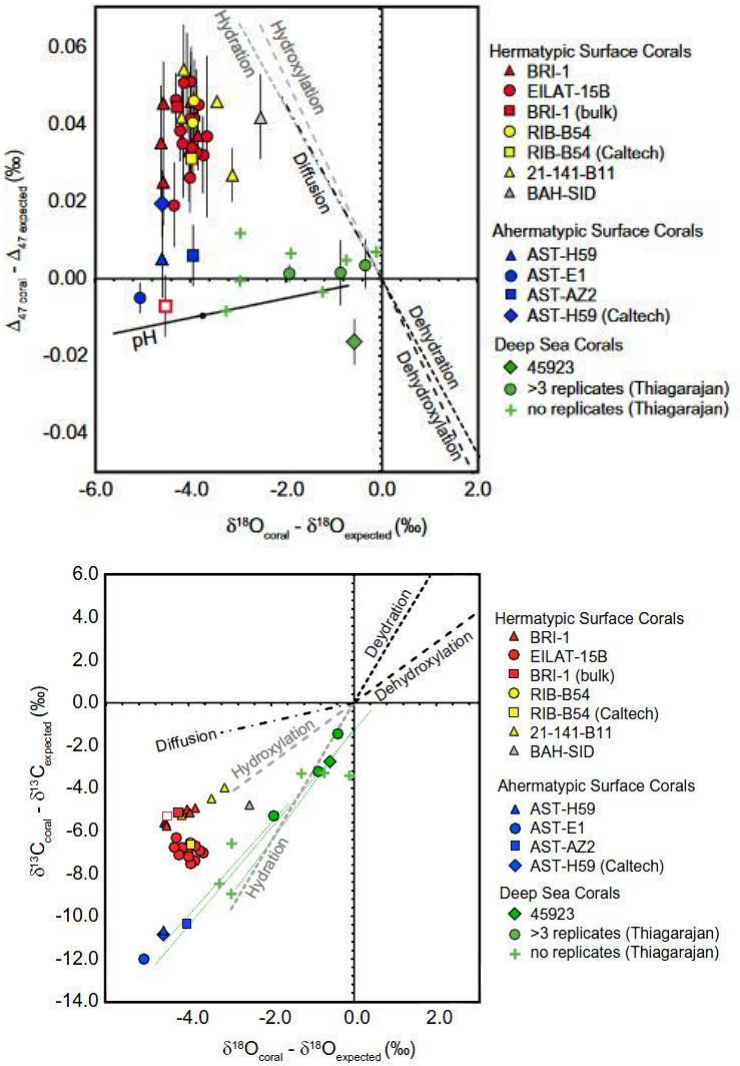

(Seanger et al., GCA, 2012)

石笋的同位素不平衡：

溶液快速去气过程，具有比平衡值更高的$\delta^{18}O$，更低的Δ_{47}值。

浅海珊瑚的同位素不平衡：

快速生长（CO_2水合过程），具有比平衡值低的$\delta^{18}O$，高的Δ_{47}值。

同位素不平衡

Available online at www.sciencedirect.com

ScienceDirect

Geochimica et Cosmochimica Acta 267 (2019) 196–226

Geochimica et Cosmochimica Acta

www.elsevier.com/locate/gca

Patterns and controls of disequilibrium isotope effects in speleothems: Insights from an isotope-enabled diffusion-reaction model and implications for quantitative thermometry

Weifu Guo [a,*], Chen Zhou [a,b]

[a] *Department of Geology and Geophysics, Woods Hole Oceanographic Institution, Woods Hole, MA 02543, United States*
[b] *School of Earth and Space Sciences, University of Science and Technology of China, Hefei, Anhui 230026, China*

Received 9 January 2019; accepted in revised form 14 July 2019; available online 29 July 2019

(Guo & Zhou, GCA, 2019)

同位素不平衡

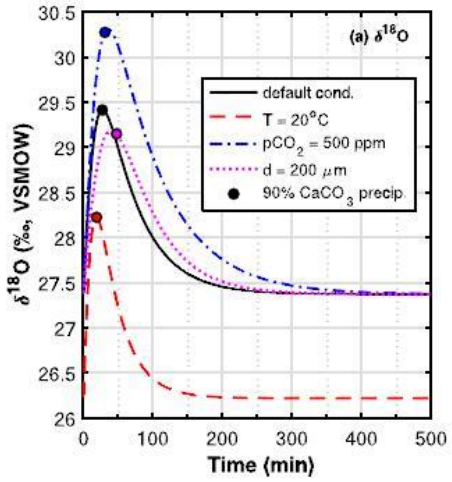

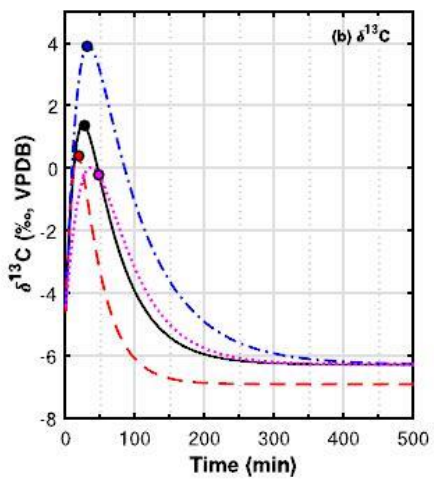

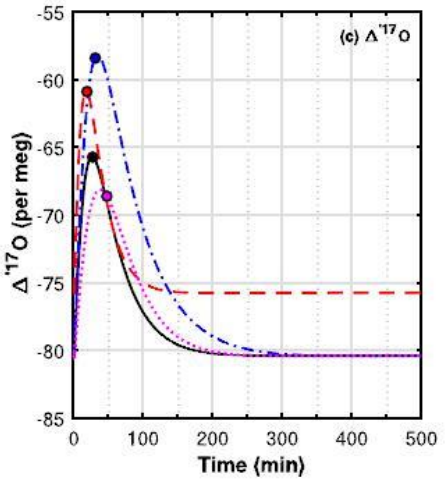

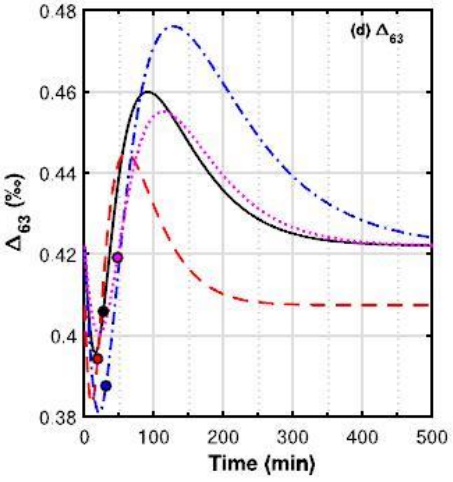

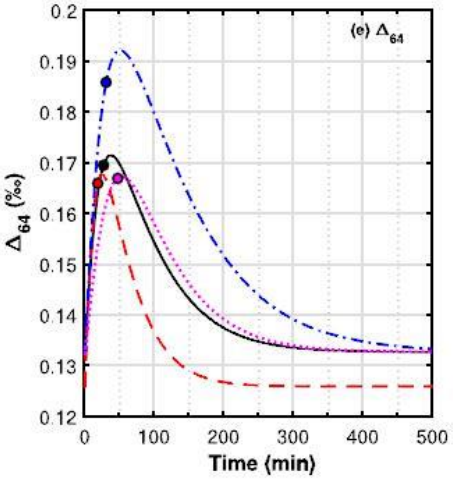

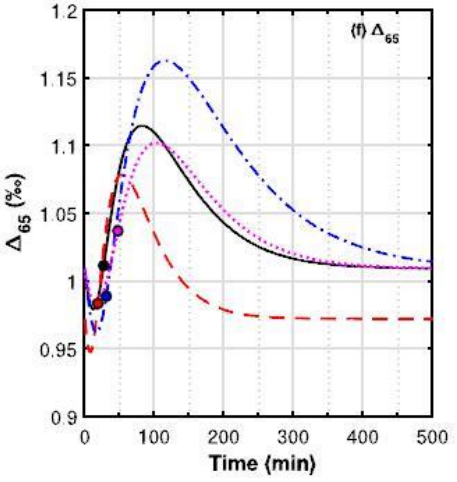

碳酸盐^{13}C-^{18}O clumped信号

(Guo & Zhou, GCA, 2019)

同位素不平衡

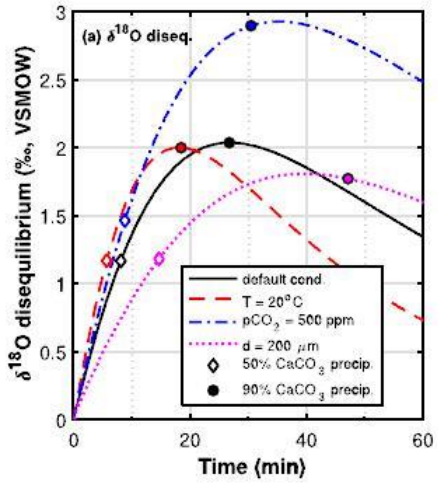

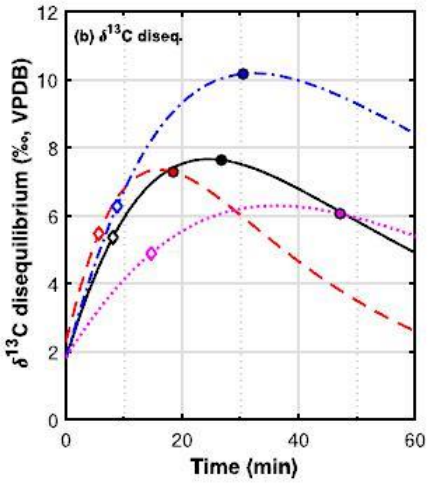

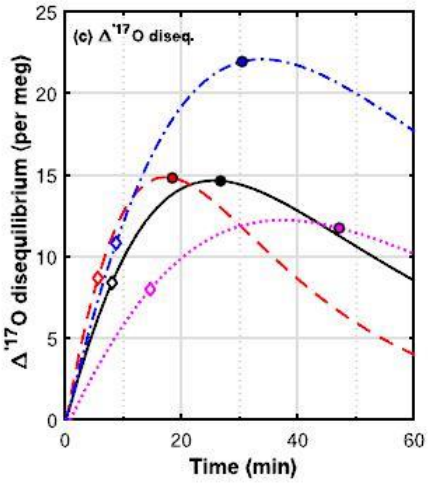

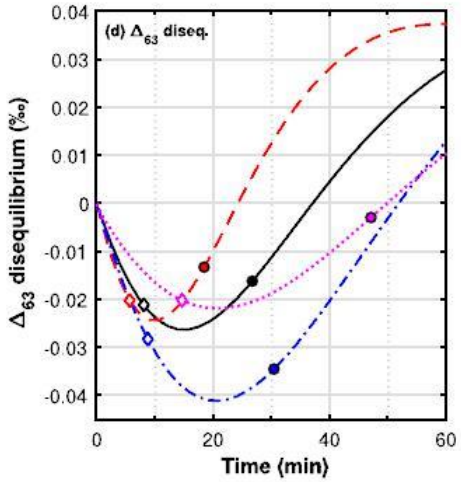

碳酸盐^{13}C-^{18}O clumped信号

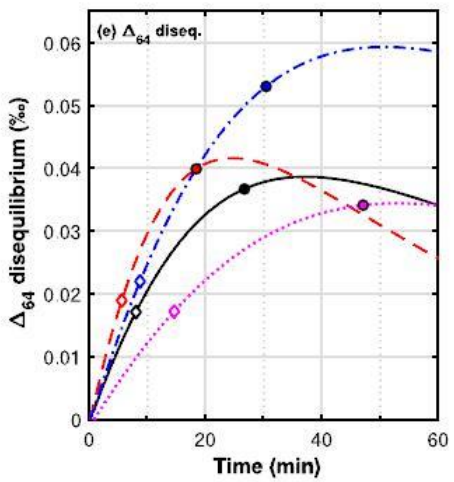

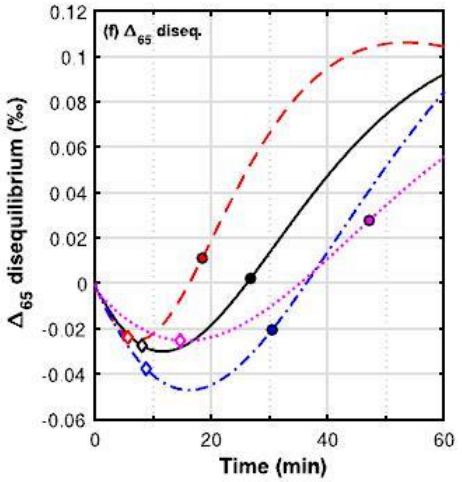

(Guo & Zhou, GCA, 2019)

知识点：

1）随机分布是高温极限下的分布状态，只受概率控制；

2）同位素平衡分馏参数，是温度（T）的函数；

3）碳酸盐Δ_{47}平衡信号可单相测温，结合碳酸盐$\delta^{18}O$值，可获得与之平衡的水体$\delta^{18}O$值。

4）动力学分馏一般造成产物富集轻同位素，clumped同位素信号稍显复杂；

^{13}C-^{18}O重组

Earth and Planetary Science Letters 351–352 (2012) 223–236

Contents lists available at SciVerse ScienceDirect

Earth and Planetary Science Letters

journal homepage: www.elsevier.com/locate/epsl

Carbonate clumped isotope bond reordering and geospeedometry

Benjamin H. Passey*, Gregory A. Henkes

Department of Earth and Planetary Sciences, Johns Hopkins University, 3400 N Charles Street, Baltimore, MD 21218, USA

封闭温度：~150-250°C

慢速冷却的碳酸盐岩比快速冷却的具有更低的Δ_{47}封闭温度。

两个问题：

1）300°C的热液中沉淀的方解石Δ_{47}值会显示300°C的结晶温度，还是比这低的封闭温度？

2）这个Δ_{47}值有没有可能记录冷却速率？

封闭温度和冷却速率存在一一对应的关系。

（Passey & Henkes, EPSL, 2012）

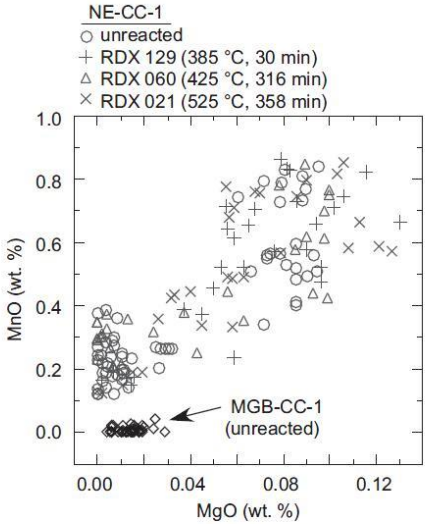

Fig. 1. MnO and MgO contents of the studied calcites based on electron microprobe analysis. Each point reflects an individual microprobe spot analysis, with the analyses performed on many individual grains from the 60–120 mesh size fraction of each material.

^{13}C-^{18}O重组

$$\ln\left[\frac{\Delta_{47}^{t}-\Delta_{47}^{eq}}{\Delta_{47}^{init}-\Delta_{47}^{eq}}\right]=\ln\left[1-\frac{\Delta_{47}^{init}-\Delta_{47}^{t}}{\Delta_{47}^{init}-\Delta_{47}^{eq}}\right]=\ln[1-F]=-kt$$

$$k=K_0\exp(-E_a/kT)$$

$\delta^{13}C$和$\delta^{18}O$无变化；
反映一阶动力学效应；

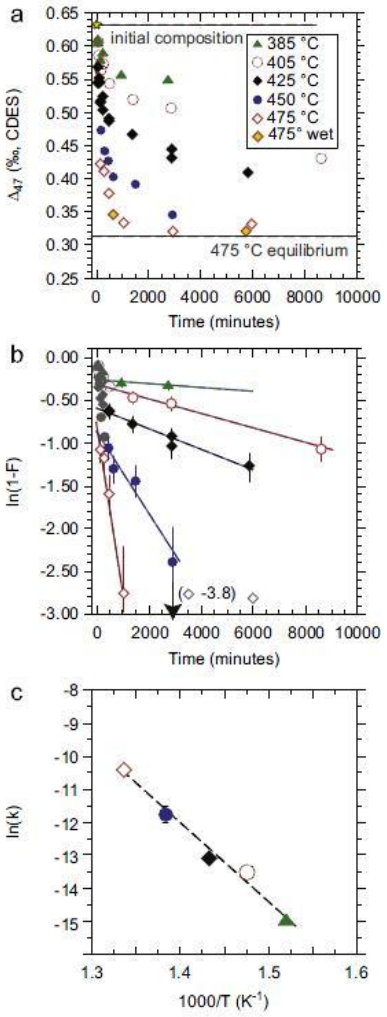

Table 2
Rate constant regressions and Arrhenius parameters for reordering reactions in MGB-CC-1 and NE-CC-1 calcite.

T (°C)	Slope (= −k) (s⁻¹)	Intercept	Fractional contribution	R^2	Stats	RDX points used in regression*
MGB-CC-1 calcite						
385	−3.18 (±0.42) × 10⁻⁷	−0.27 (±0.03)	–	na	na	181, 189
405	−1.39 (±0.15) × 10⁻⁶	−0.32 (±0.04)	–	0.99	a,b,c	169, 173, 177
425	−2.01 (±0.15) × 10⁻⁶	−0.59 (±0.02)	–	0.97	d,e,f	149, 150, 151, 153
450	−7.95 (±1.72) × 10⁻⁶	−0.88 (±0.12)	–	0.91	d,e,f	144, 145, 147, 148
475	−2.98 (±0.37) × 10⁻⁵	−0.79 (±0.08)	–	0.97	d,e,f	112, 113, 114, 115
Arrhenius regression: E_a=197 ±19 kJ/mol K_0=1.39 × 10⁹ s⁻¹ [(+36.0/−1.34) × 10⁹]				0.97	d,e,f	
NE-CC-1 calcite, refractory component						
560	−1.29 (±0.05) × 10⁻⁵	−1.60(±0.02)	0.20 (±0.008)	0.99	d,e,f	034, 037, 036
525	−3.66 (±0.25) × 10⁻⁶	−1.47(±0.03)	0.23 (±0.014)	0.99	d,e,f	021, 010, 017, 018, 015
475	−4.48 (±0.40) · 10⁻⁷	−1.06(±0.05)	0.35 (±0.036)	0.98	d,e,f	025, 016, 042, 046
			0.26 mean			
Arrhenius regression: E_a=200 ±2 kJ/mol K_0=4.4 × 10⁷ s⁻¹ [(+1.4/−1.0) × 10⁷]				0.99	复制 d,e,f	
NE-CC-1 calcite, labile component						
525	−1.27 (±0.13) × 10⁻⁴	−1.14(±0.06)	0.32 (±0.041)	–	na	026, 019
475	−1.63 (±0.19) × 10⁻⁵	−0.74(±0.04)	0.48 (±0.038)	0.95	d,e,f	125, 123, 130, 022, 023, 027, 024
425	−1.37 (±0.19) × 10⁻⁶	-0.76(±0.04)	0.47 (±0.042)	0.93	d,e,f	065, 060, 064, 061, 063, 062
			0.42 mean			
Arrhenius regression: E_a=208 ±4 kJ/mol K_0=5.6 × 10⁹ s⁻¹ [(+4.9/−2.6) × 10⁹]				0.99	d,e,f	

不同方解石具有不同重组特质

冷却速率： $dT/dt=\dfrac{\gamma R T_{ae}^2 k_{Tae}}{E_a}$

T_{ae}：Δ_{47}值反映的封闭温度
k_{Tae}：T_{ae}温度下的速率常数
Ea：常数，通过实验获得
γ：常数，此处等于2
R：理想气体常数

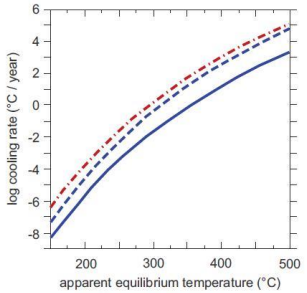

Fig. 7. Relationship between cooling rate and apparent equilibrium temperature for the three different sets of Arrhenius parameters derived in this study. Red dot-dashed line: MGB-CC-1 (optical calcite). Blue dashed line: NE-CC-1 labile component. Blue solid line: NE-CC-1 refractory component. (For interpretation of the references to color in this figure legend, the reader is referred to the web version of this article.)

成岩作用可以导致^{13}C-^{18}O重组，而最后记录的温度信号受冷却速率控制。

(Passey & Henkes, EPSL, 2012)

^{13}C-^{18}O重组

Available online at www.sciencedirect.com
ScienceDirect
Geochimica et Cosmochimica Acta 242 (2018) 1–20
Geochimica et Cosmochimica Acta
www.elsevier.com/locate/gca

Experimental calibration of clumped isotope reordering in dolomite

Max K. Lloyd*, Uri Ryb, John M. Eiler

Division of Geological and Planetary Sciences, California Institute of Technology, Pasadena, CA 91125, USA

Received 7 February 2018; accepted in revised form 23 August 2018; available online 1 September 2018

白云石可以在长时间的地质历史中，记录不高于150°C的温度记录。

Available online at www.sciencedirect.com
ScienceDirect
Geochimica et Cosmochimica Acta 258 (2019) 156–173
Geochimica et Cosmochimica Acta
www.elsevier.com/locate/gca

Mechanism of solid-state clumped isotope reordering in carbonate minerals from aragonite heating experiments

Sang Chen[a,*], Uri Ryb[b,a], Alison M. Piasecki[a,c], Max K. Lloyd[a,d]
Michael B. Baker[a], John M. Eiler[a]

[a] *Division of Geological and Planetary Sciences, California Institute of Technology, Pasadena, CA 91125, United States*
[b] *Fredy and Nadine Herrmann Institute of Earth Sciences, The Hebrew University of Jerusalem, Jerusalem 9190401, Israel*
[c] *Department of Earth Science, University of Bergen, Bergen, Norway*
[d] *Department of Earth and Planetary Science, University of California, Berkeley, CA 94720, United States*

Received 16 October 2018; accepted in revised form 13 May 2019; available online 22 May 2019

文石的Δ_{47}值随加热进行而降低，但随转变为方解石而增加0.05–0.15‰；重组能力强于方解石和白云石，容易受成岩作用影响。

知识点：

1）随机分布是高温极限下的分布状态，只受概率控制；

2）同位素平衡分馏参数，是温度（T）的函数；

3）碳酸盐Δ_{47}平衡信号可单相测温，结合碳酸盐$\delta^{18}O$值，可获得与之平衡的水体$\delta^{18}O$值。

4）动力学分馏一般造成产物富集轻同位素，clumped同位素信号稍显复杂；

5）碳酸盐无法记录Δ_{47}平衡温度时，可以记录受冷却速率控制的封闭温度；

磷酸酸解

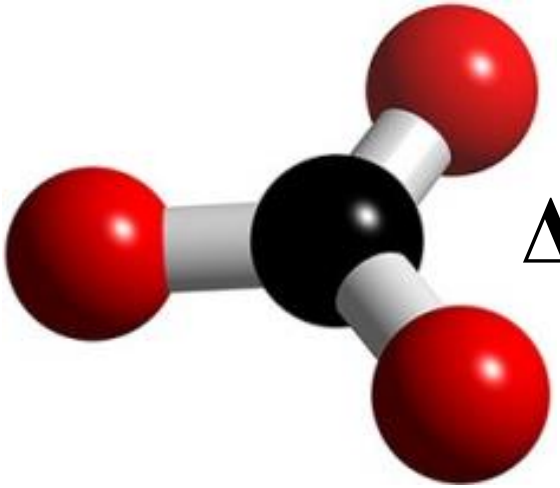

Δ_{63} $\delta^{18}O$ Δ_{47}

动力学分馏：

源自一个氧原子丢失；

影响Δ_{47}和$\delta^{18}O$的分析结果。

分析结果：

碳酸盐同位素信号

+

动力学分馏值

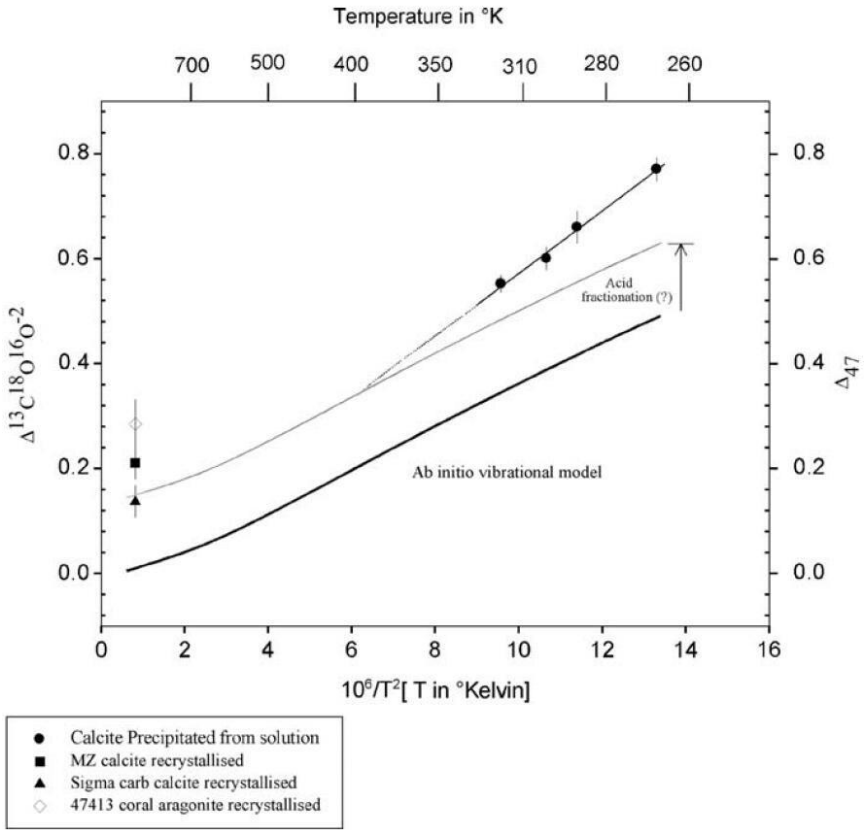

磷酸酸解

Available online at www.sciencedirect.com
ScienceDirect
Geochimica et Cosmochimica Acta 73 (2009) 7203–7225
Geochimica et Cosmochimica Acta
www.elsevier.com/locate/gca

Isotopic fractionations associated with phosphoric acid digestion of carbonate minerals: Insights from first-principles theoretical modeling and clumped isotope measurements

Weifu Guo [a,*], Jed L. Mosenfelder [a], William A. Goddard III [b], John M. Eiler [a]

[a] Division of Geological and Planetary Sciences, California Institute of Technology, Pasadena, CA 91125, USA
[b] Materials and Process Simulation Center, California Institute of Technology, Pasadena, CA 91125, USA

Received 28 July 2008; accepted in revised form 27 May 2009; available online 23 June 2009

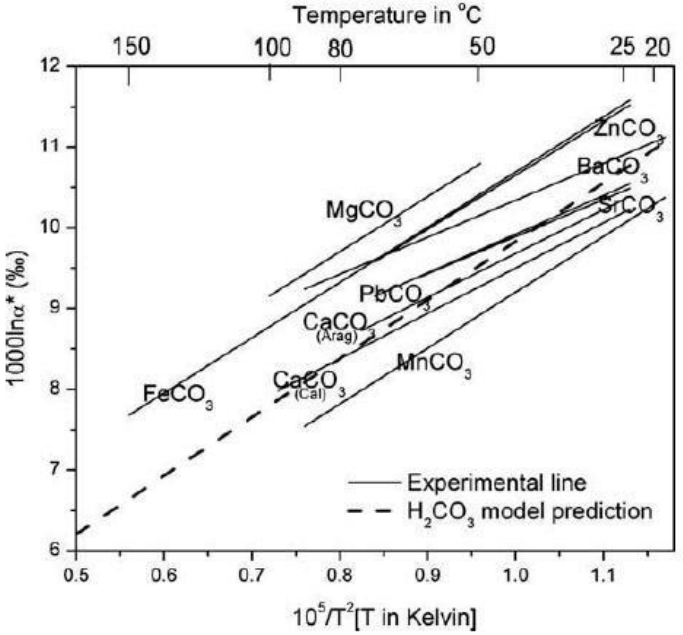

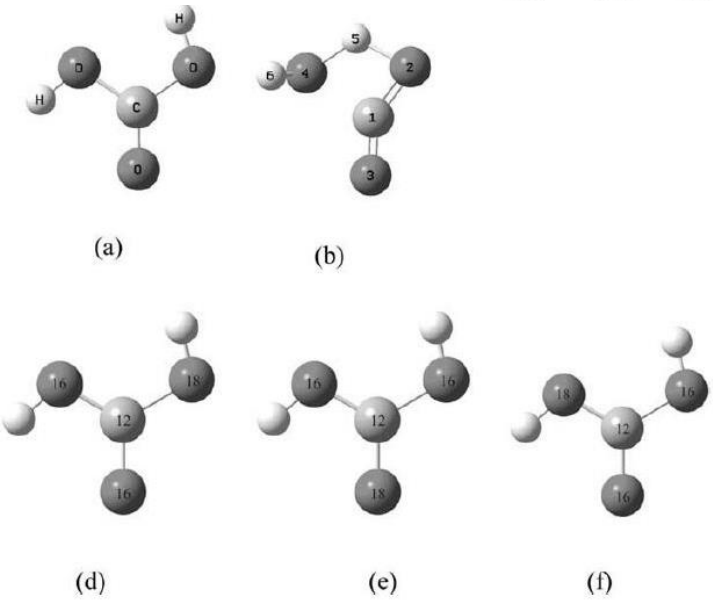

(Guo et al., GCA, 2009)

磷酸酸解

ACS EARTH AND SPACE CHEMISTRY

http://pubs.acs.org/journal/aesccq Article

Molecular-Level Mechanism of Phosphoric Acid Digestion of Carbonates and Recalibration of the $^{13}C-^{18}O$ Clumped Isotope Thermometer

Siting Zhang, Qi Liu, Mao Tang, and Yun Liu*

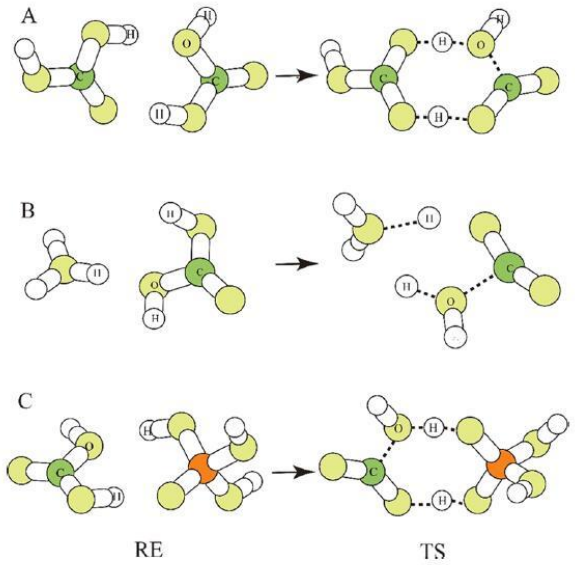

Figure 1. Optimized reactant and transition-state structures of the carbonic acid decomposition reaction. "RE" denotes the reactants, and "TS" denotes the transition-state complexes. (A) H_2CO_3-catalyzed reaction, (B) H_2O-catalyzed reaction (H_2O is as H_3O^+ under acidic conditions), and (C) H_3PO_4-catalyzed reaction.

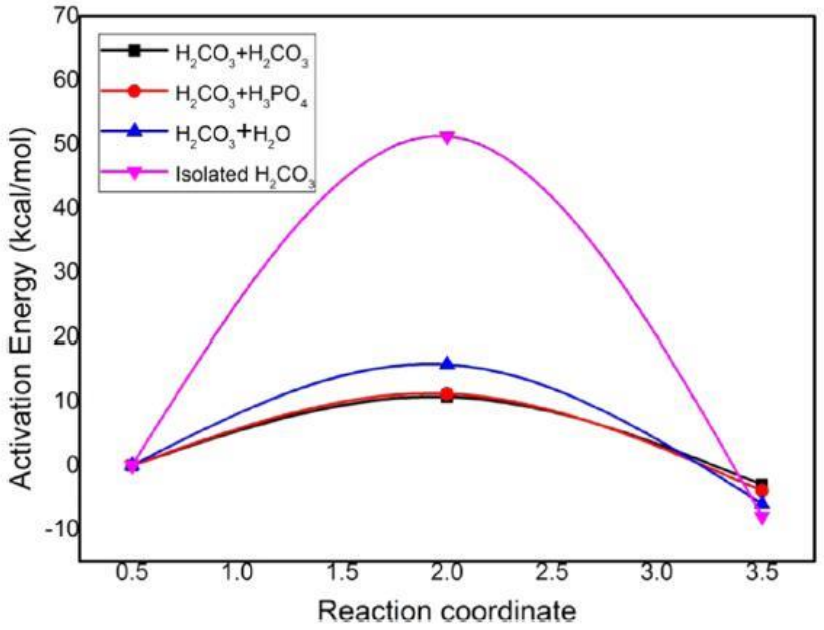

Figure 6. Calculated reaction energy profiles of the transition state for the dissociation of cis−cis H_2CO_3 to CO_2 and H_2O via isolated or three different catalyzed pathways.

(Zhang et al., ACS Earth Space Chem. , 2019)

磷酸酸解

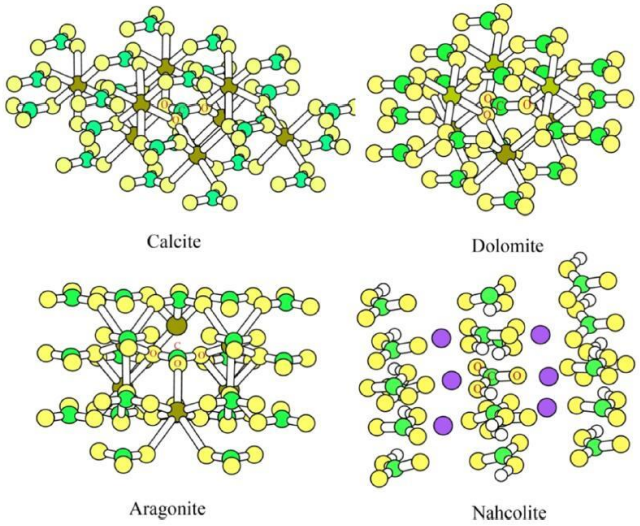

Figure 3. Cluster models used for calcite, aragonite, dolomite, and nahcolite. The $[CO_3^{2-}]$ unit at the central place of the cluster is the atom of interest.

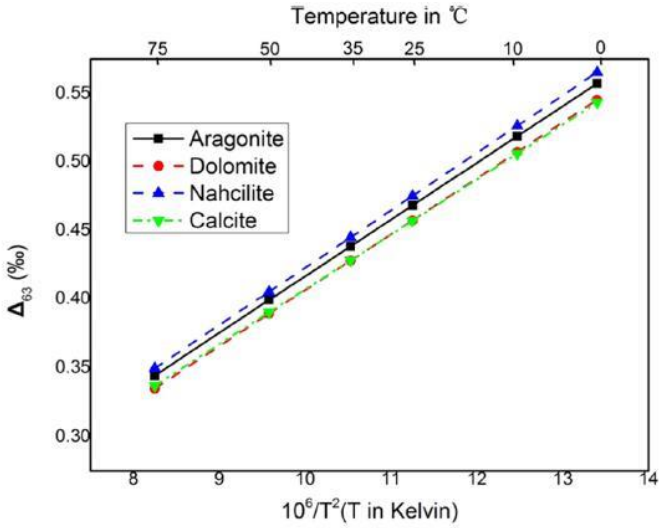

Figure 5. Calculated equilibrium Δ_{63} values of calcite, aragonite, dolomite, and nahcolite with anharmonic corrections.

Table 2. Equilibrium Δ_{63}-Value-Based Harmonic Calculation Using the VVCM Method (‰) and the Comparison with Schauble et al.[14] and Hill et al.[55]

	0 °C		25 °C			100 °C	
minerals	this study	Schauble et al.[14]	this study	Schauble et al.[14]	Hill et al.[55]	this study	Schauble et al.[14]
calcite	0.519	0.490	0.437	0.410	0.394	0.268	0.247
aragonite	0.532	0.513	0.448	0.430		0.273	0.260
dolomite	0.518	0.484	0.437	0.406		0.268	0.245
nahcolite	0.540	0.490	0.454	0.410		0.280	0.247

(Zhang et al., ACS Earth Space Chem. , 2019)

磷酸酸解

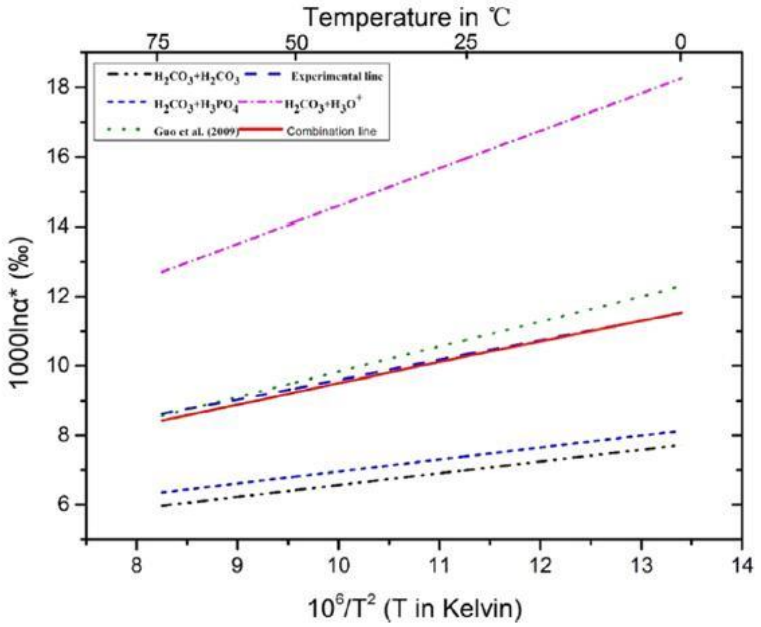

Figure 7. Oxygen isotope enrichment ($1000 \ln \alpha^*$) during phosphoric acid digestion under different pathways. The combination line is the net result of the three parallel pathways. The experimental line is from Kim et al.[10]

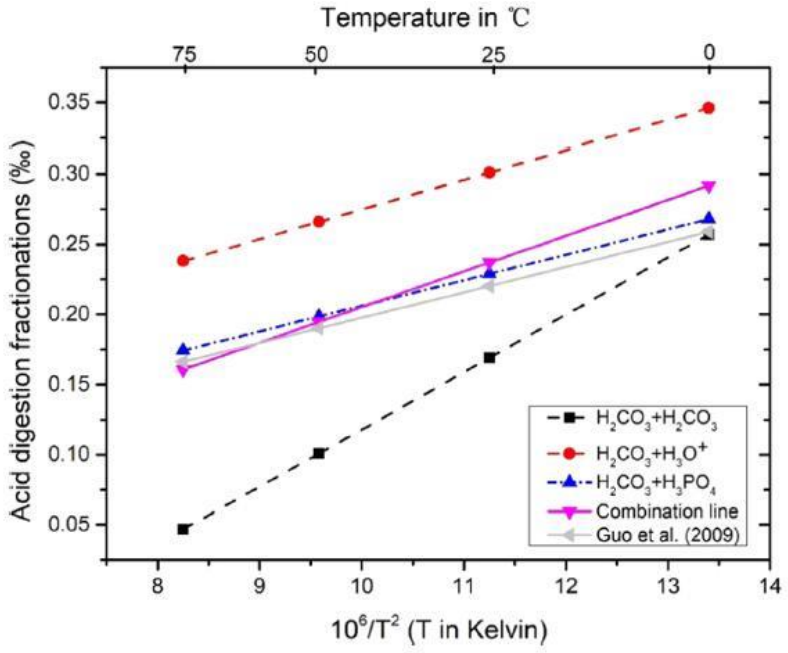

Figure 8. Δ^*_{47} values ($\Delta^*_{47} = \Delta_{47} - \Delta_{63}$) of CO_2 by different pathways and the comparison with Guo et al.[16] The combination lines are possible net results of the 3PP contributions.

$$1000 \ln \alpha^*_{(H_2O-catalyzed)} = 1.079 \times 10^6/T^2 + 3.800$$

$$1000 \ln \alpha^*_{(H_2CO_3-catalyzed)} = 0.3409 \times 10^6/T^2 + 3.151$$

$$1000 \ln \alpha^*_{(H_3PO_4-catalyzed)} = 0.3465 \times 10^6/T^2 + 3.489$$

$$\Delta^*_{47\,(H_2O-catalyzed)} = 0.0255 \times 10^6/T^2 + 0.0045$$

$$\Delta^*_{47\,(H_2CO_3-catalyzed)} = 0.0449 \times 10^6/T^2 - 0.3440$$

$$\Delta^*_{47\,(H_3PO_4-catalyzed)} = 0.0182 \times 10^6/T^2 + 0.0241$$

(Zhang et al., ACS Earth Space Chem. , 2019)

磷酸酸解

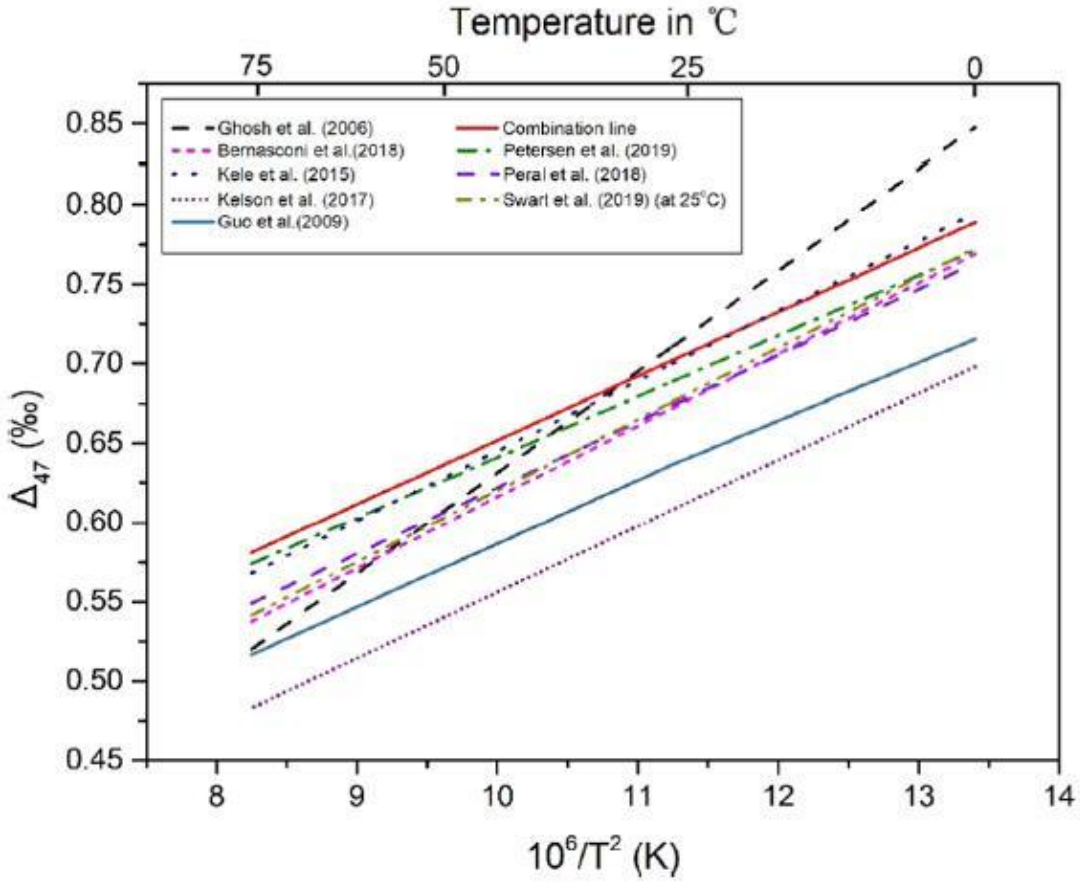

Figure 9. Comparison of calibration lines of this study, the experimental calibration lines, and the theoretical calibration line of Guo et al.[16] in ARF.[18] According to the 3PP model, the line of "this study" can be varied parallelly up or down to an extent due to the change of individual contributions.

(Zhang et al., ACS Earth Space Chem. , 2019)

磷酸酸解

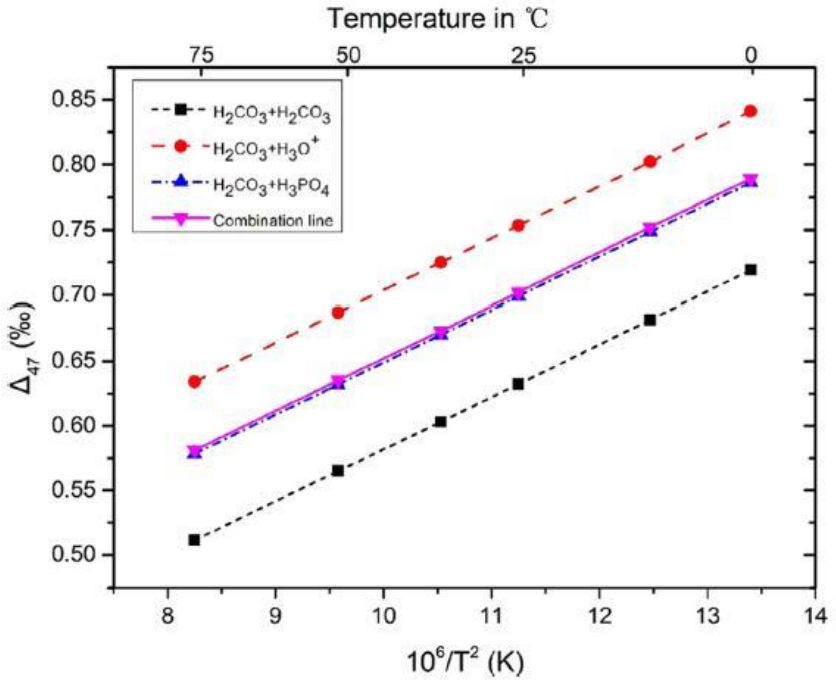

Figure 10. Possible distributions of calibration lines of the 3PP model in ARF (25 °C).

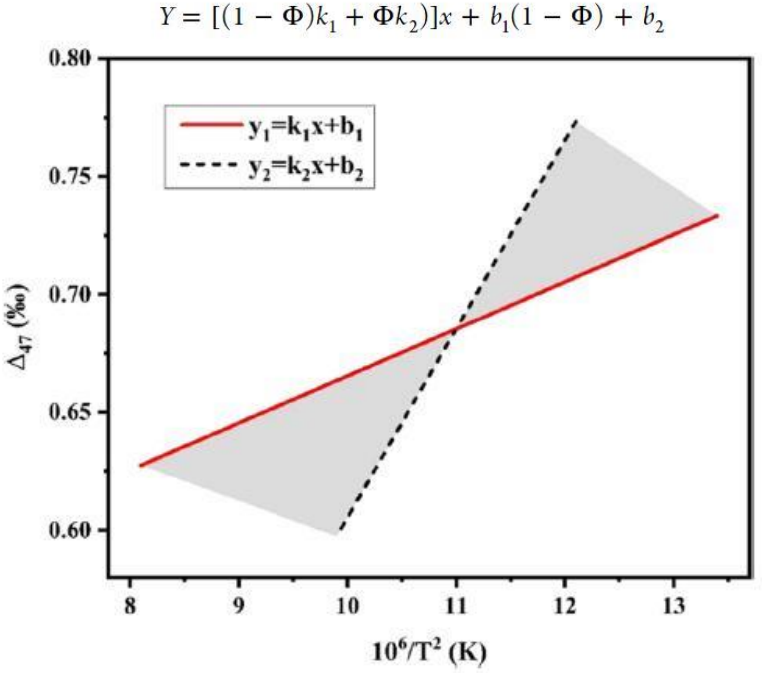

Figure 11. Schematic diagram of possible variations of the predicted slope (y_1) with different contributions from a hidden factor (y_2).

提供了多种碳酸盐岩平衡Δ_{63}值，即25°C是约为0.46‰；
建立了碳酸盐酸解过程的3路径反应机理，及动力学分馏参数；
推荐90°C的酸解处理方式。

(Zhang et al., ACS Earth Space Chem. , 2019)

磷酸酸解

Geochemical Perspectives Letters

Clumped isotope temperature calibration for calcite: Bridging theory and experimentation

J.J. Jautzy[1*], M.M. Savard[1], R.S. Dhillon[2], S.M. Bernasconi[3], A. Smirnoff[1]

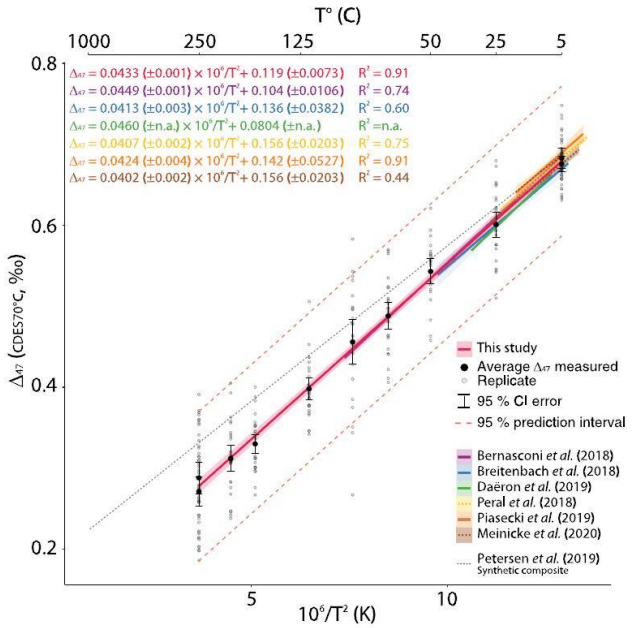

Figure 2 Δ_{47}–T linear relationship in the CDES70°C for the studies fully referenced to ETH carbonate standards; lines represent each study's linear models, with shaded envelopes representing their respective 95 % CI. For more information on the reprocessing of the different datasets, see Supplementary Information S-6.

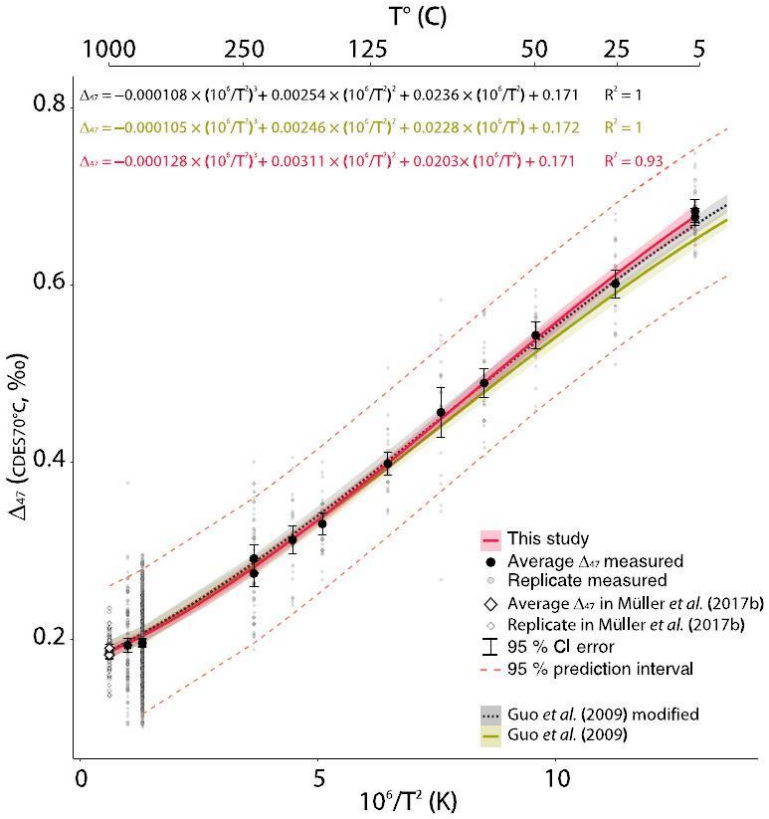

在低、中、高温，分别合成和加热方解石；
利用70°C酸解，建立涵盖5°C-726°C的Δ_{47}温度曲线。

与Guo et al. (2009)在高温段吻合的比较好，但是低温段略高于Guo et al. (2009);
Zhang et al. (2019)的温度曲线略高于Guo et al. (2009)。

(Jautzy et al., GPL. , 2020)

知识点：

1）随机分布是高温极限下的分布状态，只受概率控制；

2）同位素平衡分馏参数，是温度（T）的函数；

3）碳酸盐Δ_{47}平衡信号可单相测温，结合碳酸盐$\delta^{18}O$值，可获得与之平衡的水体$\delta^{18}O$值。

4）动力学分馏一般造成产物富集轻同位素，clumped同位素信号稍显复杂；

5）碳酸盐无法记录Δ_{47}平衡温度时，可以记录受冷却速率控制的封闭温度；

6）Δ_{47}值温度曲线的精确性，是测温的关键；

Clumped同位素的分馏理论

组合效应

Isotope clumping and anticlumping in oxygen and methane

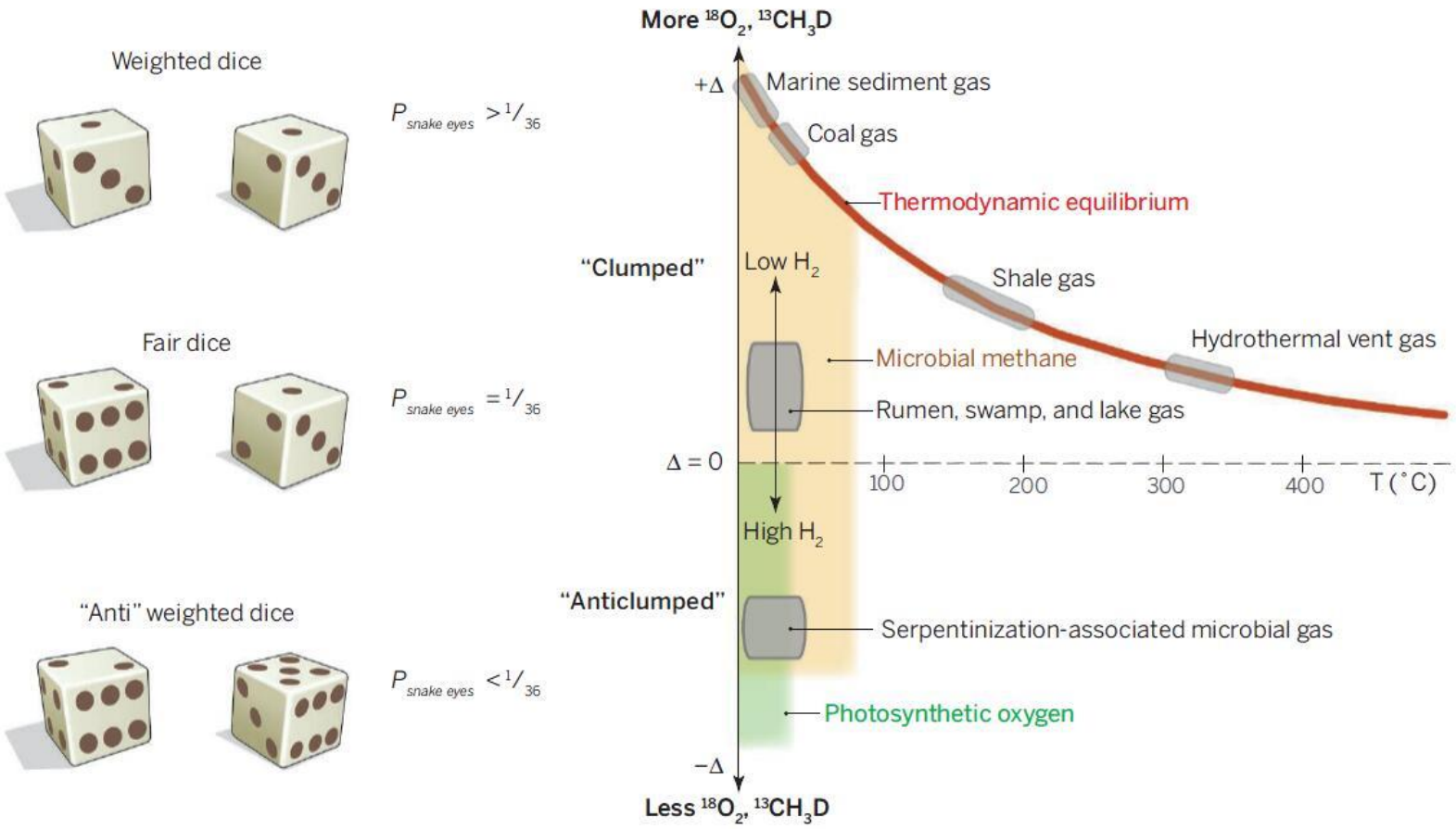

More than a roll of the dice. The appearance of more than one rare, heavy isotope in a molecule (a heavy isotope "clump") is not random. Instead, the isotopic dice are weighted. Clumps are strongly favored under conditions of chemical equilibrium, whereas kinetic processes related to biosynthesis may have lower preference for clumps and in some cases may select against clumps, leading to "anticlumped" products. Natural methane gas shows both behaviors (*6*), whereas the isotope content of photosynthetic oxygen is random or anticlumped (i.e., below chance levels) (*5*).

(Passey, Science, 2015)

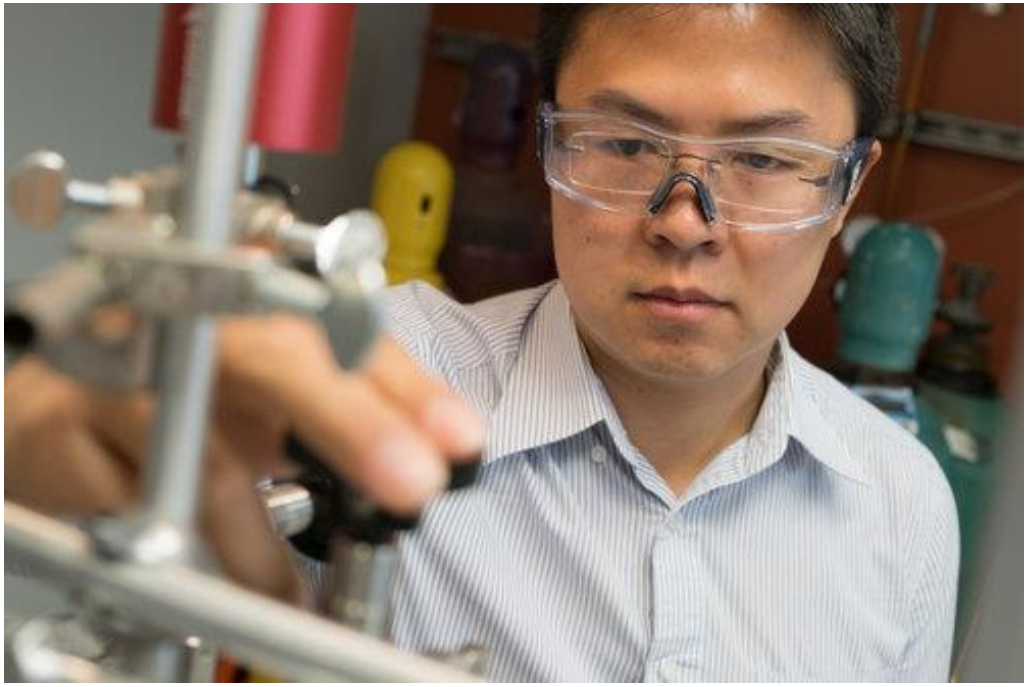

Laurence Yeung

Rice University

2016 F. W. Clarke Medal,
Geochemical Society

继张有学（1993）、Cin-Ty Lee（2009）后，第三位获得该奖的华人/华裔科学家。

Frank Wigglesworth Clarke (1847-1931)

F.W. Clarke was a chemist who determined the composition of the Earth's crust. He has been called the Father of Geochemistry.

The **F.W. Clarke Award** honors a single outstanding contribution to geochemistry or cosmochemistry, published by an early-career scientist as a single paper or a series of papers on a single topic.

Eligibility for this award is met if either of the following criteria is satisfied on the first day of the year in which the award is given: (1) the candidate must have received a recognized doctorate or its equivalent within six years; or (2) must not have celebrated his/her thirty-fifth birthday. An individual may not receive the Patterson and Clarke Awards for the same body of work. Nominations from all fields of geochemistry are encouraged. (For 2021: Nominee must either be born on/after Jan 1, 1986, or have received a PhD on/after Jan 1, 2015.)

Go to Make a Nomination for eligibility and nomination requirements.

双原子分子

不可逆反应（平衡，生物地球化学过程，例如光合作用的O_2）

$$A + E_1 \underset{k_{-1}}{\overset{k_1}{\rightleftharpoons}} AE_1 \quad (R1)$$

$$A + E_2 \underset{k_{-2}}{\overset{k_2}{\rightleftharpoons}} AE_2 \quad (R2)$$

$$AE_1 + AE_2 \xrightarrow{k_3} A\text{–}A + E_1 + E_2 \quad (R3)$$

A：兴趣原子，E：反应底物

R1，R2：可以是可逆反应，R3：不可逆反应

如果指定A′为稀有同位素，A无限多，且[A′]/[A]恒定：

$$\frac{d[(AA)]}{dt} = k_3[AE_1][AE_2]$$

$$\frac{d[(AA')]}{dt} = k_{31'}[A'E_1][AE_2] + k_{32'}[AE_1][A'E_2]$$

$$\frac{d[(A'A')]}{dt} = k_{3''}[A'E_1][A'E_2]$$

$$\frac{d[(AE_1)]}{dt} = k_1[A][E_1] - k_{-1}[AE_1]$$

$$\frac{d[(AE_2)]}{dt} = k_2[A][E_2] - k_{-2}[AE_2]$$

（Yeung, GCA, 2016）

双原子分子

$$\frac{d[(\mathrm{AA})]}{dt} = k_3[\mathrm{AE}_1][\mathrm{AE}_2]$$

$$\frac{d[(\mathrm{AA}')]}{dt} = k_{31'}[\mathrm{A}'\mathrm{E}_1][\mathrm{AE}_2] + k_{32'}[\mathrm{AE}_1][\mathrm{A}'\mathrm{E}_2]$$

$$\frac{d[(\mathrm{A}'\mathrm{A}')]}{dt} = k_{3''}[\mathrm{A}'\mathrm{E}_1][\mathrm{A}'\mathrm{E}_2]$$

$$\frac{d[(\mathrm{AE}_1)]}{dt} = k_1[\mathrm{A}][\mathrm{E}_1] - k_{-1}[\mathrm{AE}_1]$$

$$\frac{d[(\mathrm{AE}_2)]}{dt} = k_2[\mathrm{A}][\mathrm{E}_2] - k_{-2}[\mathrm{AE}_2]$$

酶催化反应：反应达到稳态时，中间产物的产生速率为0

即，$d[(\mathrm{AE}_1)]/dt=0$，$d[(\mathrm{AE}_2)]/dt=0$

$$k_1[\mathrm{A}][\mathrm{E}_1] = k_{-1}[\mathrm{AE}_1]$$

$$k_2[\mathrm{A}][\mathrm{E}_2] = k_{-2}[\mathrm{AE}_2]$$

$$[\mathrm{AE}_1] = k_1[\mathrm{A}][\mathrm{E}_1]/k_{-1}$$

$$[\mathrm{AE}_2] = k_2[\mathrm{A}][\mathrm{E}_2]/k_{-2}$$

$$k_{1'}[\mathrm{A}'][\mathrm{E}_1] = k_{-1'}[\mathrm{A}'\mathrm{E}_1]$$

$$k_{2'}[\mathrm{A}'][\mathrm{E}_2] = k_{-2'}[\mathrm{A}'\mathrm{E}_2]$$

$$[\mathrm{A}'\mathrm{E}_1] = k_{1'}[\mathrm{A}'][\mathrm{E}_1]/k_{-1'}$$

$$[\mathrm{A}'\mathrm{E}_2] = k_{2'}[\mathrm{A}'][\mathrm{E}_2]/k_{-2'}$$

(Yeung, GCA, 2016)

双原子分子

$$[AE_1] = k_1[A][E_1]/k_{-1}$$
$$[AE_2] = k_2[A][E_2]/k_{-2}$$
$$[A'E_1] = k_{1'}[A'][E_1]/k_{-1'}$$
$$[A'E_2] = k_{2'}[A'][E_2]/k_{-2'}$$

$$\frac{d[(AA)]}{dt} = k_3[AE_1][AE_2]$$
$$\frac{d[(AA')]}{dt} = k_{31'}[A'E_1][AE_2] + k_{32'}[AE_1][A'E_2]$$
$$\frac{d[(A'A')]}{dt} = k_{3''}[A'E_1][A'E_2]$$

$$\frac{d[(AA)]}{dt} = k_3\left(\frac{k_1k_2}{k_{-1}k_{-2}}\right)[A]^2[E_1][E_2]$$
$$\frac{d[(AA')]}{dt} = \left(k_{31'}\frac{k_{1'}k_2}{k_{-1'}k_{-2}} + k_{32'}\frac{k_1k_{2'}}{k_{-1}k_{-2'}}\right)[A'][A][E_1][E_2]$$
$$\frac{d[(A'A')]}{dt} = k_{3''}\left(\frac{k_{1'}k_{2'}}{k_{-1'}k_{-2'}}\right)[A']^2[E_1][E_2]$$

(Yeung, GCA, 2016)

双原子分子

$$\frac{d[(AA)]}{dt} = k_3\left(\frac{k_1k_2}{k_{-1}k_{-2}}\right)[A]^2[E_1][E_2]$$ **Eq.(1)**

$$\frac{d[(AA')]}{dt} = \left(k_{31'}\frac{k_{1'}k_2}{k_{-1'}k_{-2}} + k_{32'}\frac{k_1k_{2'}}{k_{-1}k_{-2'}}\right)[A'][A][E_1][E_2]$$ **Eq.(2)**

$$\frac{d[(A'A')]}{dt} = k_{3''}\left(\frac{k_{1'}k_{2'}}{k_{-1'}k_{-2'}}\right)[A']^2[E_1][E_2]$$ **Eq.(3)**

当R3反应中，A-A的形成没有任何动力学分馏效应：$k_3 = k_{31'} = k_{32'} = k_{3''}$

AE_1+AE_2
反应物

没有过渡态

$A\text{-}A+E_1+E_2$
生成物

$$^{A\text{–}A'}R_{sample} = \frac{[(AA')]}{[(AA)]} = \frac{[A']}{[A]}\alpha_1 + \frac{[A']}{[A]}\alpha_2$$ **Eq.(2)/Eq.(1)**

$$^{A'\text{–}A'}R_{sample} = \frac{[(A'A')]}{[(AA)]} = \left(\frac{[A']}{[A]}\alpha_1\right)\left(\frac{[A']}{[A]}\alpha_2\right)$$ **Eq.(3)/)/Eq.(1)**

$$\alpha_1 = (k_{1'}/k_{-1'})/(k_1/k_{-1}) \quad \& \quad \alpha_2 = (k_{2'}/k_{-2'})/(k_2/k_{-2})$$

(Yeung, GCA, 2016)

双原子分子

当R3反应中，A-A的形成没有任何动力学分馏效应：$k_3=k_{31'}=k_{32'}=k_{3''}$

$$^{A-A'}R_{sample} = \frac{[(AA')]}{[(AA)]} = \frac{[A']}{[A]}\alpha_1 + \frac{[A']}{[A]}\alpha_2$$

Eq.(2)/Eq.(1)

$$^{A'-A'}R_{sample} = \frac{[(A'A')]}{[(AA)]} = \left(\frac{[A']}{[A]}\alpha_1\right)\left(\frac{[A']}{[A]}\alpha_2\right)$$

Eq.(3)/)/Eq.(1)

$$\alpha_1 = (k_{1'}/k_{-1'})/(k_1/k_{-1}) \quad \& \quad \alpha_2 = (k_{2'}/k_{-2'})/(k_2/k_{-2})$$

A′-A′随机分布时的R值：

$$^{A'-A'}R_{stochastic} = \left(\frac{[A']_{product}}{[A]_{product}}\right)^2 = \left\{\frac{[(AA')] + 2[(A'A')]}{2[(AA)] + [(AA')]}\right\}^2$$

$$= \left\{\frac{^{A-A'}R_{sample} + 2^{A'-A'}R_{sample}}{2 + {}^{A-A'}R_{sample}}\right\}^2$$

(Yeung, GCA, 2016)

双原子分子

$$^{A-A'}R_{sample} = \frac{[(AA')]}{[(AA)]} = \frac{[A']}{[A]}\alpha_1 + \frac{[A']}{[A]}\alpha_2$$

$$^{A'-A'}R_{sample} = \frac{[(A'A')]}{[(AA)]} = \left(\frac{[A']}{[A]}\alpha_1\right)\left(\frac{[A']}{[A]}\alpha_2\right)$$

$$^{A'-A'}R_{stochastic} = \left(\frac{[A']_{product}}{[A]_{product}}\right)^2 = \left\{\frac{[(AA')] + 2[(A'A')]}{2[(AA)] + [(AA')]}\right\}^2$$

$$= \left\{\frac{^{A-A'}R_{sample} + 2^{^{A'-A'}R_{sample}}}{2 + ^{A-A'}R_{sample}}\right\}^2$$

基于Δ定义： $\Delta_n = \left(\frac{^nR_{sample}}{^nR_{stochastic}} - 1\right)$

$$\Delta_{A'-A'} = \left[\frac{\alpha_1\alpha_2\left\{2 + \frac{[A']}{[A]}(\alpha_1 + \alpha_2)\right\}^2}{\left\{\alpha_1 + \alpha_2 + 2\frac{[A']}{[A]}\alpha_1\alpha_2\right\}^2} - 1\right]$$

(Yeung, GCA, 2016)

双原子分子

$$\Delta_{A'-A'} = \left[\frac{\alpha_1 \alpha_2 \left\{ 2 + \frac{[A']}{[A]} (\alpha_1 + \alpha_2) \right\}^2}{\left\{ \alpha_1 + \alpha_2 + 2 \frac{[A']}{[A]} \alpha_1 \alpha_2 \right\}^2} - 1 \right]$$

$$[A']/[A] \to 0 ,$$

$$\Delta_{A'-A'} \approx \left[\frac{\alpha_1 \alpha_2}{\frac{1}{4}(\alpha_1 + \alpha_2)^2} - 1 \right] = \left[\frac{(\alpha_1 \alpha_2)^{\frac{1}{2}}}{\frac{1}{2}(\alpha_1 + \alpha_2)} \right]^2 - 1$$

(Yeung, GCA, 2016)

双原子分子

$$\Delta_{A'-A'} \approx \left[\frac{\alpha_1\alpha_2}{\frac{1}{4}(\alpha_1+\alpha_2)^2}-1\right]$$

$$= \left[\frac{(\alpha_1\alpha_2)^{\frac{1}{2}}}{\frac{1}{2}(\alpha_1+\alpha_2)}\right]^2 - 1$$

$$\leqslant 0$$

$$(a-b)^2 \geq 0$$

$$a^2-2ab+b^2 \geq 0$$

$$a^2+b^2 \geq 2ab$$

$$a^2+2ab+b^2 \geq 4ab$$

$$(a+b)^2 \geq 4ab$$

$$\frac{a+b}{2} \geq \sqrt{ab}$$

双原子分子

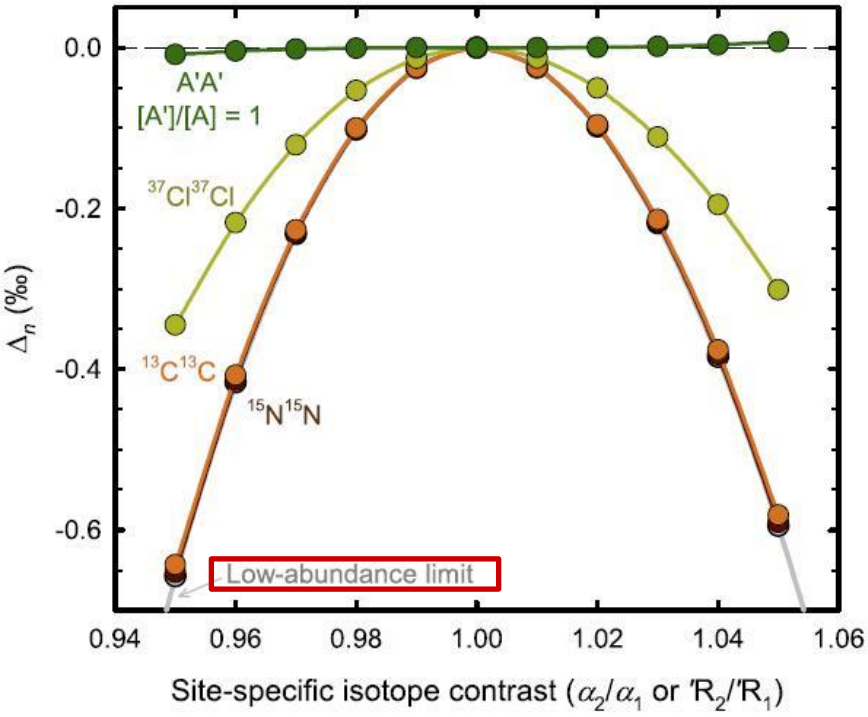

Fig. 1. Calculated clumped-isotope signatures for irreversible isotope-pairing reactions R1, R2, and R3 for $\alpha_1 = 1$. Combinatorial effects, driven here by a difference in isotopic fractionation for the two halves of a symmetric dimer, cause Δ_n values to be less than zero. As the isotopic contrast deviates from unity (plotted here as $\alpha_2/\alpha_1 = 1$ for no isotopic contrast), the magnitude of the combinatorial effect increases quadratically. The sensitivity of Δ_n values to site-specific isotope contrast decreases as rare-isotope abundance increases ($^{15}N \rightarrow {}^{13}C \rightarrow {}^{37}Cl$ at natural abundances covers two orders of magnitude).

以$\alpha_1 = 1$为例：

如果 $\alpha_1 = \alpha_2$，$\Delta_n = 0$，即催化底物不同位点对同位素的选取没有差异；

如果 $\alpha_1 \neq \alpha_2$，$\Delta_n < 0$，即催化底物对同位素的选取有不同的喜好（[AA′]≠[A′A]）；

稀有同位素占比越少，曲线越陡；

储库的同位素组成影响可忽略，当δD=0‰和500 ‰导致 Δ_4 的差别只有0.0001‰；

从不同储库分别获取同位素（例如一个点位从δD=0‰的储库获得同位素，另一点位从δD=500‰的储库获得同位素），即使$\alpha_1 = \alpha_2$也可以导致$\Delta_n < 0$，$\alpha_1 \neq \alpha_2$也可以产生$\Delta_n = 0$。

（Yeung, GCA, 2016）

双原子分子

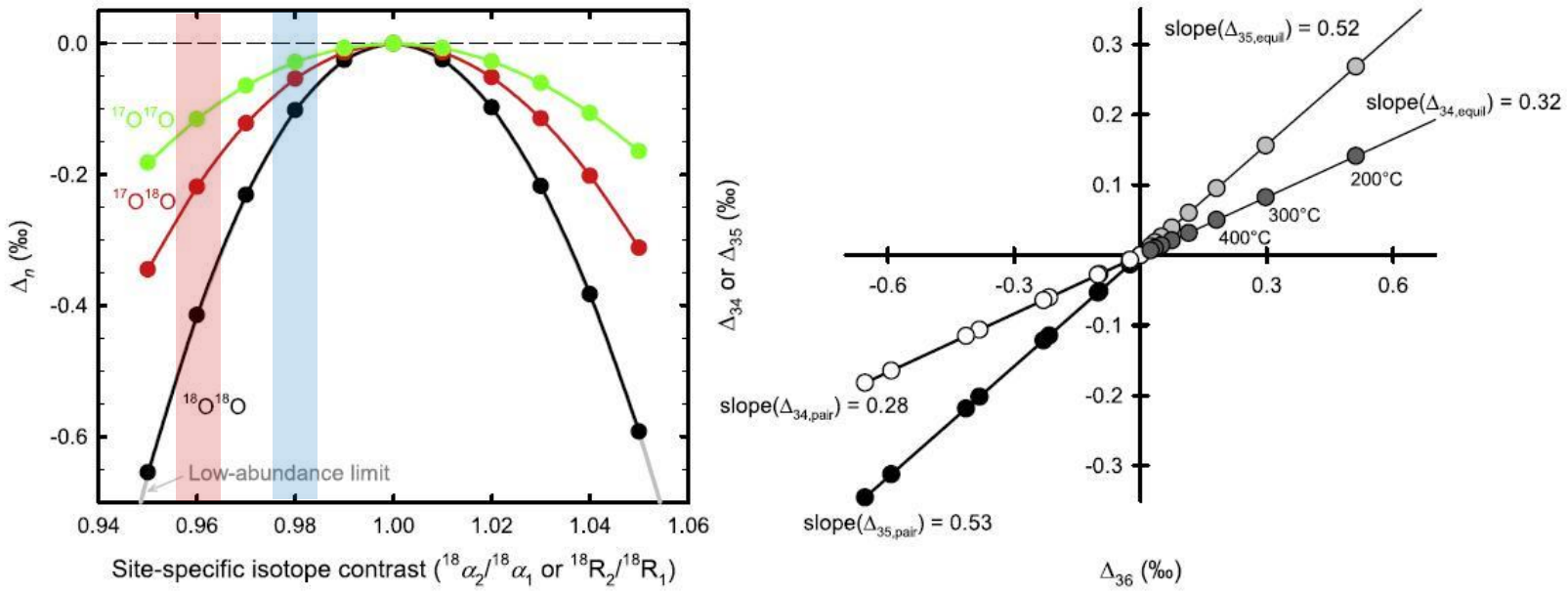

Fig. 2. Calculated combinatorial effects for rare-isotope pairing in O_2. (Left) Dependence of Δ_{34} ($^{17}O^{17}O$), Δ_{35} ($^{17}O^{18}O$), and Δ_{36} ($^{18}O^{18}O$) on site-specific isotope contrast, where the mass-dependent relationship $^{17}R = (^{18}R)^{0.528}$ was used. The smaller fractionation of ^{17}O vs. ^{18}O at each binding site results in Δ_{34} and Δ_{35} values being less sensitive to $^{18}R_2/^{18}R_1$ compared to Δ_{36}. (Right) Covariation in Δ_{34}, Δ_{35}, and Δ_{36} values for combinatorial isotope pairing (black and white points) and isotopic equilibrium (grey points). Combinatorial effects result in clumped-isotope compositions in quadrant III, while isotopic equilibrium yields clumped-isotope compositions in quadrant I. The slopes of the trends in Δ–Δ space are also unique to each process within each quadrant.

对于O_2 clumped同位素的组合效应：

只会产生负的Δ_n信号；

随底物点位对同位素喜好的程度加剧而差异明显；

符合质量分馏关系。

(Yeung, GCA, 2016)

双原子分子

存在过渡态的反应： $k_3 \neq k_{31'} \neq k_{32'} \neq k_{3''}$

$$A + E_1 \rightleftharpoons AE_1 \qquad (R1)$$

$$A + E_2 \rightleftharpoons AE_2 \qquad (R2)$$

$$AE_1 + AE_2 \rightleftharpoons (E_1A\text{–}AE_2)^{\ddagger} \rightarrow A\text{–}A + E_1 + E_2 \qquad (R4)$$

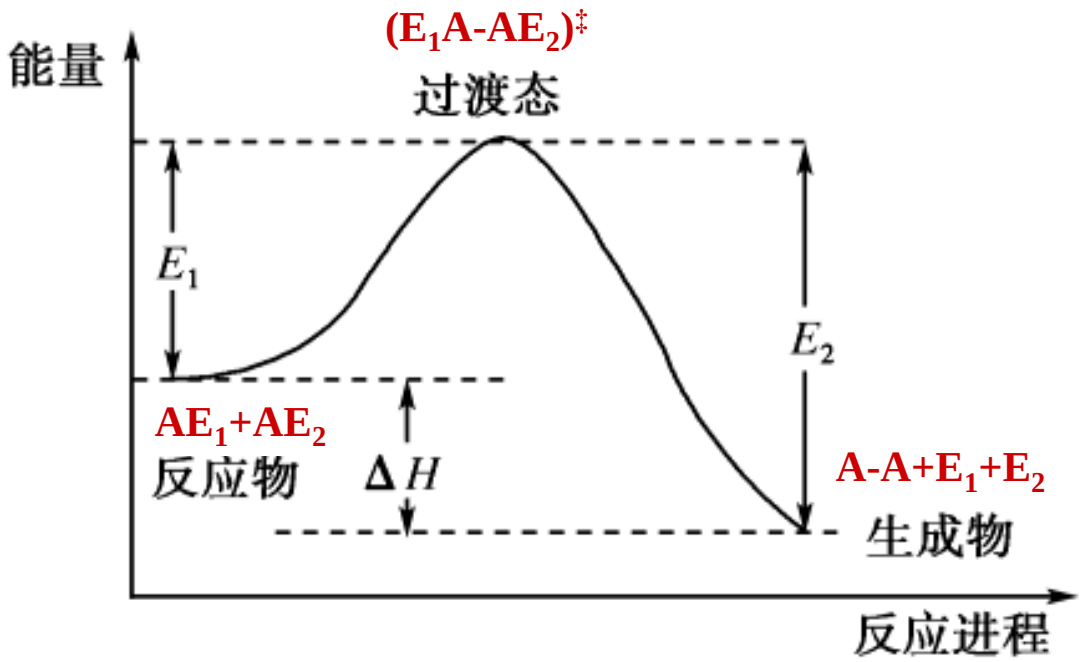

(Yeung, GCA, 2016)

双原子分子

存在过渡态的反应： $k_3 \neq k_{31'} \neq k_{32'} \neq k_{3''}$

$$AE_1 + AE_2 \underset{k_{-3}}{\overset{k_3}{\rightleftharpoons}} (E_1A\text{–}AE_2)^{\ddagger} \xrightarrow{k_4} A\text{–}A + E_1 + E_2 \qquad (R4)$$

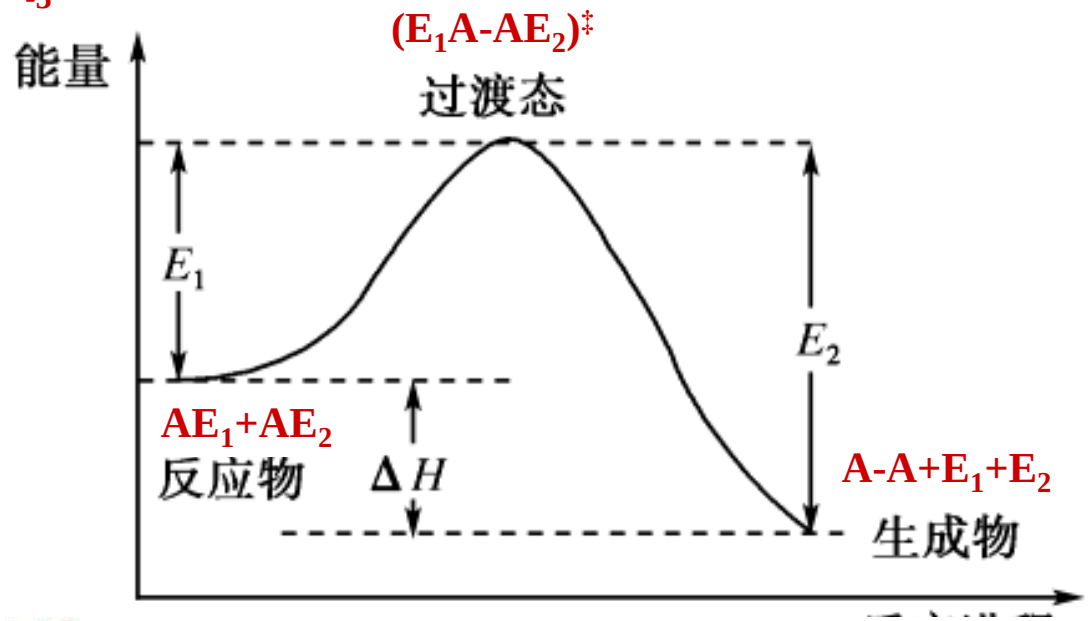

$$\frac{d[(AA)]}{dt} = k_4[(E_1A\text{–}AE_2)^{\ddagger}]$$

$$\frac{d[(E_1A\text{–}AE_2)^{\ddagger}]}{dt} = k_3[AE_1][AE_2] - k_{-3}[(E_1A\text{–}AE_2)^{\ddagger}]$$

(Yeung, GCA, 2016)

双原子分子

存在过渡态的反应：$k_3 \neq k_{31'} \neq k_{32'} \neq k_{3''}$

$$AE_1 + AE_2 \underset{k_{-3}}{\overset{k_3}{\rightleftharpoons}} (E_1A\text{–}AE_2)^{\ddagger} \xrightarrow{k_4} A\text{–}A + E_1 + E_2 \qquad (R4)$$

$$\frac{d[(AA)]}{dt} = \frac{k_3k_4}{k_{-3}}\left(\frac{k_1k_2}{k_{-1}k_{-2}}\right)[A]^2[E_1][E_2]$$

$$\frac{d[(AA')]}{dt} = \left[\left(\frac{k_{31'}k_{41'}}{k_{-31'}}\right)\left(\frac{k_{1'}k_2}{k_{-1'}k_{-2}}\right) + \left(\frac{k_{32'}k_{42'}}{k_{-32'}}\right)\left(\frac{k_1k_{2'}}{k_{-1}k_{-2'}}\right)\right] \times [A'][A][E_1][E_2]$$

$$\frac{d[(A'A')]}{dt} = \frac{k_{3''}k_{4''}}{k_{-3''}}\left(\frac{k_{1'}k_{2'}}{k_{-1'}k_{-2'}}\right)[A']^2[E_1][E_2]$$

$${}^{A\text{–}A'}R_{sample} = \frac{[(AA')]}{[(AA)]} = \left(\frac{[A']}{[A]}\right)(\alpha_1\alpha_{k1'} + \alpha_2\alpha_{k2'})$$

$${}^{A'\text{–}A'}R_{sample} = \frac{[(A'A')]}{[(AA)]} = \alpha_{k''}\left(\frac{[A']}{[A]}\right)^2\alpha_1\alpha_2$$

$${}^{A'\text{–}A'}R_{stochastic} = \left(\frac{[A']_{product}}{[A]_{product}}\right)^2 = \left\{\frac{[(AA')] + 2[(A'A')]}{2[(AA)] + [(AA')]}\right\}^2 = \left\{\frac{{}^{A\text{–}A'}R_{sample} + 2^{A'\text{–}A'}R_{sample}}{2 + {}^{A\text{–}A'}R_{sample}}\right\}^2$$

in which $\alpha_{k1'} = (k_{31'}k_{41'}/k_{-31'})/(k_3k_4/k_{-3})$, $\alpha_{k2'} = (k_{32'}k_{42'}/k_{-32'})/(k_3k_4/k_{-3})$, and $\alpha_{k''} = (k_{3''}k_{4''}/k_{-3''})/(k_3k_4/k_{-3})$

(Yeung, GCA, 2016)

双原子分子

存在过渡态的反应： $k_3 \neq k_{31'} \neq k_{32'} \neq k_{3''}$

$$\mathrm{AE_1 + AE_2} \underset{k_{-3}}{\overset{k_3}{\rightleftharpoons}} (\mathrm{E_1A\text{–}AE_2})^{\ddagger} \xrightarrow{k_4} \mathrm{A\text{–}A + E_1 + E_2} \qquad \text{(R4)}$$

$$\Delta_{\mathrm{A'\text{–}A'}} = \left[\frac{\alpha_1\alpha_2\alpha_{k''}\left\{2 + \frac{[\mathrm{A'}]}{[\mathrm{A}]}\left(\alpha_1\alpha_{k1'} + \alpha_2\alpha_{k2'}\right)\right\}^2}{\left\{\alpha_1\alpha_{k1'} + \alpha_2\alpha_{k2'} + 2\frac{[\mathrm{A'}]}{[\mathrm{A}]}\alpha_1\alpha_2\alpha_{k''}\right\}^2} - 1 \right]$$

$$= \left[\frac{{}'R_1{}'R_2\alpha_{k''}\left(2 + {}'R_1\alpha_{k1'} + {}'R_2\alpha_{k2'}\right)^2}{\left({}'R_1\alpha_{k1'} + {}'R_2\alpha_{k2'} + 2{}'R_1{}'R_2\alpha_{k''}\right)^2} - 1 \right]$$

$$\Delta_{\mathrm{A'\text{–}A'}} \approx \left[\frac{\alpha_1\alpha_2\left\{2 + \frac{[\mathrm{A'}]}{[\mathrm{A}]}\left(\alpha_1 + \alpha_2\right)\alpha_{k'}\right\}^2}{\left\{\alpha_1 + \alpha_2 + 2\left(\frac{\alpha_{k''}}{\alpha_{k'}}\right)\frac{[\mathrm{A'}]}{[\mathrm{A}]}\alpha_1\alpha_2\right\}^2} \times \frac{\alpha_{k''}}{\left(\alpha_{k'}\right)^2} - 1 \right]$$

（指定$\alpha_{k1'} = \alpha_{k2'} = \alpha_{k'}$）

$$\Delta_{\mathrm{A'\text{–}A'}} \approx \left[\frac{\alpha_1\alpha_2}{\frac{1}{4}\left(\alpha_1 + \alpha_2\right)^2} \times \frac{\alpha_{k''}}{\left(\alpha_{k'}\right)^2} - 1 \right]$$

（[A′]/[A] → 0）

（Yeung, GCA, 2016）

双原子分子

存在过渡态的反应： $k_3 \neq k_{31'} \neq k_{32'} \neq k_{3''}$

$$AE_1 + AE_2 \underset{k_{-3}}{\overset{k_3}{\rightleftharpoons}} (E_1A\text{–}AE_2)^{\ddagger} \xrightarrow{k_4} A\text{–}A + E_1 + E_2 \qquad (R4)$$

$$\Delta_{A'-A'} \approx \left[\frac{\alpha_1 \alpha_2}{\frac{1}{4}(\alpha_1 + \alpha_2)^2} \times \frac{\alpha_{k''}}{(\alpha_{k'})^2} - 1 \right]$$

$$\alpha_{k''}/(\alpha_{k'})^2 > 1,\ \Delta_{A'-A'} > 0$$

$$\alpha_{k''}/(\alpha_{k'})^2 < 1,\ \Delta_{A'-A'} < 0$$

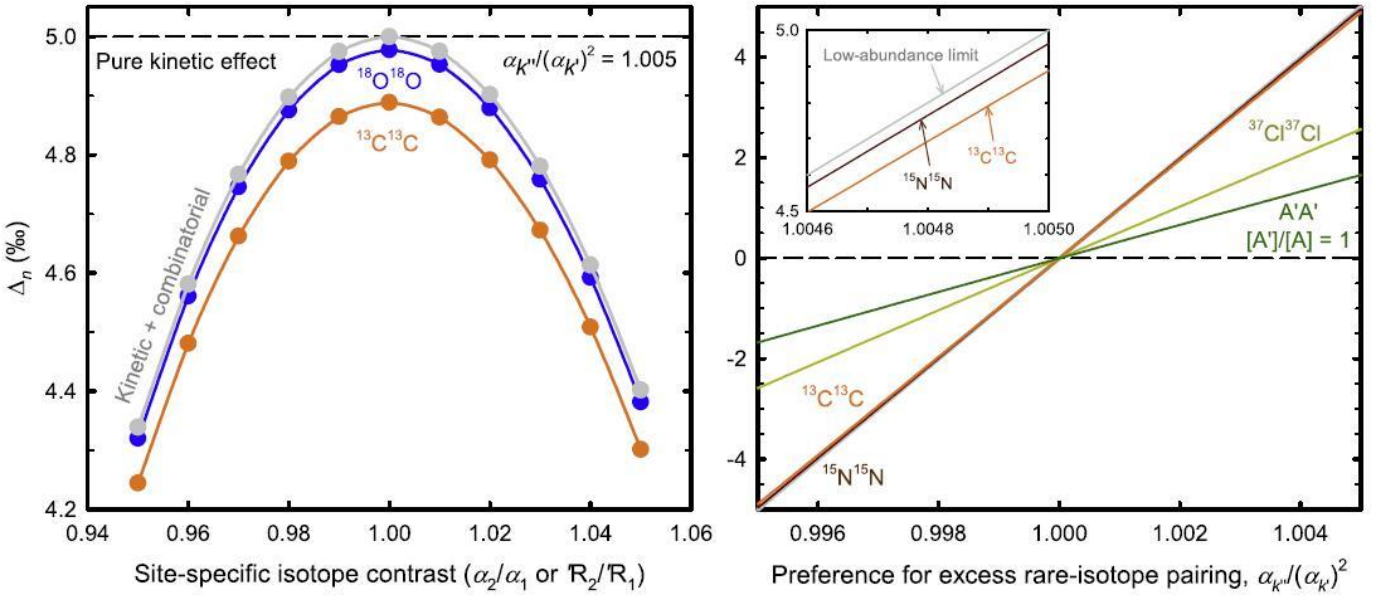

Fig. 3. Calculated combinatorial effects for reversible (but kinetically controlled) rare-isotope pairing. (Left) Rare-isotope paring is strongly dependent on intrinsic kinetic clumping/anticlumping preferences, i.e., $\alpha_{k''}/(\alpha_{k'})^2$ in Eq. (35), but depletions in Δ_n values caused by combinatorial effects are still relevant. (Left and right) Increasing abundance of the rare isotope reduces the sensitivity of Δ_n values to clumping/anticlumping preferences; $^{15}N \rightarrow {}^{13}C \rightarrow {}^{37}Cl$ at natural abundances covers two orders of magnitude. This secondary combinatorial effect arises from the [A′]/[A]-dependent terms in Eqs. 33–35.

(Yeung, GCA, 2016)

双原子分子

不同兴趣原子（例如，CO）：

A-B的形成没有任何动力学分馏效应：

$$\mathrm{A} + \mathrm{E}_1 \rightleftharpoons \mathrm{AE}_1 \quad (\mathrm{R6})$$

$$\mathrm{B} + \mathrm{E}_2 \rightleftharpoons \mathrm{BE}_2 \quad (\mathrm{R7})$$

$$\mathrm{AE}_1 + \mathrm{BE}_2 \rightarrow \mathrm{A{-}B} + \mathrm{E}_1 + \mathrm{E}_2 \quad (\mathrm{R8})$$

$$\Delta_{\mathrm{A'{-}B'}} = \left[\frac{\left({}^{\mathrm{A'{-}B}}R_{sample}\right)\left({}^{\mathrm{A{-}B'}}R_{sample}\right)}{\left({}^{\mathrm{A'{-}B}}R_{sample}\right)\left({}^{\mathrm{A{-}B'}}R_{sample}\right)} - 1 \right] = 0$$

A-B的形成受过渡态控制：

$$\mathrm{AE}_1 + \mathrm{BE}_2 \rightleftharpoons (\mathrm{E}_1\mathrm{A{-}BE}_2)^{\ddagger} \rightarrow \mathrm{A{-}B} + \mathrm{E}_1 + \mathrm{E}_2 \quad (\mathrm{R9})$$

${}^{\mathrm{A}}\alpha_{k'}$:生成A'-B的分馏系数，${}^{\mathrm{B}}\alpha_{k'}$:生成A-B'的分馏系数

${}^{\mathrm{A'}}R = \alpha_A[\mathrm{A'}]/[\mathrm{A}]$ and ${}^{\mathrm{B'}}R = \alpha_{\mathrm{B}}[\mathrm{B'}]/[\mathrm{B}]$

$$\Delta_{\mathrm{A'{-}B'}} = \left[\left(\frac{\alpha_{k''}}{{}^{\mathrm{A}}\alpha_{k'}\,{}^{\mathrm{B}}\alpha_{k'}} \right) \frac{\left(1 + {}^{\mathrm{B}}\alpha_{k'}\frac{[\mathrm{B'}]}{[\mathrm{B}]}\alpha_{\mathrm{B}}\right)\left(1 + {}^{\mathrm{A}}\alpha_{k'}\frac{[\mathrm{A'}]}{[\mathrm{A}]}\alpha_{\mathrm{A}}\right)}{\left(1 + \frac{\alpha_{k''}}{{}^{\mathrm{A}}\alpha_{k'}}\frac{[\mathrm{B'}]}{[\mathrm{B}]}\alpha_{\mathrm{B}}\right)\left(1 + \frac{\alpha_{k''}}{{}^{\mathrm{B}}\alpha_{k'}}\frac{[\mathrm{A'}]}{[\mathrm{A}]}\alpha_{\mathrm{A}}\right)} - 1 \right]$$

$$= \left[\left(\frac{\alpha_{k''}}{{}^{\mathrm{A}}\alpha_{k'}\,{}^{\mathrm{B}}\alpha_{k'}} \right) \frac{\left(1 + {}^{\mathrm{B}}\alpha_{k'}\,{}^{\mathrm{B'}}R\right)\left(1 + {}^{\mathrm{A}}\alpha_{k'}\,{}^{\mathrm{A'}}R\right)}{\left(1 + \frac{\alpha_{k''}}{{}^{\mathrm{A}}\alpha_{k'}}\,{}^{\mathrm{B'}}R\right)\left(1 + \frac{\alpha_{k''}}{{}^{\mathrm{B}}\alpha_{k'}}\,{}^{\mathrm{A'}}R\right)} - 1 \right]$$

$$\Delta_{\mathrm{A'{-}B'}} \approx \left[\frac{\alpha_{k''}}{{}^{\mathrm{A}}\alpha_{k'}\,{}^{\mathrm{B}}\alpha_{k'}} - 1 \right]$$（极低丰度近似，只与过渡态有关）

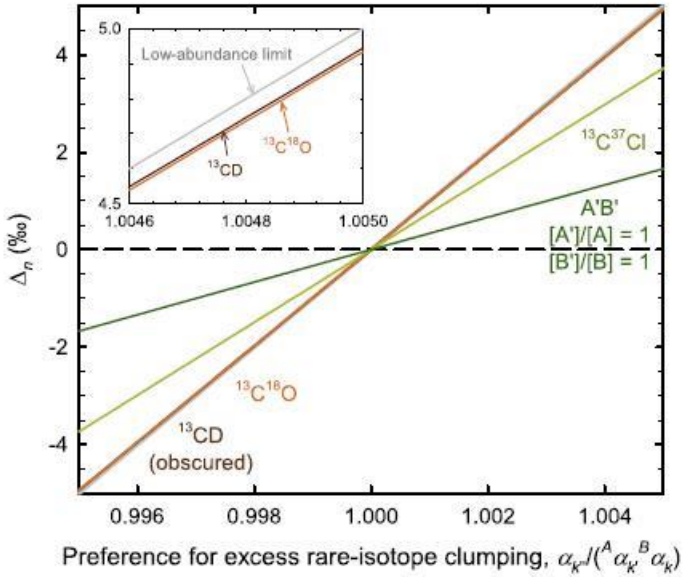

（Yeung, GCA, 2016）

组合效应

组合效应倾向产生anticlumped同位素信号：

源于反应底物对于同位素的**不同偏好**。

稀有同位素丰度会影响组合效应：

组合过程的**同位素分馏**也有影响。

主要影响相同兴趣原子的anticlumped同位素信号：
（例如，$^{18}O^{18}O$和CD_2H_2）

组合效应**主要**发生在**无过渡态**的情况；
可以发生在**有过渡态**的情况。

次要影响不同兴趣原子的anticlumped同位素信号：
（例如，$^{13}C^{18}O$和$^{13}CDH_3$）

组合效应**只可能**发生在**有过渡态**的情况。

（Yeung, GCA, 2016）

知识点：

1）随机分布是高温极限下的分布状态，只受概率控制；

2）同位素平衡分馏参数，是温度（T）的函数；

3）碳酸盐Δ_{47}平衡信号可单相测温，结合碳酸盐$\delta^{18}O$值，可获得与之平衡的水体$\delta^{18}O$值。

4）动力学分馏一般造成产物富集轻同位素，clumped同位素信号稍显复杂；

5）碳酸盐无法记录Δ_{47}平衡温度时，可以记录受冷却速率控制的封闭温度；

6）Δ_{47}值温度曲线的精确性，是测温的关键；

7）组合效应主要导致相同兴趣原子的Δ_n值<0;

新兴clumped同位素体系

甲烷

Available online at www.sciencedirect.com

ScienceDirect

Geochimica et Cosmochimica Acta 126 (2014) 169–191

Geochimica et Cosmochimica Acta

www.elsevier.com/locate/gca

Combined ^{13}C–D and D–D clumping in methane: Methods and preliminary results

D.A. Stolper [a,*], A.L. Sessions [a], A.A. Ferreira [b], E.V. Santos Neto [b], A. Schimmelmann [c], S.S. Shusta [d], D.L. Valentine [d], J.M. Eiler [a]

Relative abundances and masses of the isotopologues of methane.

Cardinal mass	Isotopologue	Proportional relative abundance of CH_4*	Exact mass (amu)
16	$^{12}CH_4$	$9.88^{*}10^{-1}$	16.031
17	$^{13}CH_4$	$1.11^{*}10^{-2}$	17.035
	$^{12}CH_3D$	$6.16^{*}10^{-4}$	17.038
18	$^{13}CH_3D$	$6.92^{*}10^{-6}$	18.041
	$^{12}CH_2D_2$	$1.44^{*}10^{-7}$	18.044
19	$^{13}CH_2D_2$	$1.62^{*}10^{-9}$	19.047
	$^{12}CHD_3$	$1.49^{*}10^{-11}$	19.050
20	$^{13}CHD_3$	$1.68^{*}10^{-13}$	20.053
	$^{12}CD_4$	$5.82^{*}10^{-16}$	20.056
21	$^{13}CD_4$	$6.54^{*}10^{-18}$	21.060

* Assumes that isotopes are randomly distributed throughout all isotopologues and that $\delta^{13}C = 0‰$ and $\delta D = 0‰$ (relative to VPDB and VSMOW respectively).

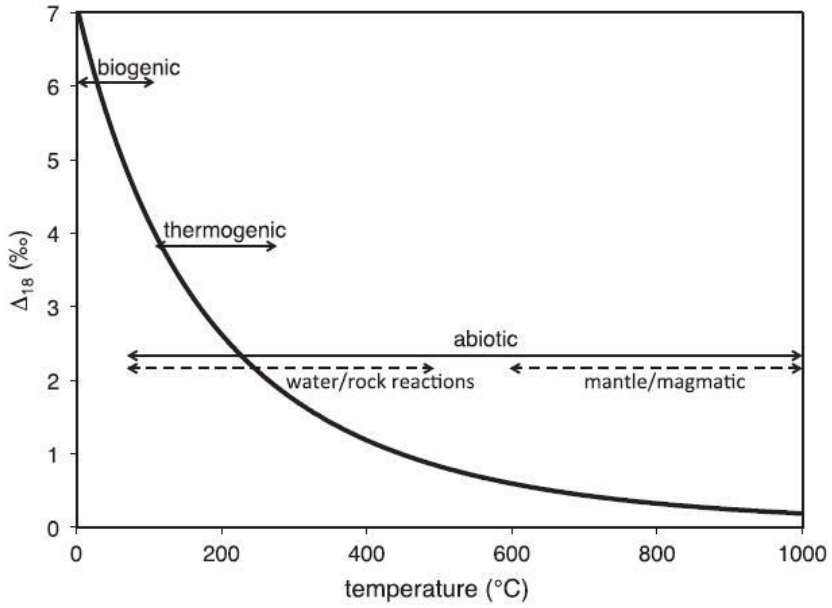

(Stolper et al., GCA, 2014)

甲烷

$$\Delta_{^{13}CH_3D} = \left[\left(\frac{^{13}CH_3DR}{^{13}CH_3DR^*} - 1\right) - \left(\frac{^{13}CH_4R}{^{13}CH_4R^*} - 1\right) - \left(\frac{^{12}CH_3DR}{^{12}CH_3DR^*} - 1\right)\right] * 1000 \qquad \Delta_{18} = \left(\frac{^{18}R}{^{18}R^*} - 1\right) * 1000$$

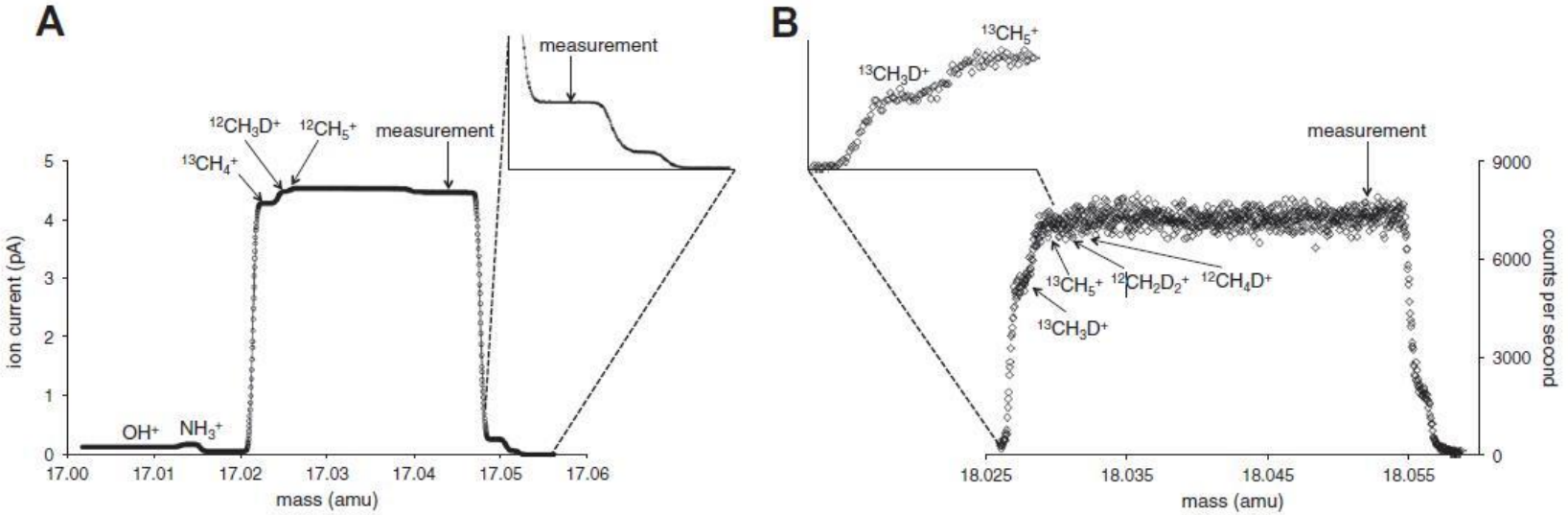

Fig. 2. (A) Mass spectrum at mass 17. The full spectrum was measured at medium resolution (16,000–17,000 mass resolving power) on a Faraday cup read through a 10^{12} Ω resistor while using the instrument's 16 μm entrance slit. The partial mass spectrum in the smaller inset was measured at high resolution (20,000–22,000 mass resolving power) on a Faraday cup read through 10^{12} Ω resistor using the instrument's 5 μm entrance slit. Measurements and adduct lines are made where indicated. (B) High-resolution (~20,000 mass resolving power) scan of mass 18 registered on a secondary electron multiplier. $H_2{}^{16}O^+$ is baseline resolved but not shown due to its higher intensity (100,000 counts per second). Measurements are made where indicated at medium resolution (16,000–17,000 mass resolving power) to increase sensitivity to about 20,000 counts per second. The $^{13}CH_3D^+$ shoulder is shown to demonstrate that it can be resolved from $^{13}CH_5^+$ at the highest resolution setting of the instrument.

(Stolper et al., GCA, 2014)

甲烷

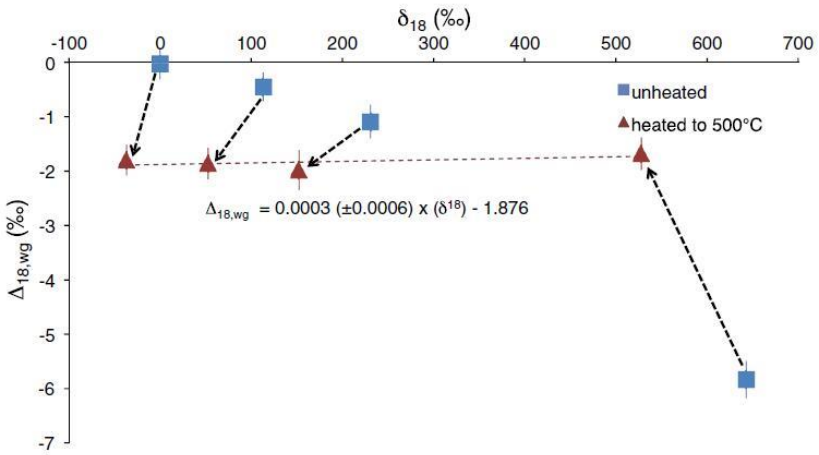

Fig. 6. Bracketed heating experiments at 500 °C. Samples of methane with varying Δ_{18} and bulk isotopic compositions were heated at 500 °C in the presence of a nickel catalyst. The bulk isotopic composition is tracked through δ^{18} values and all samples are referenced such that the working reference gas is defined to have a $\Delta_{18,wg} = 0$. For these samples, the changes in δ^{18} are controlled dominantly by changes in the concentration of D in each sample. All heated samples converge to the same value $\Delta_{18,wg}$ value (~−2‰), within error. Additionally, there is no statistical dependence on the bulk isotopic compositions (tracked through δ^{18}) and $\Delta_{18,wg}$ values.

Table 6
Heating experiment. Samples were heated for the given amounts of time in the presence of a nickel catalyst.

Temperature (°C)	Time (days)	Δ_{18} (‰)	± (‰)
200*	1	−0.603	0.258
300	3.8	−1.242	0.270
300*	0.9	−1.254	0.296
400	3.8	−2.033	0.272
400*	0.2	−1.676	0.244
500	4	−2.079	0.283
500	3.9	−1.979	0.370
500	3	−1.794	0.281
500†	3	−1.678	0.299
500	2.9	−1.855	0.290
500	2	−2.364	0.222
500	2	−1.7669	0.242
500	2	−1.941	0.248
500	2	−2.225	0.271
500	2	−2.002	0.256
500	2	−2.188	0.242

* Denotes correction by subtracting 0.49‰ to account for sieve fractionation artifact.
† Not used in calibration as this sample is ~500‰ different in δ^{18} from typical samples. As such if there are unknown scale compressions or analytical artifacts over such ranges, this sample would be the most susceptible.

In the absence of any statistically significant evidence for scale compression or other artifacts, we assume here that our measurements follow the same functional form as the theoretically predicted dependence of Δ_{18} on temperature (i.e., we assume our measurements are 1:1 with the theoretical values), with a constant offset equal to the Δ_{18} value of our intralaboratory standard, which we take to be +2.981‰. This set of assumptions lets us create a $\Delta_{18,wg}$ vs. temperature (in Kelvin) calibration where the dependent variable is $10^6/T^2$ (Fig. 7B), which results in the following equation:

$$\Delta_{18,wg} = -0.0117\left(\frac{10^6}{T^2}\right)^2 + 0.708\left(\frac{10^6}{T^2}\right) - 3.318. \qquad (11)$$

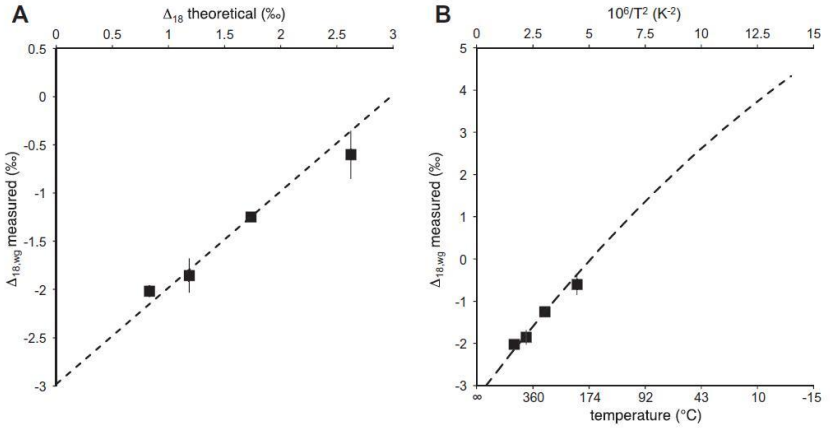

Fig. 7. Heating experiments from 200–500 °C. Samples were heated with a nickel catalyst for varying amounts of time (Table 5). Each point represents an average of experiments if multiple samples were measured. (A) Comparison of measured values vs. theoretically expected values for equilibrium. A 1:1 line has been fit through the data. Data are offset from the origin as all samples are measured relative to a working reference gas, which has a real, but unknown Δ_{18} value. If this line is used to find that value, the standard has a Δ_{18} value of ~2.981‰, or 170 °C. (B) Experimentally derived $\Delta_{18,wg}$ vs. temperature calibration. 2.981‰ has been subtracted from the theoretical line to account for the difference between the theoretical and working gas reference frames.

(Stolper et al., GCA, 2014)

甲烷

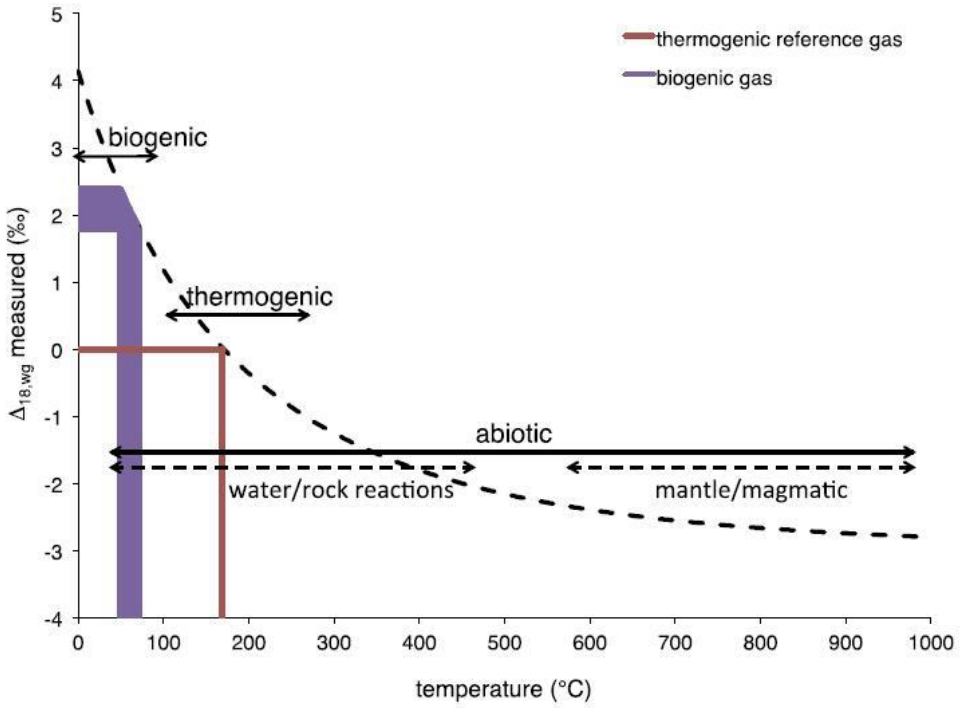

Fig. 8. Samples measured compared to their calculated $\Delta_{18,wg}$-based temperatures. Ranges include 1 standard error of the measurement. As seen, the thermogenic reference gas gives a high but reasonable temperature of 170 °C while the biogenic sample from a methanogen grown at 65 °C yields a temperature of 63 °C.

结论：

(1)获得精确的甲烷Δ_{18}值；

(2)甲烷Δ_{18}可能作为温度计。

(Stolper et al., GCA, 2014)

甲烷

GAS FORMATION

Formation temperatures of thermogenic and biogenic methane

D. A. Stolper,[1]* M. Lawson,[2] C. L. Davis,[2] A. A. Ferreira,[3] E. V. Santos Neto,[3] G. S. Ellis,[4] M. D. Lewan,[4] A. M. Martini,[5] Y. Tang,[6] M. Schoell,[7] A. L. Sessions,[1] J. M. Eiler[1]

生物成因甲烷：
形成于80°C以下；

热成因甲烷模型:
受时间、温度、有机质组成等动力学因素控制；
150°C 以下~ 160°C，油气共生；
石油或干酪根裂解，形成于150°C ~ 160°C以上。

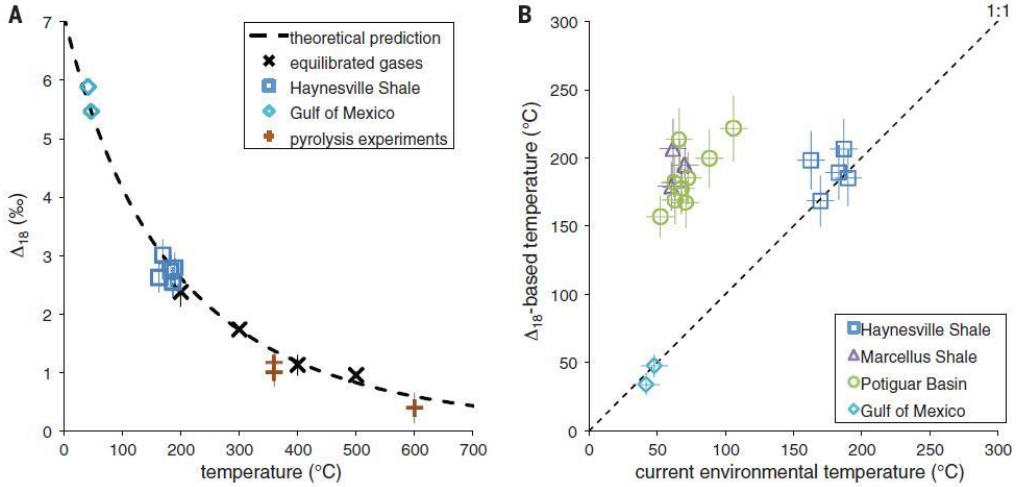

Fig. 1. Comparisons of Δ_{18} temperatures to environmental/formation temperatures. (**A**) Formation/reservoir temperatures versus Δ_{18} values. The dashed line is the theoretical dependence of Δ_{18} on temperature (*19*). Equilibrated gas data are from (*19*). Temperatures are formation/equilibration temperatures for the pyrolysis and equilibrated samples and current reservoir temperatures for the Haynesville Shale and Gulf of Mexico samples. (**B**) Current reservoir temperatures versus Δ_{18} temperatures for all natural samples investigated except the Antrim Shale samples, which are excluded because they are a mixture of thermogenic and biogenic gases. The dotted line is a 1:1 line. Uncertainty for well temperatures is estimated to be ~±10°C. Error bars are 1σ.

Potiguar Basin：

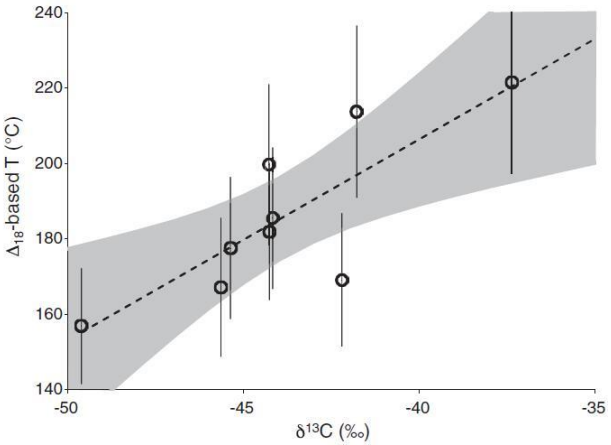

Fig. 2. $\delta^{13}C$ values versus Δ_{18} temperatures for methane from the Potiguar Basin. A positive correlation (P = 0.008) between $\delta^{13}C$ values and Δ_{18}-based temperatures of methane is observed. The gray band is the 95% confidence interval for the linear regression through the data. Error bars are 1σ.

Haynesville Shale：
经历极小的抬升，现今的环境温度为163°C至190°C，Δ_{18} 温度范围169° C至207°C；

Marcellus Shale：
经历抬升，冷却和长期储存，模拟最高埋藏温度为183°C至219°C，现今温度为60°C至70°C， Δ_{18}温度范围179° C至207°C；

Potiguar Basin：
深层到浅层运移，现今温度66°C至106°C，Δ_{18}温度范围157° C至221°C，反映源区性质（与$\delta^{13}C$线性相关，混合）和迁移历史；

Gulf of Mexico：
石油生物降解，现今储库温度42°C和48°C，Δ_{18}温度34±8°C至48±8°C。

实验室产甲烷菌的培养：
同位素不平衡。

说明热成因甲烷的Δ_{18} 温度反映形成温度；200°C以上地质环境会发生同位素再平衡；

(Stolper et al., Science, 2014)

Daniel Stolper

University of California, Berkeley

Education

Ph.D., 2014
Geobiology, Caltech

M.S., 2011
Geobiology, Caltech

A.B., 2018
Earth and Planetary Sciences *Magna Cum Laude*, Harvard College

2020 F. W. Clarke Medal,
Geochemical Society

His interests are currently centered on the following questions.

(1) The application of carbonate clumped-isotope paleothermometry to solve geological problems including the formation of carbonates during crustal alteration reactions off mid-ocean ridge flanks, the temperature history of the Neogene ocean, and controls on carbonate crystal growth and recrystallization.

(2) The use of methane clumped isotope thermometry to understand the methane cycle. I am especially interested in applying this technique to understand the origin of methane in natural settings and studying the fundamental mechanisms of methane generation.

(3) The study of the O_2 cycle in the present and past using the isotopic composition and concentration of O_2 in samples retrieved from the atmosphere, ice cores, and dissolved in the ocean.

甲烷

METHANE CYCLING

Nonequilibrium clumped isotope signals in microbial methane

David T. Wang,[1,2] Danielle S. Gruen,[1,2] Barbara Sherwood Lollar,[3] Kai-Uwe Hinrichs,[4] Lucy C. Stewart,[5] James F. Holden,[5] Alexander N. Hristov,[6] John W. Pohlman,[7] Penny L. Morrill,[8] Martin Könneke,[4] Kyle B. Delwiche,[9] Eoghan P. Reeves,[1] Chelsea N. Sutcliffe,[3] Daniel J. Ritter,[10] Jeffrey S. Seewald,[2] Jennifer C. McIntosh,[10] Harold F. Hemond,[9] Michael D. Kubo,[11] Dawn Cardace,[12] Tori M. Hoehler,[11] Shuhei Ono[1]*

甲烷的$\delta^{13}C$和δD会受动力学分馏控制：
利用红外激光光谱仪（TILDAS）研究生物过程对甲烷clumped同位素的影响:

取样：湖泊、湿地、牛胃、实验室培养的产甲烷菌，以及非生物成因的天然气藏。

基于$\Delta^{13}CH_3D$的温度
热成因甲烷：
反映甲烷的形成温度（平衡）；
湖泊、沼泽、牛胃：
明显远高于环境温度（不平衡）；

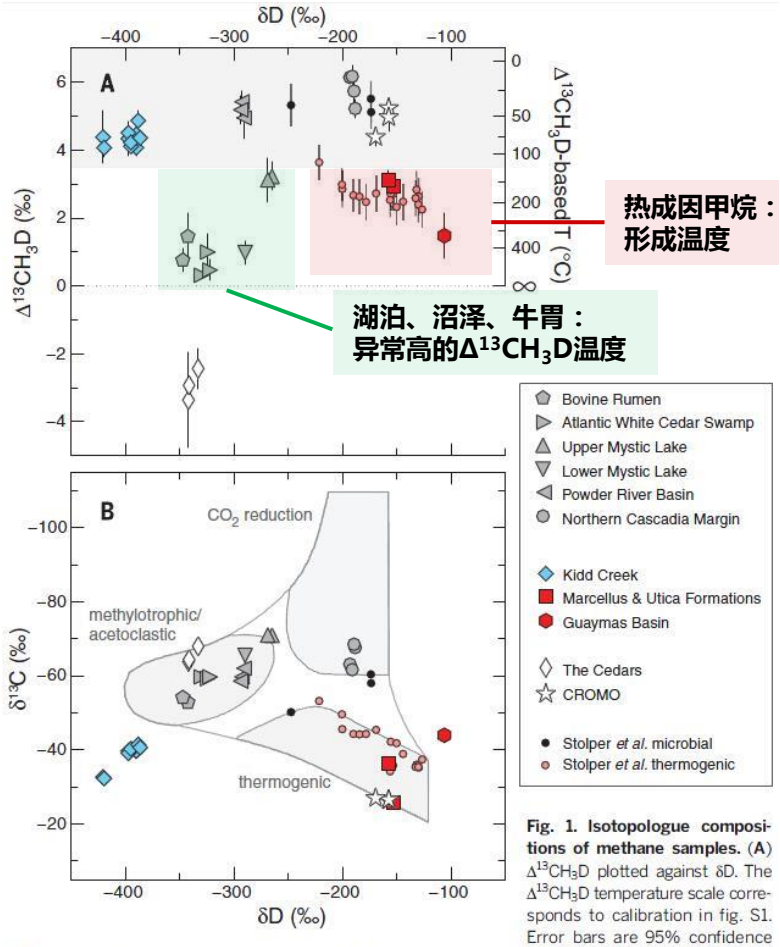

Fig. 1. Isotopologue compositions of methane samples. (**A**) $\Delta^{13}CH_3D$ plotted against δD. The $\Delta^{13}CH_3D$ temperature scale corresponds to calibration in fig. S1. Error bars are 95% confidence intervals (table S1). Data from (*16*) were scaled to their corresponding $\Delta^{13}CH_3D$ values (*15*). The shaded area represents the temperature range within which microbial life has been demonstrated to date (*35*). The dotted line represents $\Delta^{13}CH_3D$ = 0‰ (temperature $T \rightarrow \infty$); data plotting below this line cannot yield corresponding apparent temperatures. (**B**) $\delta^{13}C$ plotted against δD, showing characteristic fields for different methane sources from (*13*).

（Wang et al., Science, 2015）

甲烷

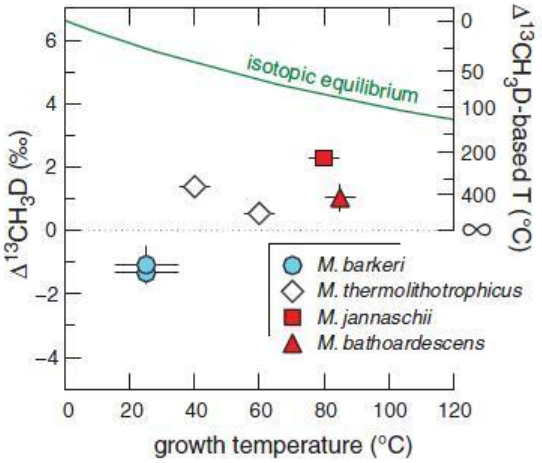

Fig. 3. $\Delta^{13}CH_3D$ values of methane produced by hydrogenotrophic methanogens in batch cultures reflect kinetic effects. Data and error bars are from table S2. The green line represents clumped isotopologue equilibrium (i.e., samples for which $\Delta^{13}CH_3D$ temperature is equal to growth temperature) (fig. S1).

产甲烷古菌（高[H_2]和高[CO_2] 环境）

高温厌氧产甲烷菌(培养温度40-85°C）：明显远高于环境温度（不平衡）；

嗜中温产甲烷菌（室温培养）：$\Delta^{13}CH_3D < 0$；

都与环境水发生了大的D/H同位素分馏。

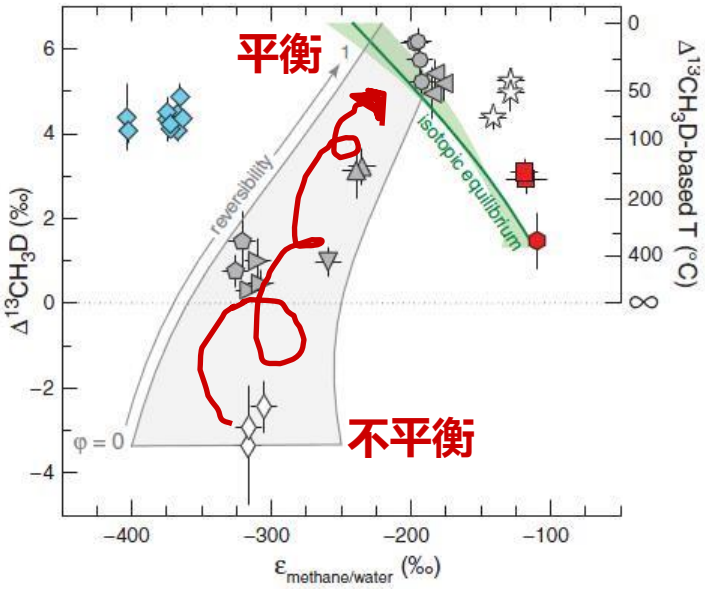

Fig. 2. Extent of clumped and hydrogen isotopic disequilibria in methane. Symbols and vertical error bars are the same as those in Fig. 1. Horizontal error bars represent uncertainties on estimates of $\varepsilon_{methane/water}$ (*23*) (table S4). The solid green curve represents isotopic equilibrium, with the $\varepsilon_{methane/water}$ calibration given by (*36*). Green shading represents ranges of $\varepsilon_{methane/water}$ calibrations from published reports (fig. S3). Gray shading represents model predictions from this study, for microbial methane formed between 0° and 40°C. Metabolic reversibility (φ) increases from bottom (φ = 0, fully kinetic) to top (φ → 1, equilibrium) within this field (*19*).

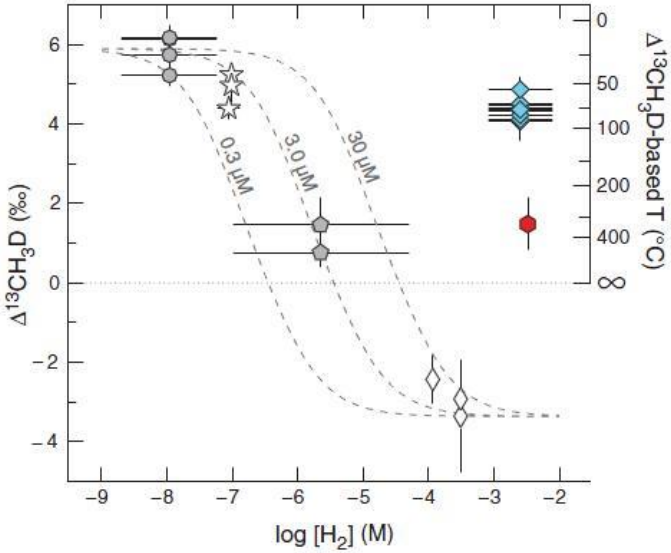

Fig. 4. Relationships between $\Delta^{13}CH_3D$ and H_2 concentration for microbial methane. Symbols and vertical error bars are the same as in Fig. 1. The H_2 data are from table S4; when a range of [H_2] values is given, points are plotted at the geometric mean of the maximum and minimum values. Dashed lines represent model predictions for microbial methane produced at 20°C, calculated using Michaelis-Menten constants (K_M) of 0.3, 3.0, and 30 μM H_2. Data for samples of dominantly nonmicrobial methane from Guaymas Basin and Kidd Creek are plotted for comparison.

$\Delta^{13}CH_3D$信号：与甲烷/环境水体间D/H同位素分馏成正相关；随着反应可逆程度的增强，可由同位素不平衡转变为平衡；

$\Delta^{13}CH_3D$值、H_2浓度、D/H同位素分馏：[H_2]越高，电子供体越多，产甲烷过程越不可逆，$\Delta^{13}CH_3D$值越低；与用于判别生物过程甲烷来源。

（Wang et al., Science, 2015）

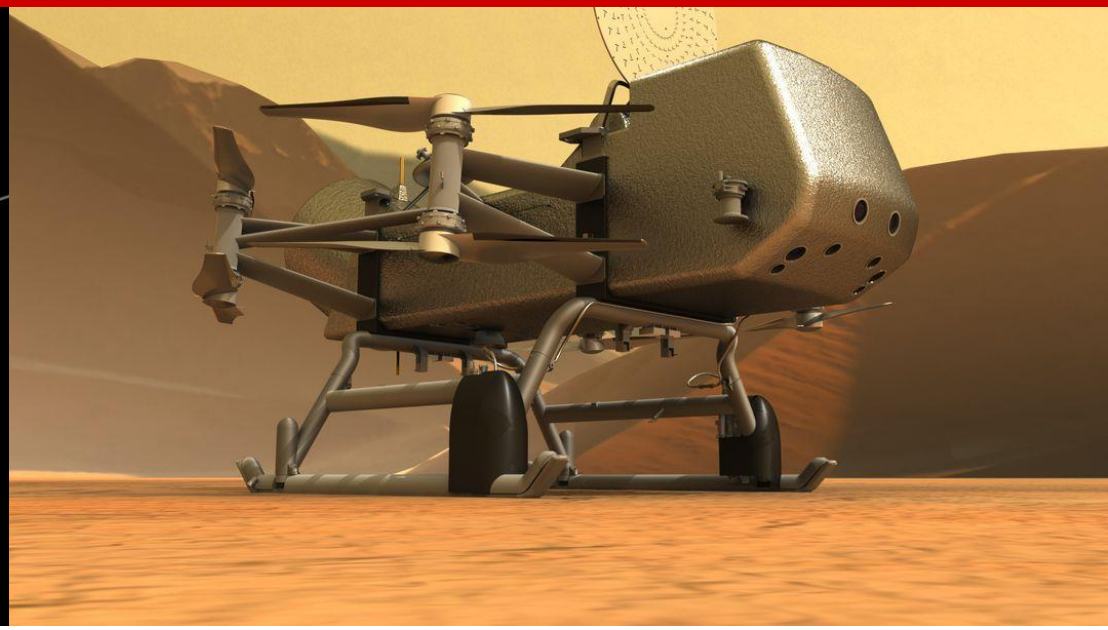

NASA

蜻蜓号（Dragonfly）：2026年发射，预计2034年抵达土星最大的卫星——“泰坦”。

泰坦（Titan）：

木卫六，大气以氮气为主，表面冰冷，存在液态湖泊，以碳氢化合物为主（甲烷和乙烷）。

TILDAS：

Tunable Infrared Laser Direct Absorption Spectrometer

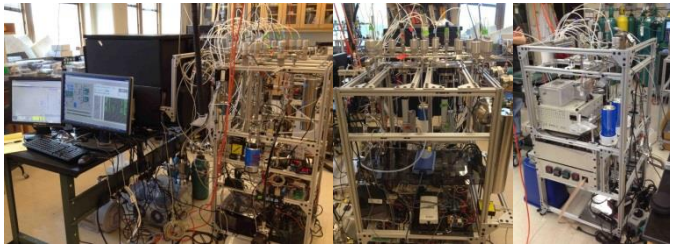

知识点：

1）随机分布是高温极限下的分布状态，只受概率控制；

2）同位素平衡分馏参数，是温度（T）的函数；

3）碳酸盐Δ_{47}平衡信号可单相测温，结合碳酸盐$\delta^{18}O$值，可获得与之平衡的水体$\delta^{18}O$值。

4）动力学分馏一般造成产物富集轻同位素，clumped同位素信号稍显复杂；

5）碳酸盐无法记录Δ_{47}平衡温度时，可以记录受冷却速率控制的封闭温度；

6）Δ_{47}值温度曲线的精确性，是测温的关键；

7）组合效应主要导致相同兴趣原子的Δ_n值<0;

8）生物效应可以产生异常的Δ_n值，可用于示踪；

氧气

ISOTOPE GEOCHEMISTRY

Biological signatures in clumped isotopes of O_2

Laurence Y. Yeung,[1,2]*† Jeanine L. Ash,[1]*† Edward D. Young[1]

$$\Delta_{36,p} = \left[\frac{\alpha_A \alpha_B}{\frac{1}{4}(\alpha_A + \alpha_B)^2} - 1\right]$$

组合效应：光合作用产生的O_2，相对随机分布亏损$^{18}O^{18}O$和$^{17}O^{18}O$同位素体。

酶催化反应通过5步，讲O_A和O_B组合成O_2：

$\Delta_{36} < 0$ 和 $\Delta_{35} < 0$ （ $\alpha_A \neq \alpha_B$ ）

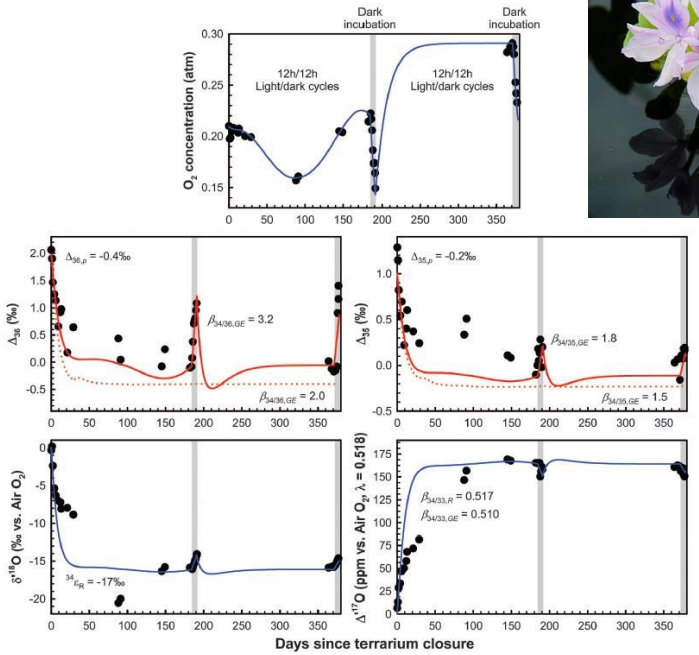

Fig. 2. Evolution of concentration and O_2 isotopologue composition in the terrarium. Observations (data points) are compared with model results (curves). Uncertainties are not shown for clarity, but long-term analytical uncertainties in O_2 concentration, $\delta^{18}O$, $\Delta^{17}O$, Δ_{36}, and Δ_{35} are 1%, 0.04‰, 5 ppm, 0.17‰, and 0.3‰, respectively. A single isotopologue discrimination factor ($^{34}\varepsilon_R$ = −17‰) is used here to illustrate steady-state behavior in $\delta^{18}O$ and $\Delta^{17}O$; a more detailed model run yields better agreement for $\delta^{18}O$ and $\Delta^{17}O$ but similar results for Δ_{36} and Δ_{35}. Mass-dependent exponents used in the model, $\beta_{34/n}$, are labeled, with subscripts *R* and *GE* denoting values for respiration and gas exchange, respectively. For $\beta_{34/35,GE}$ and $\beta_{34/36,GE}$, two model runs are shown to illustrate their effects on the Δ_{36} and Δ_{35} time traces (*17*).

大气O_2因为光化学反应导致同位素平衡，基本不受生物效应影响。

(Yeung, Science, 2015)

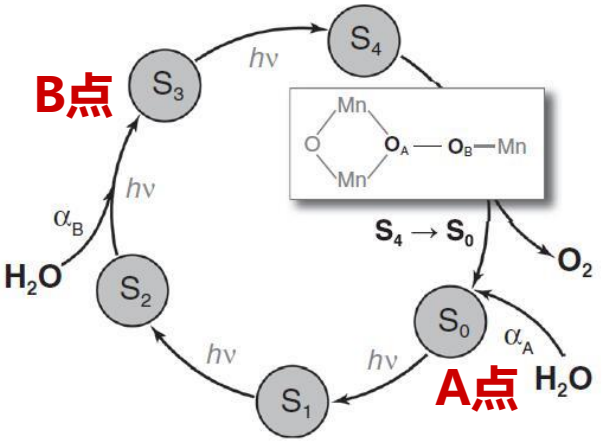

Fig. 1. Conceptual diagram of O_2 formation at the OEC. The five-step Kok cycle for the water-splitting reaction $2H_2O + 4h\nu \rightarrow O_2 + 4H^+ + 4e^-$ is shown without electron flow (*32*). Transitions between intermediate oxidation states of the OEC (S_0 to S_4) occur upon absorption of visible light. The water-binding sequence is based on experimental results (*19*, *33*, *34*), which also indicate that water substrates are exchangeable at least up to state S_3 on chemically distinct binding sites (*18*, *19*). The O–O bond is formed during the S_4-to-S_0 transition, expressing the isotopic fractionations α_A and α_B from water substrate binding.

氮气

Article

Hydrothermal $^{15}N^{15}N$ abundances constrain the origins of mantle nitrogen

https://doi.org/10.1038/s41586-020-2173-4
Received: 4 July 2019
Accepted: 4 February 2020

J. Labidi[1,11]✉, P. H. Barry[2], D. V. Bekaert[3], M. W. Broadley[3], B. Marty[3], T. Giunta[4], O. Warr[4], B. Sherwood Lollar[4], T. P. Fischer[5], G. Avice[6], A. Caracausi[7], C. J. Ballentine[8], S. A. Halldórsson[9], A. Stefánsson[9], M. D. Kurz[2], I. E. Kohl[1,10] & E. D. Young[1]✉

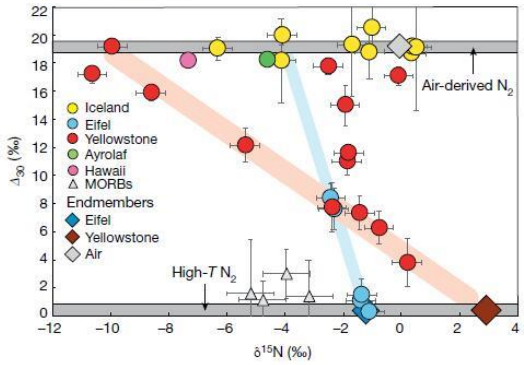

Fig. 1 | The nitrogen isotopic composition of volcanic gases and volatile-rich MORBs. Volcanic gases were collected in hydrothermal systems from Iceland, Hawaii (USA), Yellowstone (Wyoming, United States), Ayrolaf (Ethiopia) and Eifel (Germany). MORBs are popping glasses from the Mid-Atlantic Ridge. Data can be found in Supplementary Table 1. Error bars are 2σ and their magnitude is a function of counting statistics. The nitrogen isotopic and isotopologue compositions of air are shown. Atmospheric N_2 has a known Δ_{30} of +19.1 ± 0.3‰ (2 s.d.), relative to high-temperature nitrogen with Δ_{30} = 0‰ (ref. [25]). Icelandic samples have exclusively air-derived N_2 as shown by atmospheric Δ_{30} values. The varying $\delta^{15}N$ values at any given atmospheric Δ_{30} value are evidence for isotopic fractionation of air-derived N_2 in the geotherma system. Similar fractionation is observed in the gases from all of the investigated locations. Since high-temperature nitrogen has by definition a Δ_{3} of 0‰, mixing relationships can be confidently extrapolated to this value along straight lines. This allows the endmember $\delta^{15}N$ of the degassing magmas to be determined from volcanic gases. Shaded areas demarcate the mixing trends defined by the data for Eifel (blue) and Yellowstone (red). We find that Eifel and Yellowstone gases have mantle-derived $\delta^{15}N$ values of −1.4 and +3‰, respectively. Note that the Yellowstone data are also affected by a third component resembling air in both Δ_{30} and $\delta^{15}N$ values.

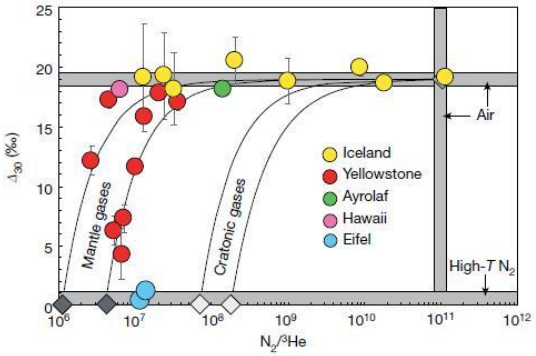

Fig. 2 | The relationship between Δ_{30} and $N_2/^3He$ ratios in volcanic gases. Δ_{30} and $N_2/^3He$ ratios are shown for samples collected at the same time from gases in Iceland, Yellowstone, Hawaii and Ayrolaf. The error bars are 2σ. Data can be found in Supplementary Table 1. Two estimates for mantle gases are shown as the dark grey diamonds with $N_2/^3He$ ratios of 1×10^6 and 4×10^6, after Marty et al.[11]. These are consistent with the popping rock estimate[11] of $(2.9 \pm 0.1) \times 10^6$. Two estimates for cratonic gases are shown as light grey diamonds. These are derived from our data on cratonic gases from two locations in the Canadian Shield (see Supplementary Information). For $N_2/^3He$ ratios, the cratonic endmembers are 0.7×10^8 and 1.8×10^8 (see Methods for details and Supplementary Table 2 for data). The samples show a clear mixing between air and mantle-derived gases, with a negligible cratonic crustal contribution. Icelandic samples have $N_2/^3He$ ratios ranging down to 10^7, but no substantial contribution of mantle N_2 is observed. Note that no He concentrations were obtained for Eifel as the samples were collected in glass vials, leading to appreciable He diffusion out of the containers. Existing data obtained with no Δ_{30} measurements suggest a $N_2/^3He$ value below 3.0×10^7 (ref. [10]).

建立模型显示，对流地幔一直流失氮，因此观察到幔源$\delta^{15}N$值变化是经历地球形成和早期分异的残留。

（Labidi et al., Nature, 2020）

地球大气富含N_2，会污染地幔N_2样品；

如何扣除大气N_2对地幔N_2的污染？

Δ_{30}：

大气：19.1±0.3‰

深部地幔：0‰

同位素平衡：0-5 ‰（100K以上）

可以作为指示空气混染的指标。

冰岛：

大气N_2，经过热液系统后改变$\delta^{15}N$值；

黄石地幔柱：

混染部分大气N_2，外推深部幔源$\delta^{15}N$值为+3±2‰；

Eifel：

混染部分大气N_2，外推深部幔源$\delta^{15}N$值为-1.2±0.5‰；

利用端元混合模型：

黄石：反映地幔源区；

Eifel：有俯冲脱水洋壳的加入；

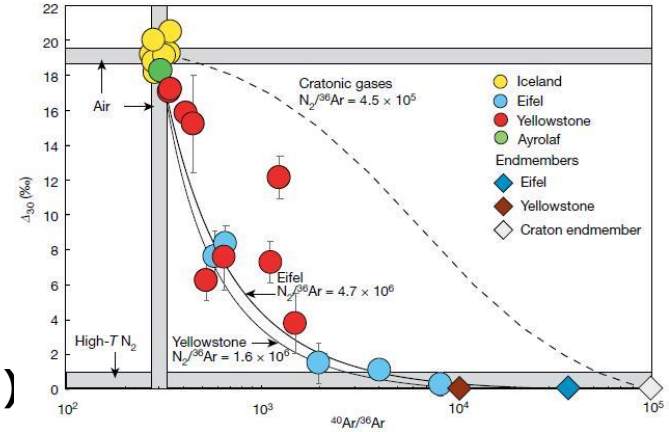

知识点：

1）随机分布是高温极限下的分布状态，只受概率控制；

2）同位素平衡分馏参数，是温度（T）的函数；

3）碳酸盐Δ_{47}平衡信号可单相测温，结合碳酸盐$\delta^{18}O$值，可获得与之平衡的水体$\delta^{18}O$值。

4）动力学分馏一般造成产物富集轻同位素，clumped同位素信号稍显复杂；

5）碳酸盐无法记录Δ_{47}平衡温度时，可以记录受冷却速率控制的封闭温度；

6）Δ_{47}值温度曲线的精确性，是测温的关键；

7）组合效应主要导致相同兴趣原子的Δ_i值<0;

8）生物效应可以产生异常的Δ_i值，可用于示踪；

9）异常的Δ_n值还可以用于扣除污染；

国内相关领域的发展

理论研究

2007：唐茂，赵辉，刘耘. 天然气中甲烷和CO_2的二元同位素特征. 矿物学报, (3-4): 396-399.

[中科院地球化学研究所]

首次将“clumped同位素” 译为“二元同位素”；

最早计算甲烷的clumped同位素平衡分馏信号。

第27卷 第3/4期
2007年12月

矿 物 学 报
ACTA MINERALOGICA SINICA

Vol.27, No.3/4
Dec., 2007

文章编号：1000-4734(2007)03-0396-04

天然气中甲烷和 CO_2的二元同位素特征

唐茂，赵辉，刘耘

（中国科学院 地球化学研究所 矿床地球化学国家重点实验室，贵州 贵阳 550002）

摘要：不同成因的天然气由于形成温度不同，往往会有不同的稳定同位素特征。但是，由于经常不能同时获得天然气以及它的生成母体的同位素成分，很难用单独的C或H同位素成分来确定它的形成温度。在形成天然气时，不同的温度会形成不同的二元同位素的浓度，温度越低，二元同位素的比例越大，因此只需要知道天然气本身的二元同位素的浓度，就可以确定形成温度，从而避免了需要知道天然气生成母体的同位素成分这一难题。本文利用高级量子化学计算，预测了不同温度下天然气中甲烷和 CO_2气体的二元同位素（Clumped isotope）的特征，提供用于天然气成因分析的新方法。

关键词：天然气；甲烷；CO_2；同位素；二元同位素；量子化学计算

中图分类号：P597；P618.13　　**文献标识码**：A

作者简介：唐茂，1970年出生，助理研究员，主要从事计算地球化学研究工作.

理论研究

会议报告：

刘琪, 唐茂, 刘耘, 2009. 二元同位素(clumped isotope)方法的介绍.第九届全国同位素地质年代学和同位素地球化学学术讨论会.

张思亭, 刘耘, 2013. 碳酸盐中^{13}C-^{18}O “clumped” 同位素Δ_{47}值与温度的理论校准线.第十届全国同位素地质年代学与同位素.

刘琪, 刘耘, 2013. 采用超越简谐水平对H_2O, H_2S, SO_2, NH_3和CH_4的 “clumped” 同位素平衡分馏信号的理论预测.第十届全国同位素地质年代学与同位素.

刘琪, 刘耘. 2015. 有机化合物 “Clumped” 同位素平衡分馏信号的理论预测.第七届全国成矿理论和找矿方法学术讨论会.

张思亭, 刘耘, 2017. 动力学分馏对碳酸盐中^{13}C-^{18}O “clumped” 同位素及三氧同位素关系的影响.中国矿物岩石地球化学学会第 16 届学术年会.

理论研究

Available online at www.sciencedirect.com
SciVerse ScienceDirect
Geochimica et Cosmochimica Acta 77 (2012) 292–303
Geochimica et Cosmochimica Acta
www.elsevier.com/locate/gca

Cao & Liu, GCA, 2012

Theoretical estimation of the equilibrium distribution of clumped isotopes in nature

Xiaobin Cao, Yun Liu *

State Key Laboratory of Ore Deposit Geochemistry, Institute of Geochemistry, Chinese Academy of Sciences, Guiyang 550002, China

Received 18 October 2010; accepted in revised form 7 November 2011

Available online at www.sciencedirect.com
ScienceDirect
Geochimica et Cosmochimica Acta 175 (2016) 252–270
Geochimica et Cosmochimica Acta
www.elsevier.com/locate/gca

Liu & Liu, GCA, 2012

Clumped-isotope signatures at equilibrium of CH_4, NH_3, H_2O, H_2S and SO_2

Qi Liu, Yun Liu *

State Key Laboratory of Ore Deposit Geochemistry, Institute of Geochemistry, Chinese Academy of Sciences, Guiyang 550002, China

Received 6 January 2015; accepted in revised form 26 November 2015; Available online 8 December 2015

http://pubs.acs.org/journal/aesccq
Article

Zhang et al., ACS.ESC, 2012

Molecular-Level Mechanism of Phosphoric Acid Digestion of Carbonates and Recalibration of the $^{13}C-^{18}O$ Clumped Isotope Thermometer

Siting Zhang, Qi Liu, Mao Tang, and Yun Liu*

Cite This: *ACS Earth Space Chem.* 2020, 4, 420–433
Read Online

译名

2012：马秀峰，张兆峰，严爽，韦刚健，邓文峰，孙卫东. 耦合同位素简介. 地球环境学报，3: 950-959.

[中科院广州地球化学研究所]

将“clumped同位素”译为“耦合同位素”。

第3卷 第4期 地球环境学报 Vol. 3 No. 4
2012年8月 Journal of Earth Environment Aug. 2012
doi:10.7515/JEE201204005

耦合同位素简介

马秀峰[1,4]，张兆峰[2]，严 爽[2,4]，韦刚健[3]，邓文峰[2]，孙卫东[1]
（1. 中国科学院广州地球化学研究所 中国科学院矿物学与成矿学重点实验室，广州 510640；
2. 中国科学院广州地球化学研究所 同位素地球化学国家重点实验室，广州 510640；3. 中国科学院广州地球化学研究所 中国科学院边缘海地质重点实验室，广州 510640；4. 中国科学院研究生院，北京 100049）

摘 要：耦合同位素（Clumped isotope），是新兴的同位素地球化学方法。该方法从同位素互相结合程度的角度研究“同位素体”的地球化学行为，获得了传统同位素总体组成研究无法提供的新信息，目前已经在测定碳酸盐形成温度等领域展示了广阔的发展前景。本文简要介绍了耦合同位素地球化学的基本原理、测试方法、应用范围及存在问题，展望了其发展趋势，讨论了其发展中需注重的问题。

关键词：耦合同位素；碳酸盐耦合同位素温度计；原理；方法；应用
中图分类号：P597 **文献标志码**：A **文章编号**：1674-9901(2012)04-0950-10

译名

团簇同位素：

郑永飞院士最早提议使用；

中国矿物岩石地球化学会同位素地球化学专业委员会推荐；

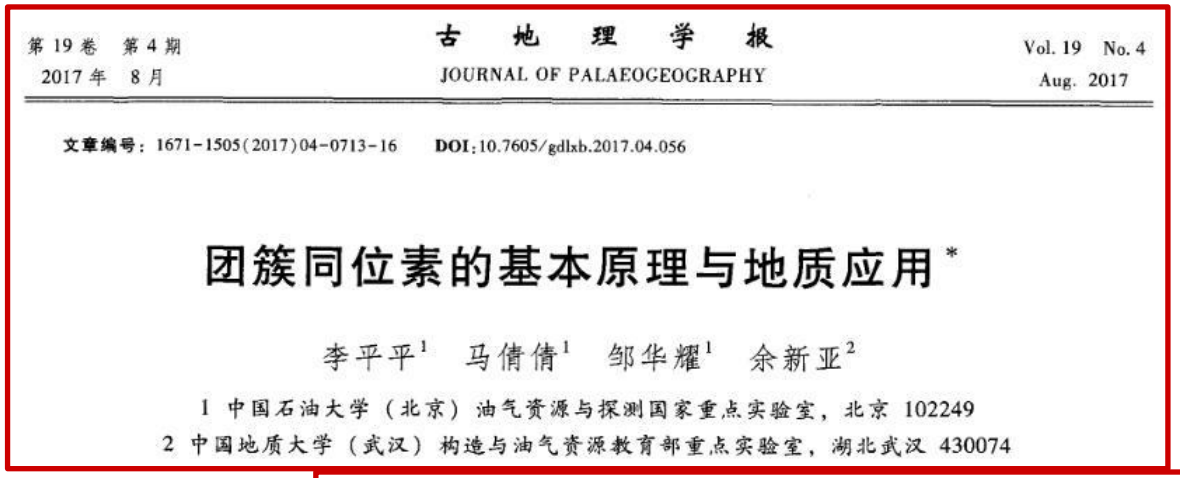

第 19 卷 第 4 期
2017 年 8 月

古 地 理 学 报
JOURNAL OF PALAEOGEOGRAPHY

Vol. 19 No. 4
Aug. 2017

文章编号：1671-1505(2017)04-0713-16 DOI:10.7605/gdlxb.2017.04.056

团簇同位素的基本原理与地质应用*

李平平[1] 马倩倩[1] 邹华耀[1] 余新亚[2]

1 中国石油大学（北京）油气资源与探测国家重点实验室，北京 102249
2 中国地质大学（武汉）构造与油气资源教育部重点实验室，湖北武汉 430074

·综述·

矿物岩石地球化学通报
Bulletin of Mineralogy, Petrology and Geochemistry
Vol. 38 No. 4, July, 2019

珊瑚碳酸盐团簇同位素研究进展

郭炀锐[1,2], 邓文峰[1*], 韦刚健[1]

1. 中国科学院 广州地球化学研究所, 同位素地球化学国家重点实验室, 广州 510640;
2. 中国科学院大学 地球与行星科学学院, 北京 100049

实验研究

建立实验室并发表论文：

中国科学院地质与地球物理研究所、中国科学院广州地球化学研究所、中国地质大学（武汉）·

与国外实验室合作：

北京大学、中国科学院地球环境研究所、中国地质大学（北京）、中国石油勘探开发研究院、中国石油杭州地质研究院、中国石油大学（北京） ……

实验研究

中国科学院地质与地球物理研究所：

Contents lists available at ScienceDirect

International Journal of Mass Spectrometry

journal homepage: www.elsevier.com/locate/ijms

Determination of clumped isotopes in carbonate using isotope ratio mass spectrometer: Effects of extraction potential and long-term stability

Linlin Cui [a,*], Xu Wang [b]

[a] Institute of Geology and Geophysics, Chinese Academy of Sciences, P.O. Box 9825, Beijing 100029, China
[b] Key Laboratory of Cenozoic Geology and Environment, Institute of Geology and Geophysics, Chinese Academy of Sciences, P.O. Box 9825, Beijing 100029, China

Contents lists available at ScienceDirect

International Journal of Mass Spectrometry

journal homepage: www.elsevier.com/locate/ijms

Determination of clumped isotopes in carbonate using isotope ratio mass spectrometry: Toward a systematic evaluation of a sample extraction method using a static Porapak™ Q absorbent trap

Xu Wang [a,*], Linlin Cui [b], Yangyang Li [a], Xiaofang Huang [a], Jixuan Zhai [a], Zhongli Ding [a]

[a] Key Laboratory of Cenozoic Geology and Environment, Institute of Geology and Geophysics, Chinese Academy of Sciences, P.O. Box 9825, Beijing 100029, China
[b] Institute of Geology and Geophysics, Chinese Academy of Sciences, P.O. Box 9825, Beijing 100029, China

AGU PUBLICATIONS

Geochemistry, Geophysics, Geosystems

RESEARCH ARTICLE
10.1002/2015GC006182

Stable and clumped isotopes in shell carbonates of land snails *Cathaica* sp. and *Bradybaena* sp. in north China and implications for ecophysiological characteristics and paleoclimate studies

Key Points:
- Clumped isotopes of snail shells are a season-specific geothermometer in monsoonal region
- *Cathaica* sp. snails had calcification temperatures 3–5°C higher than *Bradybaena* sp. snails
- Climatic seasonality determined the faunal assemblages of land snails in north China

Xu Wang[1], Linlin Cui[2], Jixuan Zhai[1,3], and Zhongli Ding[1]

[1]Key Laboratory of Cenozoic Geology and Environment, Institute of Geology and Geophysics, Chinese Academy of Sciences, Beijing, China, [2]Institute of Geology and Geophysics, Chinese Academy of Sciences, Beijing, China, [3]University of Chinese Academy of Sciences, Beijing, China

2014：

采用90%的离子源提取电压；
取得可重复的可信Δ_{47}值（NBS 19）；
无需经常加热CO_2做参考标准；
内部精度：0.010-0.014 ‰ ；
外部精度：0.010-0.020‰。

2016：

使用Porapak ™ Q吸附剂纯化CO_2；
系统比对使用Porapak ™ Q吸附剂的效率；
提出液氮+高真空泵+吸附剂可以节省时间；
不同前处理方法得到的Δ_{47}值略有差别。

2016：

分析两种陆生蜗牛壳体的Δ_{47}值；
认为Δ_{47}值反映蜗牛生长的环境温度；
Cathaica sp.比Bradybaena sp.高3–5°C；
温暖潮湿 vs. 寒冷干燥 ；
认为蜗牛Δ_{47}值有潜力重建陆地古环境。

实验研究

中国科学院地质与地球物理研究所：

ELSEVIER

Available online at www.sciencedirect.com

ScienceDirect

Geochimica et Cosmochimica Acta 257 (2019) 68–79

Geochimica et Cosmochimica Acta

www.elsevier.com/locate/gca

Clumped isotopes in land snail shells over China:
Towards establishing a biogenic carbonate paleothermometer

Jixuan Zhai [a,b,c,d], Xu Wang [a,b,c,*], Ben Qin [e], Linlin Cui [c,f], Shuhua Zhang [g]
Zhongli Ding [a,b,c]

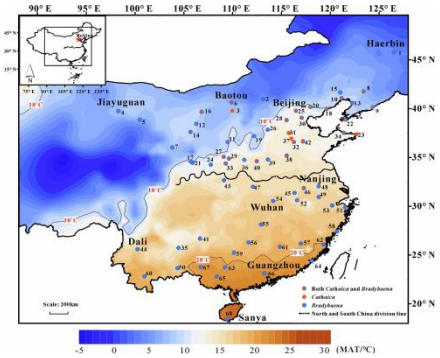

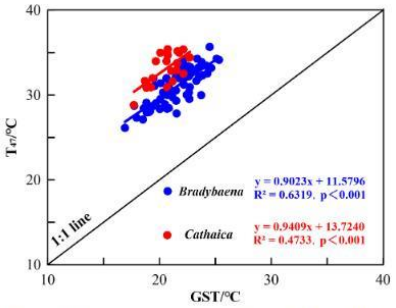

Fig. 6. Plot showing the positive correlation of T_{47} to GST for *Bradybaena* and *Cathaica*. All data were combined together for each species. The GST means growing season temperature.

$$Bradybaena\ \Delta_{47} = (0.0513 \pm 0.0036) \times 10^6/T^2 + (0.0930 \pm 0.0413), \quad R^2 = 0.9360$$

$$Cathaica\ \Delta_{47} = (0.0552 \pm 0.0111) \times 10^6/T^2 + (0.0351 \pm 0.1293), \quad R^2 = 0.8036$$

2019：

68个采样点的177个陆生蜗牛壳体样本；
发现壳体Δ_{47}温度与全年平均温度不一致，但与蜗牛生长季节温度具有相关性；
两种陆生蜗牛的壳体Δ_{47}温度有别，反应不同种蜗牛具有不同的生物效应；
建立了蜗牛壳体Δ_{47}值与生长温度的校正关系；
利用Δ_{47}温度和壳体$\delta^{18}O$ 信号，计算出蜗牛体液$\delta^{18}O$值；
认为Bradybaena sp.体液$\delta^{18}O$值可以指示其生长季节的降雨$\delta^{18}O$。

实验研究

中国科学院广州地球化学研究所：

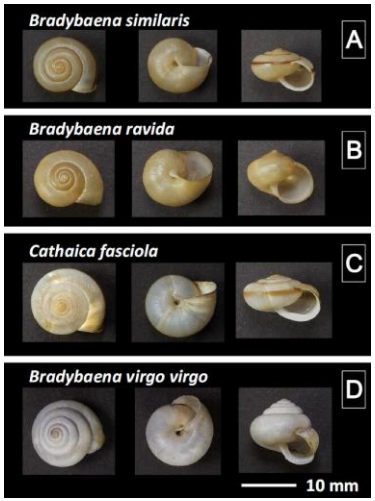

Contents lists available at ScienceDirect

Chemical Geology

journal homepage: www.elsevier.com/locate/chemgeo

Clumped isotopic signatures in land-snail shells revisited: Possible palaeoenvironmental implications

Yangrui Guo[a,b], Wenfeng Deng[a,c,*], Gangjian Wei[a], Li Lo[a], Ning Wang[a]

[a] State Key Laboratory of Isotope Geochemistry, Guangzhou Institute of Geochemistry, Chinese Academy of Sciences, Guangzhou 510640, China
[b] University of Chinese Academy of Sciences, Beijing 100039, China
[c] Radiogenic Isotope Facility, School of Earth and Environmental Sciences, The University of Queensland, Brisbane, Queensland 4072, Australia

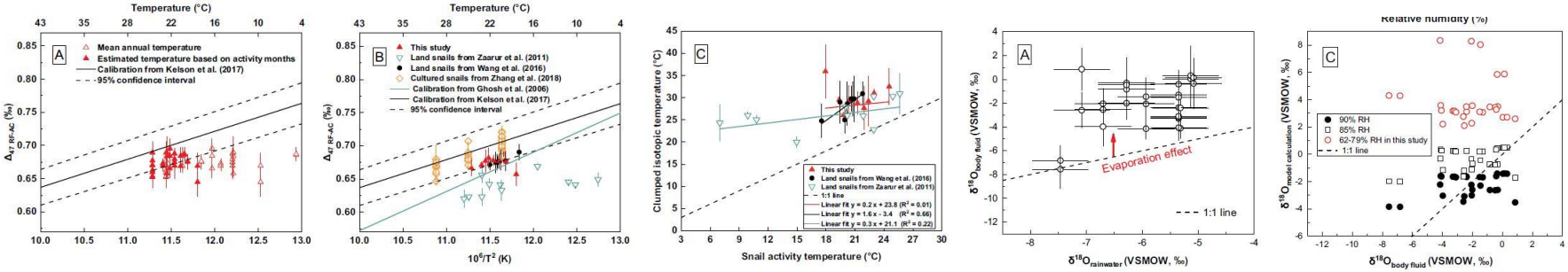

2019：

认为蜗牛壳体Δ_{47}温度与生长环境温度相关性弱，更反映蜗牛壳体钙化温度；
发现壳体Δ_{47}温度高于环境温度和活动温度，认为蜗牛可以上调体温；
壳体钙化，受蜗牛自身生理状况影响，温暖潮湿的生长环境有更多的钙化记录；
发现蜗牛体液$\delta^{18}O$值高于降雨$\delta^{18}O$，可能是钙化过程的蒸发导致；
90%湿度：体液$\delta^{18}O$值，可能反映生长区的降雨$\delta^{18}O$。

实验研究

中国科学院广州地球化学研究所：

JGR Biogeosciences

RESEARCH ARTICLE
10.1029/2019JG005402

Exploring the Temperature Dependence of Clumped Isotopes in Modern *Porites* Corals

Yangrui Guo[1,2,3], Wenfeng Deng[1,3,4], Gangjian Wei[1,3], Xuefei Chen[1,3], Xi Liu[1], Xijie Wang[1,2], Li Lo[1,5], Guanqiang Cai[6], and Ti Zeng[1,3]

[1]State Key Laboratory of Isotope Geochemistry, Guangzhou Institute of Geochemistry, Chinese Academy of Sciences, Guangzhou, China, [2]College of Earth and Planetary Sciences, University of Chinese Academy of Sciences, Beijing, China, [3]Southern Marine Science and Engineering Guangdong Laboratory, Guangzhou, China, [4]Radiogenic Isotope Facility, School of Earth and Environmental Sciences, The University of Queensland, Brisbane, Queensland, Australia, [5]Now at Department of Geosciences, National Taiwan University, Taipei, Taiwan, [6]Guangzhou Marine Geological Survey, China Geological Survey, Guangzhou, China

Key Points:

- There is no evidence of intercolony or intracolony variations in mean Δ_{47} values of *Porites* corals on an annual timescale
- Coral vital effects are found to cause relative disequilibrium of isotopic composition at an intracolony level
- Clumped isotopes analysis of *Porites* corals is suitable for reconstructing relative changes in seasonal sea surface temperature

2020：

珊瑚骨骼碳酸盐因生物效应无法达到热力学平衡；

相同温度条件下，滨珊瑚Δ_{47}值比无机碳酸钙的高；

滨珊瑚同时期不同部位的Δ_{47}值间存在显著差异；

$\delta^{18}O$值的差异较小；

该Δ_{47}-$\delta^{18}O$关系，可能指示新型生物分馏现象；，

总体上珊瑚Δ_{47}值与海面温度相关性明显；

具有指示季节性海水温度的应用价值。

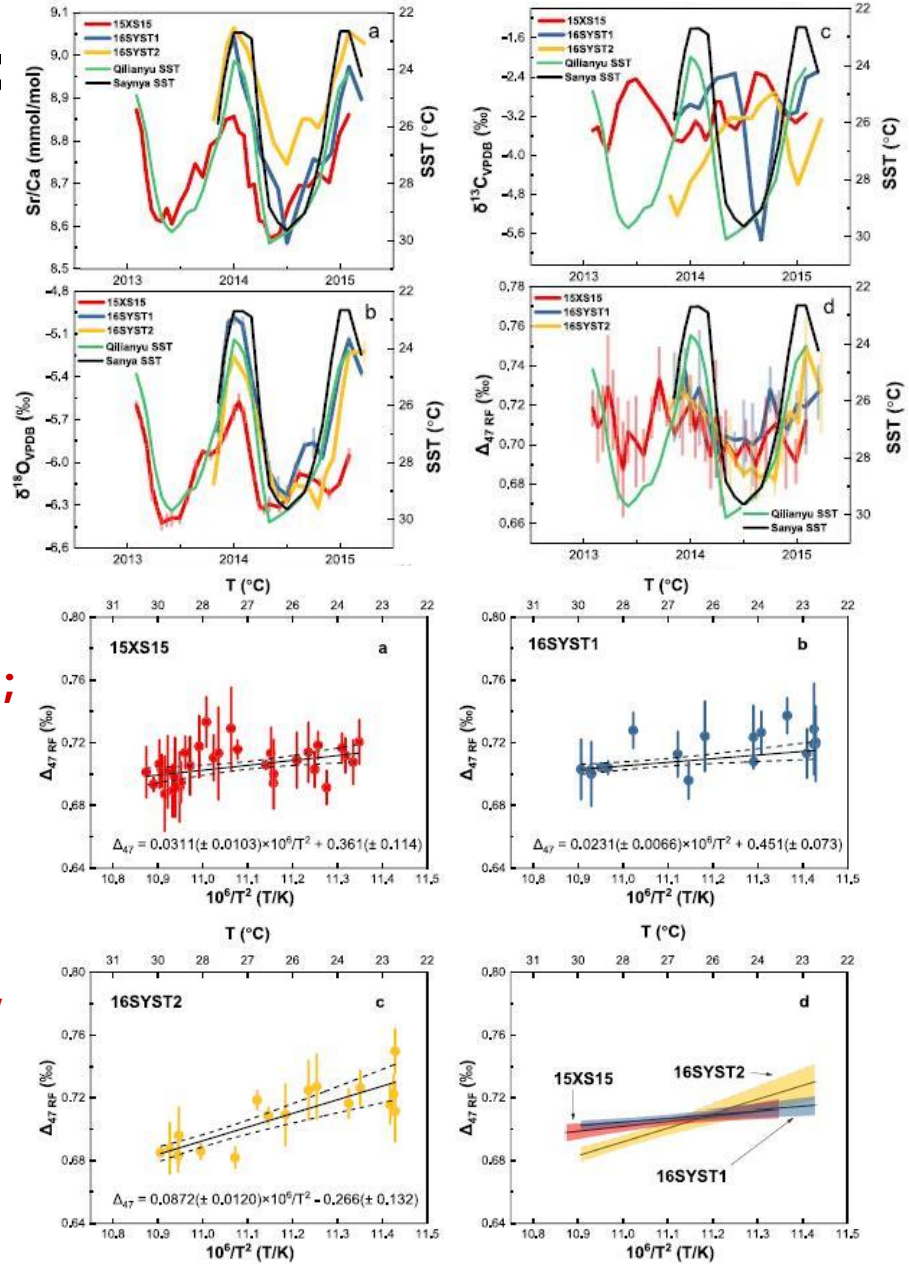

实验研究

中国科学院广州地球化学研究所：

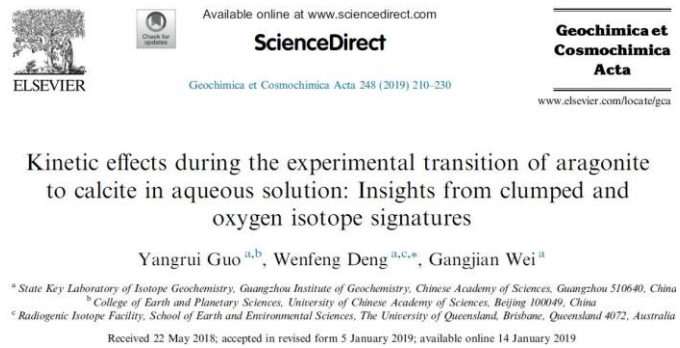

Available online at www.sciencedirect.com

ScienceDirect

Geochimica et Cosmochimica Acta 248 (2019) 210–230

Geochimica et Cosmochimica Acta

www.elsevier.com/locate/gca

Kinetic effects during the experimental transition of aragonite to calcite in aqueous solution: Insights from clumped and oxygen isotope signatures

Yangrui Guo [a,b], Wenfeng Deng [a,c,*], Gangjian Wei [a]

[a] State Key Laboratory of Isotope Geochemistry, Guangzhou Institute of Geochemistry, Chinese Academy of Sciences, Guangzhou 510640, China
[b] College of Earth and Planetary Sciences, University of Chinese Academy of Sciences, Beijing 100049, China
[c] Radiogenic Isotope Facility, School of Earth and Environmental Sciences, The University of Queensland, Brisbane, Queensland 4072, Australia

Received 22 May 2018; accepted in revised form 5 January 2019; available online 14 January 2019

2020：

文石-方解石转化是较常见的成岩作用，溶液Mg^{2+}的存在阻碍了转化的发生，Na^{+}和Ca^{2+}则促进转化发生；

H_2O-DIC-$CaCO_3$体系，转化过程的$\delta^{18}O$在90°C降低比25°C更明显，Ca^{2+}的增加会增大同位素不平衡信号；

Δ_{47}值和$\delta^{13}C$基本保持不变，不易受矿物学转化影响，记录文石的温度特征；

转化过程的动力学效应（高转化率）对Δ_{47}和$\delta^{18}O$的影响存在明显差异；

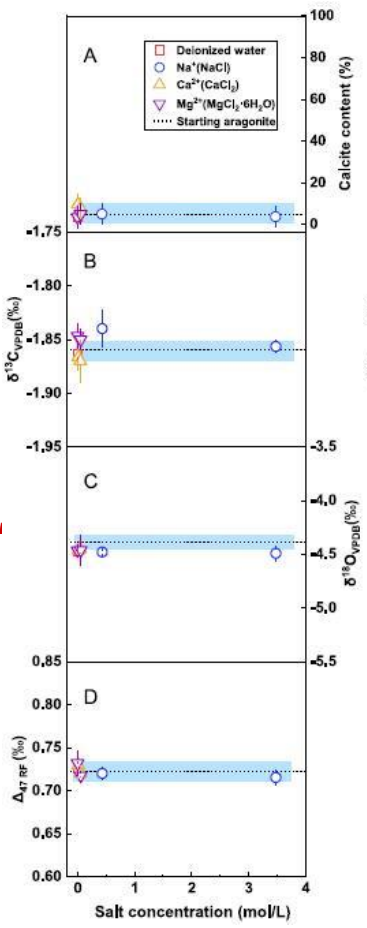

25°C

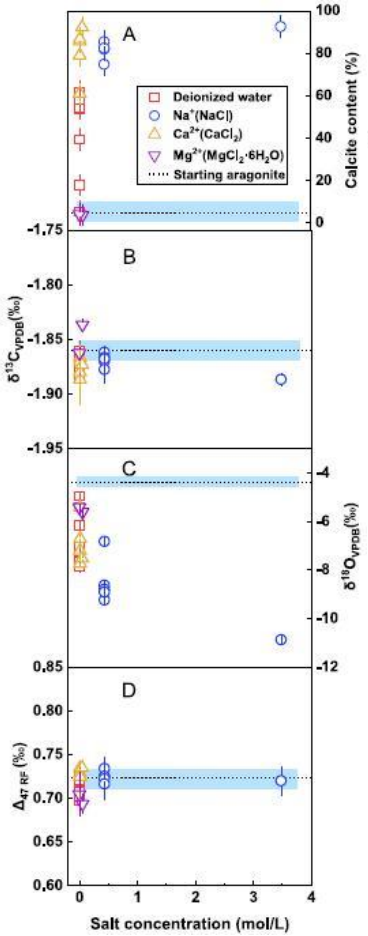

90°C

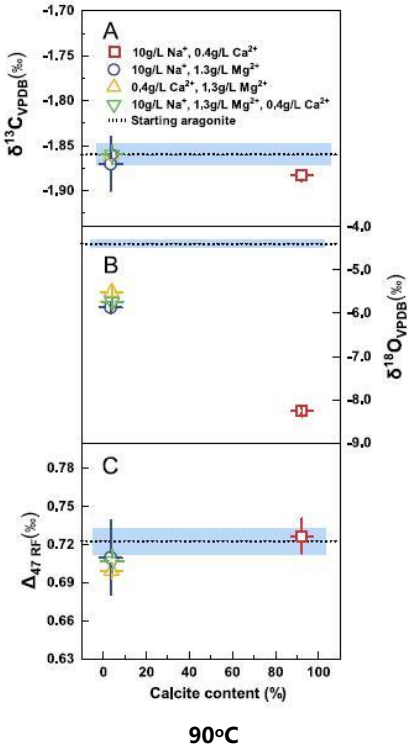

90°C

实验研究

中国地质大学（武汉）：

Received: 24 September 2019 | Revised: 27 November 2019 | Accepted: 27 November 2019
DOI: 10.1002/rcm.8678

RESEARCH ARTICLE

Rapid Communications in Mass Spectrometry

RCMS，2019

Effects of different constants and standards on the reproducibility of carbonate clumped isotope (Δ_{47}) measurements: Insights from a long-term dataset

Biao Chang[1,2] | William F. Defliese[3] | Chao Li[2] | Junhua Huang[1] | Aradhna Tripati[4] | Thomas J. Algeo[1,2,5]

PNAS，2020

Massive formation of early diagenetic dolomite in the Ediacaran ocean: Constraints on the "dolomite problem"

Biao Chang[a,b], Chao Li[a,1], Deng Liu[a], Ian Foster[c], Aradhna Tripati[c,d,e], Max K. Lloyd[f], Ingrid Maradiaga[d,e], Genming Luo[a], Zhihui An[g], Zhenbing She[a], Shucheng Xie[a], Jinnan Tong[a], Junhua Huang[b,1], Thomas J. Algeo[a,b,h], Timothy W. Lyons[i], and Adrian Immenhauser[j]

"白云石之谜" 第一作者：常标，共同通讯：李超、黄俊华

白云石在现今地表常温常压条件下难以形成，被认为是埋藏-热液白云岩化的产物；
距今5亿年的埃迪卡拉纪白云石地层的Δ_{47}温度显示，其形成于0℃—60℃地表环境；
认为白云石形成于一个低温且微生物活跃的海水溶液环境；
"白云石之谜"可能是古生代和前寒武纪海洋中特定条件下的产物；
白云石可能是早期海洋环境条件的忠实记录者。

实验研究

中国地质大学（北京）：
松辽盆地白垩纪古碳酸盐Δ_{47}温度，重建气候历史；德干火山的喷发造成了大规模生物灭绝。

THE GEOLOGICAL SOCIETY OF AMERICA®

Deccan volcanism caused coupled pCO_2 and terrestrial temperature rises, and pre-impact extinctions in northern China

Laiming Zhang[1*†], Chengshan Wang[1*], Paul B. Wignall[2], Tobias Kluge[3], Xiaoqiao Wan[1], Qian Wang[1§], and Yuan Gao[1]
[1]State Key Laboratory of Biogeology and Environmental Geology, School of Earth Sciences and Resources, China University of Geosciences Beijing, Beijing 100083, China
[2]School of Earth and Environment, University of Leeds, Leeds LS2 9JT, UK
[3]Institut für Umweltphysik, Universität Heidelberg, Im Neuenheimer Feld 229, Heidelberg 69120, Germany

中国石油大学（北京）：
湖泊叠层石Δ_{47}温度，重建准噶尔盆地南缘晚新生代气候变化。

Palaeogeography, Palaeoclimatology, Palaeoecology 514 (2019) 109–123

Contents lists available at ScienceDirect

Palaeogeography, Palaeoclimatology, Palaeoecology

journal homepage: www.elsevier.com/locate/palaeo

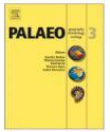

Sensitivity of lacustrine stromatolites to Cenozoic tectonic and climatic forcing in the southern Junggar Basin, NW China: New insights from mineralogical, stable and clumped isotope compositions

Wei Yang[a,b,*], Rusi Zuo[a,b], Xu Wang[c,**], Yan Song[a,b], Zhenxue Jiang[a,b], Qun Luo[a,b], Jixuan Zhai[c], Qianyou Wang[a,b], Chen Zhang[a,b], Ziya Zhang[d,e]

中国石油勘探开发研究院：
甲烷Δ_{18}温度指示天然气成因。

Contents lists available at ScienceDirect

Earth and Planetary Science Letters

www.elsevier.com/locate/epsl

Methane clumped isotopes in the Songliao Basin (China): New insights into abiotic vs. biotic hydrocarbon formation

Yanhua Shuai[a,b,*], Giuseppe Etiope[c,d], Shuichang Zhang[a], Peter M.J. Douglas[b,e], Ling Huang[a], John M. Eiler[b,*]

……

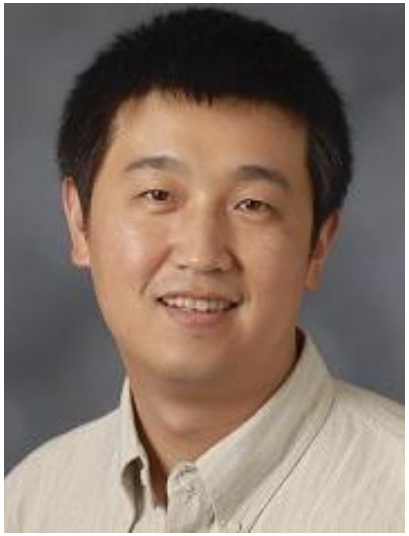

The City College of New York

Woods Hole Oceanographic Institution

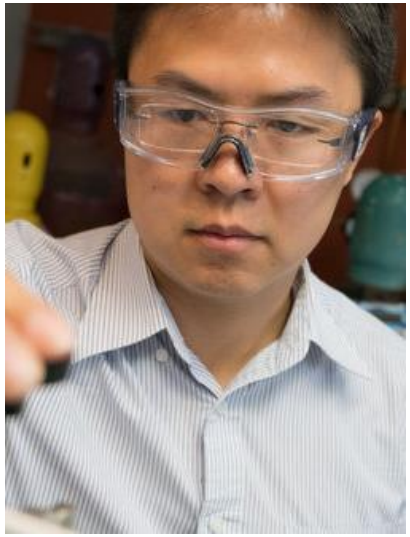

Rice University

北京大学

李姝宁

$^{15}N^{15}N$团簇同位素示踪行星大气圈的演化
碳酸盐$^{13}C^{18}O$团簇同位素用于古气候中的测温
^{13}C-D, D-D双团簇同位素体系示踪甲烷成因

Available online at www.sciencedirect.com
ScienceDirect
Geochimica et Cosmochimica Acta 203 (2017) 235–264
ELSEVIER
Geochimica et Cosmochimica Acta
www.elsevier.com/locate/gca

The relative abundances of resolved $^{12}CH_2D_2$ and $^{13}CH_3D$ and mechanisms controlling isotopic bond ordering in abiotic and biotic methane gases

E.D. Young [a,*], I.E. Kohl [a], B. Sherwood Lollar [b], G. Etiope [c,d], D. Rumble III [e], S. Li (李姝宁) [a], M.A. Haghnegahdar [a], E.A. Schauble [a], K.A. McCain [a], D.I. Foustoukos [e], C. Sutcliffe [b], O. Warr [b], C.J. Ballentine [f], T.C. Onstott [g], H. Hosgormez [h], A. Neubeck [i], J.M. Marques [j], I. Pérez-Rodríguez [k], A.R. Rowe [k], D.E. LaRowe [k], C. Magnabosco [l], L.Y. Yeung [m], J.L. Ash [a], L.T. Bryndzia [n]

SCIENCE ADVANCES | RESEARCH ARTICLE

ATMOSPHERIC SCIENCE

Extreme enrichment in atmospheric $^{15}N^{15}N$

Laurence Y. Yeung,[1]* Shuning Li,[1,2†] Issaku E. Kohl,[2] Joshua A. Haslun,[3] Nathaniel E. Ostrom,[3] Huanting Hu,[1] Tobias P. Fischer,[4] Edwin A. Schauble,[2] Edward D. Young[2]*

Molecular nitrogen (N_2) comprises three-quarters of Earth's atmosphere and significant portions of other planetary atmospheres. We report a 19 per mil (‰) excess of $^{15}N^{15}N$ in air relative to a random distribution of nitrogen isotopes, an enrichment that is 10 times larger than what isotopic equilibration in the atmosphere allows. Biological experiments show that the main sources and sinks of N_2 yield much smaller proportions of $^{15}N^{15}N$ in N_2. Electrical discharge experiments, however, establish $^{15}N^{15}N$ excesses of up to +23‰. We argue that $^{15}N^{15}N$ accumulates in the atmosphere because of gas-phase chemistry in the thermosphere (>100 km altitude) on time scales comparable to those of biological cycling. The atmospheric $^{15}N^{15}N$ excess therefore reflects a planetary-scale balance of biogeochemical and atmospheric nitrogen chemistry, one that may also exist on other planets.

" I thank Jeanine Ash, Edwin Schauble, and Ed Young for stimulating discussions that led to this manuscript being conceived, Shuning Li and Eric Hegg for comments on the manuscript, and Ed Young for coming up with the term "combinatorial" to describe the clumped-isotope effects described herein. I also thank Shuhei ……"

(Yeung, GCA, 2016)

中国地质科学院
胡斌

北京大学
周力平

第 89 卷 增刊
2015 年 10 月
地 质 学 报 ACTA GEOLOGICAL SINICA
Vol. 89 Supp.
Oct., 2015

长积分双路进样(LIDI)方法及其在Clumped 同位素测量中的应用

胡斌[1,2,3], Jens Radke[4], Hans-Jürgen Schlüter[4], Frank Torsten Heine[4], 周力平[2,5], Stefano M. Bernasconi[3]

1) 中国地质科学院矿产资源研究所，北京，100037；
2) 北京大学地表过程分析与模拟教育部重点实验室，北京，100871；
3) Geological institute, ETH Zürich, 8092 Zürich, Switzerland；
4) Thermo Fisher Scientific, 28199 Bremen, Germany；
5) 北京大学海洋研究院，北京，100871

瑞士联邦苏黎世理工学院
ETH Zurich
Stefano Bernasconi

Research Article
Rapid Communications in Mass Spectrometry
Received: 13 December 2013 Revised: 18 March 2014 Accepted: 27 March 2014 Published online in Wiley Online Library
Rapid Commun. Mass Spectrom. **2014**, *28*, 1413–1425
(wileyonlinelibrary.com) DOI: 10.1002/rcm.6909

A modified procedure for gas-source isotope ratio mass spectrometry: the long-integration dual-inlet (LIDI) methodology and implications for clumped isotope measurements

Bin Hu[1,2*], Jens Radke[3], Hans-Jürgen Schlüter[3], Frank Torsten Heine[3], Liping Zhou[1,4] and Stefano M. Bernasconi[2]

[1]Laboratory for Earth Surface Processes, Department of Geography, Peking University, 100871 Beijing, China
[2]Geological Institute, ETH Zürich, 8092 Zürich, Switzerland
[3]Thermo Fisher Scientific, 28199 Bremen, Germany
[4]Institute of Ocean Research, Peking University, 100871 Beijing, China

Caltech：真空线+气相色谱+MAT 253
3～10 mg碳酸盐（Eiler, 2011）

ETH：Kiel IV+MAT 253
2 mg碳酸盐（ Schmid & Bernasconi，2010）

采用LIDI+Kiel IV+MAT 253：
平行样测量所需样品量低至~0.1mg；
平行样数量可减少至5~6个；
测量精度~0.010‰的前提下，总样品量可低至1mg。

ELSEVIER
Available online at www.sciencedirect.com
SciVerse ScienceDirect
Geochimica et Cosmochimica Acta 108 (2013) 125–140
Geochimica et Cosmochimica Acta
www.elsevier.com/locate/gca

Calibration and application of the 'clumped isotope' thermometer to foraminifera for high-resolution climate reconstructions

Anna-Lena Grauel[a,*], Thomas W. Schmid[a], Bin Hu[a,b], Caterina Bergami[c], Lucilla Capotondi[c], Liping Zhou[b,d], Stefano M. Bernasconi[a]

[a] *Geological Institute, ETH Zurich, 8092 Zurich, Switzerland*
[b] *Department of Geography, Peking University, 100871 Beijing, China*
[c] *CNR – National Research Council of Italy, ISMAR – Institute of Marine Sciences, Bologna, Italy*
[d] *Centre for Ocean Research, Peking University, 100871 Beijing, China*

Received 12 May 2012; accepted in revised form 29 December 2012; available online 1 February 2013

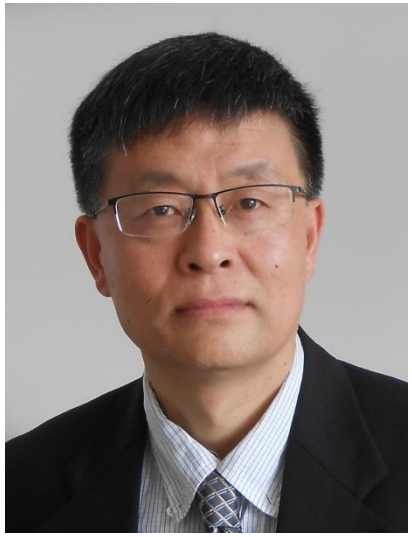

程海
西安交通大学

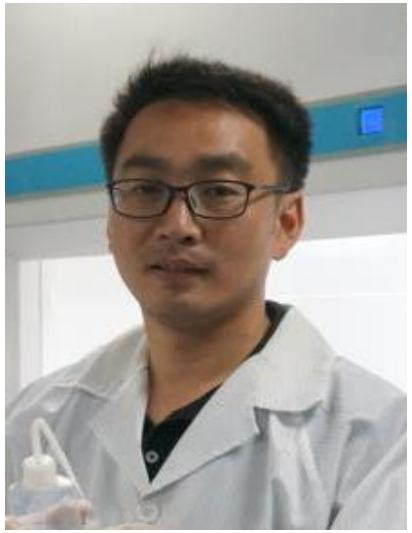

宁有丰
西安交通大学

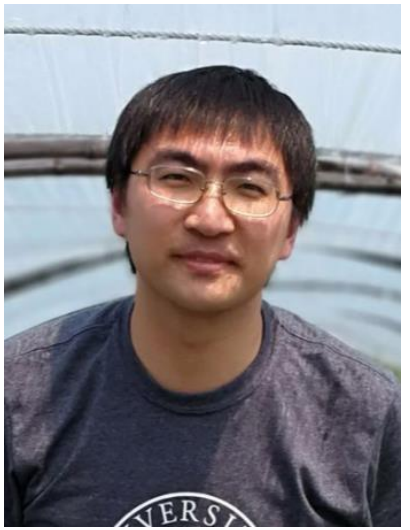

张乃忠
东京工业大学

HE Bo
芝加哥大学

TANG Jianwu
杜兰大学

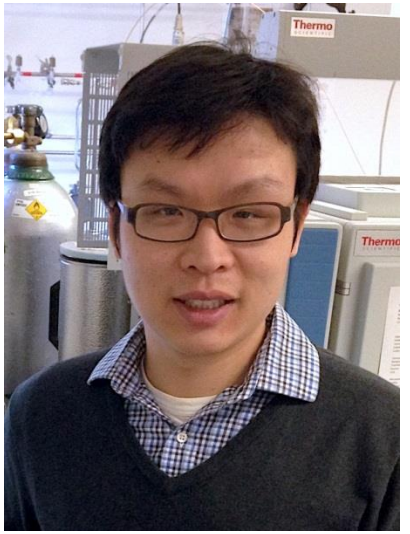

张一歌
德克萨斯农工大学

Nu Panorama：

采用全新离子光学方法；
超高分辨率、高灵敏度；
可识别质量数为18amu所有甲烷峰；
真正测定$^{13}CH_3D$和$^{12}CH_2D_2$。

上海海洋大学
全球第二台Nu Panorama

中国科学院
广州地球化学研究所
全球第四台Nu Panorama

中国地质科学院
矿产资源研究所

中国科学院
深海科学与工程研究所

https://www.nu-ins.com/products/irms/panorama

天津大学、
南京大学等

Thermo
SCIENTIFIC

MAT 253 Ultra

Explore new possibilities

- Formation temperatures of molecules
- Degradation processes of molecules
- Biochemical processes of nitrous oxide
- Photochemical processes in the atmosphere
- Metabolic processes in biochemistry

知识点：

1）随机分布是高温极限下的分布状态，只受概率控制；

2）同位素平衡分馏参数，是温度（T）的函数；

3）碳酸盐Δ_{47}平衡信号可单相测温，结合碳酸盐$\delta^{18}O$值，可获得与之平衡的水体$\delta^{18}O$值。

4）动力学分馏一般造成产物富集轻同位素，clumped同位素信号稍显复杂；

5）碳酸盐无法记录Δ_{47}平衡温度时，可以记录受冷却速率控制的封闭温度；

6）Δ_{47}值温度曲线的精确性，是测温的关键；

7）组合效应主要导致相同兴趣原子的Δ_n值<0;

8）生物效应可以产生异常的Δ_n值，可用于示踪；

9）异常的Δ_n值还可以用于扣除污染；

Clumped Isotopes
团簇同位素

谢谢